HOMOCLINIC BIFURCATIONS

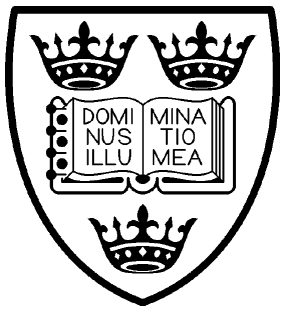

Thesis submitted for the degree of

Doctor of Philosophy

in the University of Oxford.

by

David M. Drysdale

Jesus College,

Oxford.

Michaelmas Term 1994

Acknowledgements

I would like to thank my supervisor Dr. A.C. Fowler for his help and advice, and Dr. Lenny Smith for his support, expertise and colour printer.

Financial support by the Science and Engineering Research Council, and its later incarnation, the Engineering and Physical Science Research Council, is gratefully acknowledged, as is support from Jesus College (in the form of a graduate scholarship and an extension grant).

Contents

1 Introduction

Much work has been done in the last hundred years in the study of the behaviour of parameterized systems of equations, and specifically in the study of bifurcations of solutions. However, until recently, most of this work has been done in the context of *local bifurcations*, that is bifurcations of fixed points of flows and maps. These bifurcations are termed local because they depend only upon behaviour in a neighbourhood of a fixed point.

More recently, work has been done in the field of *global bifurcations*. A global bifurcation depends on a non-local structure in the flow; the main structures that have been studied are *homoclinic* and *heteroclinic* orbits. These structures and the bifurcations associated with them display a complicated variety of behaviours, and frequently feature as an organizing centre for chaotic systems. In the present work, we concentrate entirely on homoclinic systems.

For an evolution equation

$$A_t = f(A; \mu)$$

with a parameter μ, a *homoclinic orbit* Γ associated to a fixed point p is an orbit that has the point p as its α-limit set and as its ω-limit set. That is, there exists a trajectory $x^H(t)$ such that

$$\lim_{t\to\infty} x^H(t) = \lim_{t\to-\infty} x^H(t) = p,$$

and $\Gamma = \{x^H(t) : t \in \mathbb{R}\}$. Without loss of generality, throughout the present work we will take the fixed point p to be the origin, and we will assume the existence of a homoclinic orbit at $\mu = 0$. The existence of such a homoclinic orbit is in general

a codimension one phenomenon, and thus we will consider only a one-dimensional parameter space.

The study of homoclinic equations was begun by L.P. Shil'nikov in a series of papers in the 1960's (Shil'nikov [1965], [1967a], [1968], [1969], [1970]). However, the subject was largely left untouched in the West until the recent upsurgence of interest in the study of chaos. From 1984 onwards, this has resulted in many more papers on the subject from a variety of authors.

Most of the early work on the subject considered systems of ordinary differential equations of low dimension, proving results about homoclinic systems in $n = 2, 3$ and 4 dimensions, and we review these results below. However, work by several authors considered the extension of the ideas and results to general n-dimensional systems of ordinary differential equations. Work by Fowler [1990a] also reduced the behaviour of periodic orbits of the system to fixed points of a one-dimensional map, extending previous work of Glendinning & Sparrow [1984], Sparrow [1982].

Finally, a paper by Fowler [1990b] considered a formal extension of the ideas used in the finite dimensional case to a class of partial differential equations on unbounded domains. For these systems, the behaviour of the periodic orbits of the system was shown to be related to a two-dimensional map.

In the present work, we cover the general finite dimensional case, and add in some details passed over in previous work on the subject. We also extend Fowler's work for PDEs in unbounded domains to consider the effect of symmetry considerations and vector-valued equations. This produces a finite-dimensional map, which is studied in two simple cases. These results are then applied to the complex Ginzburg-Landau equation, and compared with various numerical results.

Moreover, we also consider the case of partial differential equations on finite domains, formally corresponding to countably infinite dimensional systems of ordinary differential equations. We consider such systems in the presence of symmetry, and also consider the issues involved in the limit as the domain size tends to infinity.

Firstly, however, for the remainder of this chapter, we present briefly the results for specific low-dimensional ordinary differential equations that have been produced in the past.

1.1 Low Dimensional Cases

We will discover that the behaviour of a homoclinic ODE system is largely governed by the relative sizes and forms of those of the eigenvalues of the Jacobian matrix of the system that are closest to zero. If we consider these eigenvalues $\{\sigma\}$ ordered in a manner:

$$\ldots \leqslant \text{Re } \sigma^S < 0 < \text{Re } \sigma^U \leqslant \ldots \tag{1.1}$$

then there are three cases for the two eigenvalues with real parts closest to zero:

$$\begin{aligned}
&1)\ \sigma^U = \lambda^U, && \sigma^S = -\lambda^S && \text{(saddle)} \\
&2)\ \sigma^U = \lambda^U, && \sigma^S = -\lambda^S \pm i\omega^S && \text{(saddle-focus)} \\
&3)\ \sigma^U = \lambda^U \pm i\omega^U, && \sigma^S = -\lambda^S \pm i\omega^S && \text{(bifocal)}
\end{aligned} \tag{1.2}$$

where $\lambda^U, \lambda^S, \omega^U, \omega^S \in \mathbb{R}$ and $\lambda^U \neq 0, \lambda^S \neq 0$. (Note that the fourth possible case can be obtained from case 2) by time reversal). In each case, we will examine homoclinic systems in the lowest possible dimension for interesting behaviour. We will present the results available, as an indication of the complexity of behaviour associated with homoclinic systems, but without proofs.

Saddle-Focus Systems

In this first section, we will consider one particular homoclinic system, that of a saddle-focus system in three dimensions. This has been the most studied of the simple examples, and produces much interesting behaviour. In this case, $x \in \mathbb{R}^3$ and we assume that an appropriate (linear) change of coordinates has been performed in order to reduce the Jacobian matrix to a simple form, so that the system of ODEs is then:

$$\begin{aligned} \dot{x} &= \rho_\mu x - \omega_\mu y + P_\mu(x,y,z) \\ \dot{y} &= \omega_\mu x + \rho_\mu y + Q_\mu(x,y,z) \\ \dot{z} &= \lambda_\mu z + R_\mu(x,y,z) \end{aligned} \tag{1.3}$$

where:

1) P_μ, Q_μ, R_μ are analytic functions in (x,y,z) and μ that vanish together with their first derivatives at (0,0,0) for all μ near 0.
2) $\lambda_0 > 0 > \rho_0$ so that the origin is a saddle-focus. Note that we can also have $\lambda_0 < 0 < \rho_0$ by time reversal.
3) When $\mu = 0$, an orbit Γ homoclinic to the origin exists.

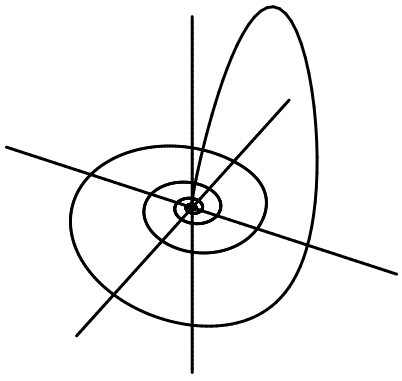

Figure 1.1 Homoclinic orbit Γ for a saddle-focus system

We then have various theorems concerning the behaviour of the system as the parameter μ varies.

Theorem 1.1.1 (Shil'nikov [1965], [1967a], [1970]): If $|\rho_0/\lambda_0| < 1$ (Shil'nikov's condition), then:

a) for $\mu \neq 0$, equation (1.3) possesses an unboundedly growing number of periodic solutions of saddle type as $\mu \to 0$

b) for $\mu = 0$, there exists countably many invariant sets of trajectories in phase space, each in one to one correspondence with a full shift on two symbols.

As is usual in such studies, when we examine the dynamics on the invariant set, by considering the symbolic dynamics of the conjugate shift map we can show that there is a countable infinity of periodic orbits of all periods, an uncountable infinity of aperiodic orbits, and an orbit that is dense in the invariant set (see e.g. Wiggins [1988] §2.2).

Theorem 1.1.2 (Glendinning & Sparrow [1984], Gaspard, Kapral & Nicolis [1984]): If $|\rho_0/\lambda_0| < 1$, then on both sides of $\mu = 0$ there exists a countable set of tangent bifurcations where periodic orbits are generated by pairs at parameter values μ_n^t accumulating at $\mu = 0$ with rate:

$$\lim_{n\to\infty} \frac{\mu_{n+1}^t - \mu_n^t}{\mu_n^t - \mu_{n-1}^t} = e^{-2\pi|\rho_0/\omega_0|} \tag{1.4}$$

Each tangent bifurcation is followed (as $\mu \to 0$) by a subharmonic (period doubling) bifurcation occurring at μ_n^h, such that:

a) If $0 < |\rho_0/\lambda_0| < 1/2$ then one orbit is a saddle and the other is an unstable node that becomes a saddle at μ_n^h.

b) If $1/2 < |\rho_0/\lambda_0| < 1$ then one orbit is a saddle and the other is a stable node that becomes a saddle at μ_n^h.

In the proofs of these two theorems, we find that the bifurcations are all connected by a *principal periodic orbit*, as depicted in Figure 1.2. The period P of this principal periodic orbit is found to be described asymptotically by $\mu \sim e^{\rho_0 P} \cos \omega_0 P$.

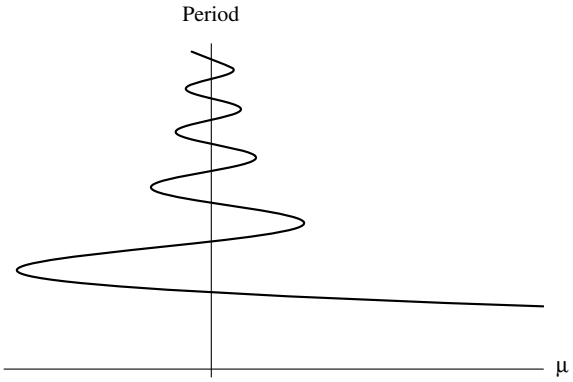

Figure 1.2 Principal periodic orbit in saddle-focus case

Theorem 1.1.3 (Gaspard [1984a], Glendinning & Sparrow [1984]): If $|\rho_0/\lambda_0| < 1$, then there exists a twofold countable set of homoclinic systems at parameter values μ_n^i $(i = 1, 2)$ with the same sign accumulating at $\mu = 0$ with rate:

$$(i = 1, 2) \qquad \lim_{n\to\infty} \frac{\mu_{n+1}^i - \mu_n^i}{\mu_n^i - \mu_{n-1}^i} = e^{-2\pi|\lambda_0/\omega_0|} \tag{1.5}$$

where each such "double-pulse" homoclinic orbit is associated to the origin and crosses twice an appropriately chosen surface transverse to Γ at $\mu = 0$.

Note that we may also apply this theorem to these subsidiary orbits, to produce further subsidiary homoclinic orbits that cross four times any surface transverse to Γ at $\mu = 0$. This process can continue indefinitely, giving a further indication of the complexity of the dynamics near the homoclinic orbit.

The main idea used in the proofs of these theorems is the construction of a Poincaré return map on a suitable surface near the fixed point. This map is the composition of two components. Near to the fixed point, we assume that the behaviour is governed by the linearization of the system about the fixed point. Away from the fixed point, we only consider those trajectories that remain close to the homoclinic orbit (in both phase space and parameter space) and thus approximate this part of the map with an affine map near to the homoclinic orbit. We will not consider this in detail here, but the method used is extended to general ordinary differential equation systems in the next chapter.

Saddle Systems

In this section we will deal with the case of a three-dimensional system possessing a homoclinic orbit to a saddle point. This is not the smallest dimension possible for this configuration of eigenvalues; however, the behaviour of a two-dimensional homoclinic system does not possess many interesting features, being completely described in the general case by the phase plane diagrams in Figure 1.3 (together with their rotations and reflections).

We consider, then, a system of form:

$$\begin{aligned} \dot{x} &= \lambda_1 x + P_\mu(x, y, z) \\ \dot{y} &= -\lambda_2 y + Q_\mu(x, y, z) \\ \dot{z} &= -\lambda_3 z + R_\mu(x, y, z) \end{aligned} \tag{1.6}$$

with $\lambda_1, \lambda_2, \lambda_3 > 0$ and where P_μ, Q_μ and R_μ are analytic functions that vanish together with their first derivatives at the origin. We assume that there is a

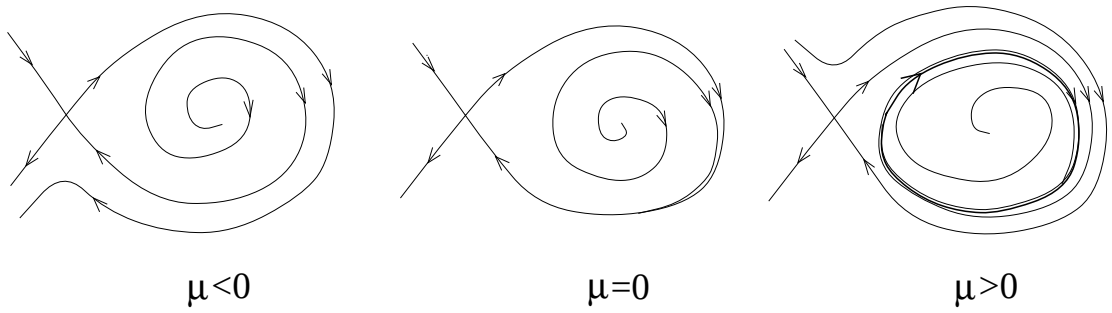

Figure 1.3 Two dimensional homoclinic system phase planes

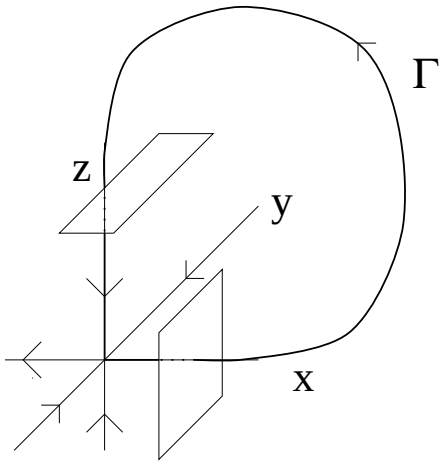

Figure 1.4 Homoclinic orbit associated to a saddle point, together with Poincaré surfaces.

homoclinic orbit Γ associated to the origin at $\mu = 0$ which approaches the origin along the z-axis.

In a similar manner to the previous section, a Poincaré return map is constructed on a suitable surface near to the origin. The main theorem is then:

Theorem 1.1.4 (Shil'nikov[1968], Wiggins [1988] §3.2): For sufficiently small

μ in the system (1.6), a periodic orbit bifurcates from the homoclinic orbit into one side of $\mu = 0$. This periodic orbit is:

a) A stable node if $\lambda_2 > \lambda_1$ and $\lambda_3 > \lambda_1$

b) A saddle point if $\lambda_2 + \lambda_3 > \lambda_1$ and ($\lambda_2 < \lambda_1$ or $\lambda_3 < \lambda_1$)

c) An unstable node if $\lambda_2 + \lambda_3 < \lambda_1$.

Moreover, if λ_m is the eigenvalue closest to zero, and P denotes the return time for the Poincaré map (that is, the period of the corresponding periodic orbit of the flow) we find that as $\mu \to 0$,

$$\mu \sim e^{-\lambda_m P}.$$

Bifocal Systems

This section will deal with the case where both the eigenvalues with real parts closest to zero are complex. This case is very similar to that of the saddle-focus; many of the results of that section are directly applicable. Specifically, Shil'nikov's original theorem (Shil'nikov [1967a], our theorem 1.1.1) was expressed in terms of bifocal systems.

If we consider a general bifocal system with the origin as the fixed point, and on which a (linear) change of coordinates has been performed in order to leave it in the form:

$$\begin{aligned} \dot{x} &= -\rho_1 x - \omega_1 y + f_1(x, y, z, w; \mu) \\ \dot{y} &= \omega_1 x - \rho_1 y + f_2(x, y, z, w; \mu) \\ \dot{z} &= \rho_2 z - \omega_2 w + f_3(x, y, z, w; \mu) \\ \dot{w} &= \omega_2 z + \rho_2 w + f_4(x, y, z, w; \mu) \end{aligned} \tag{1.7}$$

where $\rho_1, \rho_2, \omega_1, \omega_2 > 0$, the functions f_i are analytic and contain only nonlinear terms and where by time reversal if necessary we take $\rho_2 > \rho_1$. Then we may construct a Poincaré map on a surface near the origin in the same manner as mentioned before. By considering the properties of this map, we have:

Theorem 1.1.5 (Fowler & Sparrow [1991], Glendinning [1989]): If there exists a homoclinic orbit Γ at $\mu = 0$ associated to the origin of the above system, then we have:

a) there is a continuous curve in (μ, P) space $\mu = m(P)$ of periodic orbits such that the curve intersects $\mu = 0$ an infinite number of times
b) if $\omega_1/\omega_2 \neq 2n$ for any $n \in \mathbb{N}$, then there are sequences of double-pulse subsidiary homoclinic orbits that accumulate on $\mu = 0$ from both sides
c) if $\omega_1/\omega_2 = 2n$ for some $n \in \mathbb{N}$, then there are sequences of double-pulse subsidiary homoclinic orbits that accumulate on $\mu = 0$ from one side

where P denotes the period of periodic orbits.

1.2 Effects of Symmetry

The previous section presented results for homoclinic systems of ordinary differential equations under the assumption that there were no symmetries present. However, work has been done on the study of the behaviour of systems possessing both homoclinic orbits and symmetries, partly under the pervading influence of the work done on the Lorenz equations (Lorenz [1963], Sparrow [1982]), which are invariant under such a symmetry.

As we are dealing with low dimensional systems of ordinary differential equations, only discrete group actions are considered for symmetry effects (as continuous groups of symmetries for ODEs yield a reduction in order, see Olver [1986] §2.5). In fact, the level of extra complexity introduced by the addition of symmetry considerations is such that only the application of the group $\mathbb{Z}_2$ has been widely studied, although in several different representations (Tresser [1984]). The presence of such a $\mathbb{Z}_2$ symmetry means that a second homoclinic orbit will exist at $\mu = 0$, which would normally be a codimension two phenomenon.

Saddle Systems

In this case, we will give results for the saddle system (1.6) under the assumption that it is invariant under the representation $(x, y, z) \mapsto (-x, -y, z)$ of the $\mathbb{Z}_2$ symmetry. This is studied in Arneodo *et al* [1981], Glendinning [1988] and Wiggins [1988] §3.2; moreover, the Lorenz equations fall under this case. The method of analysis is still the construction of a Poincaré map, but now on pairs of symmetric Poincaré surfaces.

Theorem 1.2.1: Suppose that the system (1.6) is invariant under $(x, y, z) \mapsto (-x, -y, z)$ and that at $\mu = 0$ a pair of symmetric homoclinic orbits Γ_0 and Γ_1 exists. Moreover, suppose that $\lambda_2 > \lambda_1 > \lambda_3 > 0$ and $\lambda_2 \neq \lambda_3 - \lambda_1$. Then for sufficiently small μ, on one side of $\mu = 0$ no trajectories of the system remain in a small neighbourhood of $\Gamma_0 \cup \Gamma_1$, whilst on the other side of $\mu = 0$ there is an invariant set on which the dynamics are topologically conjugate to the full shift on two symbols.

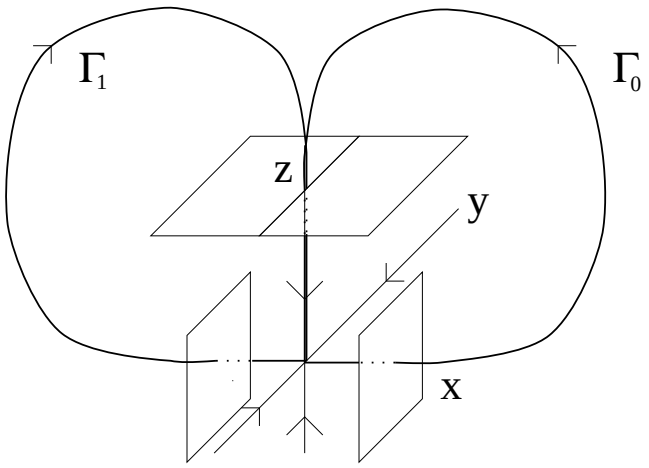

Figure 1.5 Pair of symmetric homoclinic orbits associated to a saddle point, together with pairs of symmetric Poincaré surfaces.

This theorem tells us that in the presence of symmetry, the previously simple behaviour of the homoclinic saddle system will instead display the complexity of behaviour associated with the shift map. Also, with regard to the parameterization, this complexity will appear suddenly at $\mu = 0$, in what has been called a *homoclinic explosion*.

Saddle-Focus Systems

Here we examine the results for the saddle-focus system (1.3) under the assumption that it is invariant under the representation $(x, y, z) \mapsto (-x, -y, -z)$ of the $\mathbb{Z}_2$ symmetry, as studied in Holmes [1980], Glendinning [1984] and Wiggins [1988] §3.2. We write the two homoclinic orbits as Γ_0 and Γ_1.

For such a system, all of the results presented earlier in this chapter apply to both of the homoclinic orbits. This means that when Shil'nikov's condition $|\rho_0/\lambda_0| < 1$

holds, there are two principal periodic orbits produced by the homoclinic bifurcation, which are related by the symmetry transformation. In addition, there is also a third branch of periodic orbits produced in the bifurcation that loop around once near each of the homoclinic orbits. Similarly, as well as the double pulse homoclinic orbits already mentioned, there are also sequences of double-pulse homoclinic orbits that are close to one of the homoclinic orbits for one pulse, and are close to the other for the second pulse.

When Shil'nikov's condition does not hold, that is $|\rho_0/\lambda_0| > 1$, we classify periodic orbits by assigning to each a semi-infinite sequence $\cdot a_0 a_1 a_2 \ldots$ where each a_i is 0 or 1, corresponding to whether the i-th loop of the orbit is close to Γ_0 or to Γ_1. Holmes [1980] showed that at $\mu = 0$, although the ω-limit set of the system is $\Gamma_0 \cup \Gamma_1$, every possible semi-infinite sequence is realized as an approach to $\Gamma_0 \cup \Gamma_1$. This shows that although the long time behaviour of such a system is simple, in the symmetric case the approach to this behaviour can be complex.

1.3 Summary

In this chapter, we have given the results for the systems of lowest interesting dimension for each of the three generic forms (1.2) of the eigenvalues of the Jacobian matrix at the origin. In each case, the results were originally obtained from the construction of a Poincaré map in two parts. The first part consisted of the near-linear behaviour close to the origin; the second part consisted of an affine map near to the trajectory of the homoclinic orbit. The composition of these two maps gave a Poincaré return map on a surface near to the origin, and in each case we considered the fixed point behaviour of this map.

For the saddle-focus system, which has been the most studied of the three systems, we saw that a homoclinic orbit leads to the complicated, chaotic dynamics of a symbol shift map on an invariant set near the homoclinic orbit. We also mentioned that near to any such homoclinic orbit, there exist subsidiary homoclinic orbits, which will also exhibit complicated behaviour. Most importantly, however, we deduced a pattern of bifurcations of periodic orbits near to the homoclinic orbit. When Shil'nikov's condition $|\text{Re } \sigma^S|/\sigma^U < 1$ holds, this consists of a principal periodic orbit that has a period tending to infinity in an oscillatory manner as $\mu \to 0$, with attendant subharmonic bifurcations on each branch, as depicted in Figure 1.2.

For the saddle system, we again deduced the existence of a principal periodic orbit, with period tending to infinity as $\mu \to 0$, but in all cases this orbit only existed on one side of $\mu = 0$. The stability of the periodic orbit was here governed by the relative sizes of the eigenvalues, as stated in Theorem 1.1.4.

Finally, for the bifocal system, we discovered similar behaviour to that of the saddle-focus system. We again encountered subsidiary homoclinic orbits near to the main homoclinic orbit (although in this case such subsidiary homoclinic orbits may only occur on one side of $\mu = 0$ if $|\text{Im } \sigma^S|/|\text{Im } \sigma^U|$ is an even integer), and we found a principal periodic orbit whose period tended to infinity in an oscillatory manner as $\mu \to 0$.

We have seen that for the three nondegenerate cases a principal periodic orbit is formed in a homoclinic bifurcation, with the period tending to infinity as μ tends

to zero. The asymptotic behaviour of the period P was found to be:

$$\begin{array}{llll}
\mu \sim e^{-\lambda^S P} & \sigma^U = \lambda^U, & \sigma^S = -\lambda^S, & \lambda^S < \lambda^U \\
\mu \sim e^{-\lambda^U P} & \sigma^U = \lambda^U, & \sigma^S = -\lambda^S, & \lambda^S > \lambda^U \\
\mu \sim e^{-\lambda^S P}\cos\omega^S P & \sigma^U = \lambda^U, & \sigma^S = -\lambda^S \pm i\omega^S, & \lambda^S < \lambda^U \\
\mu \sim e^{-\lambda^U P} & \sigma^U = \lambda^U, & \sigma^S = -\lambda^S \pm i\omega^S, & \lambda^S > \lambda^U \\
\mu \sim e^{-\lambda^S P}\cos\omega^S P & \sigma^U = \lambda^U \pm i\omega^U, & \sigma^S = -\lambda^S \pm i\omega^S, & \lambda^S < \lambda^U \\
\mu \sim e^{-\lambda^U P}\cos\omega^U P & \sigma^U = \lambda^U \pm i\omega^U, & \sigma^S = -\lambda^S \pm i\omega^S, & \lambda^S > \lambda^U
\end{array} \tag{1.8}$$

We thus see that in each of the cases,

$$\mu \sim e^{-\lambda_m P}\cos\omega_m P, \tag{1.9}$$

where $\lambda_m = \min\{\lambda^U, \lambda^S\}$. In the next chapter, we will derive a more general treatment of homoclinic bifurcations in ordinary differential equations, and we will be able to reduce the Poincaré map there obtained to a one-dimensional map. From this one-dimensional map, these asymptotic conditions for the period of the principal periodic orbit may be recovered.

2 Homoclinic Bifurcations in n Dimensions

In this chapter we consider the analysis of a general n-dimensional system of ordinary differential equations that possesses a homoclinic orbit. We consider all of the cases covered in the previous chapter in a more general setting, and our analysis will recover several of the properties of homoclinic systems discovered there. We will assume throughout the chapter that the system under consideration is not invariant under any symmetries, as continuous groups of symmetries would lead to a reduction of order in the equations (Olver [1986] §2.5), and specific representations of discrete groups of symmetries can not be dealt with in a generic manner.

The analysis of such n-dimensional homoclinic systems may be performed by considering matrix integral equations (as in Shil'nikov [1967b], [1968], [1970], Gaspard [1984b], Wiggins [1988] and with great rigour in Deng [1989]) or by considering functional differential equations (Lin [1986]); however, we will adopt a more symbolic approach closely following Fowler [1990a]. In either case, the analysis proceeds by the construction of a Poincaré map in two parts, in an exactly analogous manner to the standard construction for the low dimensional examples in the previous chapter.

2.1 Derivation of a Poincaré Map

We consider a system of ordinary differential equations:

$$\dot{x} = f(x;\mu) \qquad x \in \mathbb{R}^n, \mu \in \mathbb{R} \tag{2.1}$$

where f is an analytic function, and where the origin is a hyperbolic fixed point for all values of μ. We assume that a homoclinic orbit Γ exists at $\mu = 0$, and that a local change of variables has been performed so that the Jacobian matrix of f has been diagonalized. We then split the space $\mathbb{R}^n = W_U \oplus W_S$ into stable and unstable eigenspaces of the system at the origin, and throughout the chapter a subscript U or S will denote the unstable or stable component of a vector. We also let $k = \dim W_U$, giving $\dim W_S = n - k$.

If our homoclinic orbit Γ may be parameterized as $x^H(t)$, then we suppose that:

$$\begin{aligned} x^H &\sim e^{tD_0}\alpha^H \qquad \text{as } t \to -\infty, \\ x^H &\sim e^{tD_0}\beta^H \qquad \text{as } t \to +\infty, \end{aligned} \tag{2.2}$$

where $D_0 = Df(0,0)$ and $\alpha_S^H = 0$, $\beta_U^H = 0$. By suitably setting the time origin of $x^H(t)$ we may take $\alpha, \beta = \mathcal{O}(1)$.

Suppose that e^U and e^S are the eigenvectors corresponding to the unstable and stable eigenvalues with real parts closest to zero; then we define the surfaces

$$\Sigma = \{x : |\langle x, e^S\rangle| = \nu\},$$
$$\Sigma' = \{x : |\langle x, e^U\rangle| = \nu\},$$

where $\nu \ll 1$. Points on Σ sufficiently close to the homoclinic orbit will be mapped to points on Σ' near the homoclinic orbit, and we shall call this map φ. Within the region between Σ and Σ', $x = \mathcal{O}(\nu)$ and we may linearize the flow as

$$\dot{x} = Dx + g(x) \tag{2.3}$$

where $D = Df(0;\mu)$, with equivalent integral equation:

$$x(t) = e^{(t-t_0)D}x_0 + \int_{t_0}^{t} e^{(t-\tau)D}g(x(\tau))\,d\tau. \tag{2.4}$$

We have assumed that f is analytic, hence for any initial point x_0, $x(t)$ is analytic in t for t on some bounded interval (Hartman [1982] Ch. II Thm. 1.1), and also $x(t)$ is analytic in x_0 (Hartman [1982] Ch. V Thm. 4.1).

Let t_U, t_S be such that:

$$\begin{aligned} e^{-t_U D_0}\alpha^H &\in \Sigma', \\ e^{t_S D_0}\beta^H &\in \Sigma \end{aligned} \tag{2.5}$$

and we may take α^H, β^H as being such that $|\langle \alpha^H, e^U\rangle| = 1$ and $|\langle \beta^H, e^S\rangle| = 1$.

For general points x_0, x_1 on Σ and Σ' respectively, we can define an alternative representation β, α by:

$$\begin{aligned} x_0 &= e^{t_S D_0}\beta \qquad & |\langle \beta, e^S\rangle| &= 1, \\ x_1 &= e^{-t_U D_0}\alpha \qquad & |\langle \alpha, e^U\rangle| &= 1, \end{aligned} \tag{2.6}$$

and for x_0, x_1 to be close to Γ, we will require that $\alpha, \beta = \mathcal{O}(1)$. We use this alternative representation because it will enable us to use the return time P between visits to Σ to produce a one dimensional map.

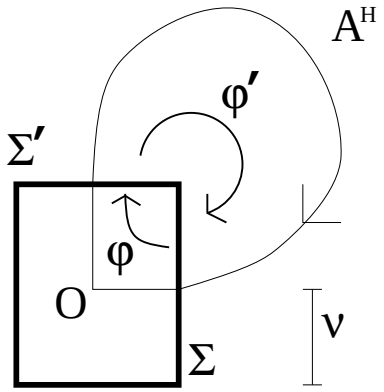

Figure 2.1 Schematic representation of the flow.

If a trajectory of the flow passes through x_0, and then through x_1 at a time $\widetilde{t}$ later, we will have from (2.4) that

$$\alpha = e^{(t_U+t_S)D_0+\widetilde{t}D}\beta + e^{t_U D_0}\int_0^{\widetilde{t}} e^{(\widetilde{t}-\tau)D} g(x(\tau))\,d\tau. \tag{2.7}$$

We will now show that this may be approximated as

$$\begin{aligned}\alpha = \varphi(\beta) &= e^{t_U D_0}\left[e^{(t_S+\widetilde{t}_L)D_0}\beta + \mathcal{O}\big(\nu^2\big)\right] \\ &= e^{PD_0}\beta + e^{t_U D_0}\mathcal{O}\big(\nu^2\big),\end{aligned} \tag{2.8}$$

where $P = t_U + t_S + \widetilde{t}_L$ and $\widetilde{t}_L$ satisfies $|\langle e^{\widetilde{t}_L D_0}x_0, e^U\rangle| = \nu$.

We adapt the analysis of Wiggins [1988] Section 3.2 to derive this result. Let Φ_t be the flow generated by the full differential equation (2.1), and let $\Pi = \{x \in \Sigma : \langle x, e^U\rangle = 0\}$ be those points on Σ that are not mapped to Σ' by the linear flow. Then for $x_0 \in \Sigma \setminus \Pi$ we define $\widetilde{t}(x_0)$ as the time taken to reach Σ', that is we define $\widetilde{t}$ by

$$|\langle \Phi_{\widetilde{t}(x_0)}(x_0), e^U\rangle| = \nu.$$

We define an exact map $\varphi\colon \Sigma \to \Sigma'$ by $\varphi(x_0) = \Phi_{\widetilde{t}(x_0)}(x_0)$ and an approximate map $\varphi_L\colon \Sigma \to \Sigma'$ by $\varphi_L(x_0) = e^{\widetilde{t}_L(x_0)D}x_0$ where $\widetilde{t}_L(x_0)$ is given by $|\langle e^{\widetilde{t}_L(x_0)D}x_0, e^U\rangle| = \nu$, and we explore the relationship between these two maps.

First scale $x = \nu y$ so that the differential equation (2.3) becomes

$$\dot{y} = Dy + h(y,\nu), \tag{2.9}$$

where $h(y,\nu) = (1/\nu)g(\nu y)$. As $g = \mathcal{O}\big(x^2\big)$, we notice that $\lim_{\nu\to 0} h(y,\nu) = 0$. We denote the flow generated by this differential equation as $\Psi_{t,\nu}$ and note that $\Psi_{t,0}(y_0) = e^{Dt}y_0$.

In these scaled coordinates φ becomes

$$\psi(y_0, \nu) = \Psi_{\widetilde{\tau}(y_0,\nu),\nu}(y_0), \tag{2.10}$$

where $\widetilde{\tau}(y_0, \nu)$ is obtained from

$$|\langle \Psi_{\widetilde{\tau}(y_0,\nu),\nu}(y_0), e^U \rangle| = 1 \tag{2.11}$$

and we have $\psi(y_0, 0) = \psi_L(y_0)$.

Lemma 2.1.1: If f is C^r then the solution $\widetilde{\tau}(t_0, \nu)$ of (2.11) is C^r for $y_0 \in \Sigma \backslash \Pi$ and sufficiently small ν.

Proof: Let

$$d(t, y_0, \nu) = |\langle \Psi_{t,\nu}(y_0), e^U \rangle| - 1, \tag{2.12}$$

so that $d(\widetilde{\tau}(y_0, \nu), y_0, \nu) = 0$. At $\nu = 0$, for all $y_0 \in \Sigma \setminus \Pi$, we have a solution $\widetilde{\tau}_L$ such that

$$d(\widetilde{\tau}_L(y_0), y_0, 0) = \left| \left\langle e^{D\widetilde{\tau}_L(y_0)} y_0, e^U \right\rangle \right| - 1 = 0.$$

Now we consider the derivative of d with respect to time:

$$\frac{\partial d}{\partial t} = \left| \left\langle \frac{\partial}{\partial t} \left(\Psi_{t,\nu}(y_0) \right), e^U \right\rangle \right|.$$

At $\nu = 0$, $t = \widetilde{\tau}_L(y_0)$ we have

$$\frac{\partial d}{\partial t}(\widetilde{\tau}_L(y_0), y_0, 0) = \left| \left\langle De^{D\widetilde{\tau}_L(y_0)} y_0, e^U \right\rangle \right|. \tag{2.13}$$

Since D_0 is hyperbolic and diagonal, and as $\left| \left\langle e^{D_0\widetilde{\tau}_L(y_0)} y_0, e^U \right\rangle \right| = 1$ we have that equation (2.13) is non-zero for sufficiently small μ. Hence, by the implicit function theorem, for sufficiently small ν the solution $\widetilde{\tau}(y_0, \nu)$ is C^r in y_0 and ν.

□

Theorem 2.1.2: $|\psi - \psi_L| = \mathcal{O}(\nu)$.

Proof: Lemma 2.1.1 tells us that we can expand

$$\begin{aligned}\widetilde{\tau}(y_0,\nu) &= \widetilde{\tau}(y_0,0) + \nu\frac{\partial\widetilde{\tau}}{\partial\nu}(y_0,0) + \mathcal{O}\big(\nu^2\big)\\ &= \widetilde{\tau}_L(y_0) + \nu T_1(y_0,0) + \mathcal{O}\big(\nu^2\big)\end{aligned}$$

thus giving

$$\begin{aligned}\psi(y_0,\nu) &= \Psi_{\widetilde{\tau}(y_0,\nu),\nu}(y_0)\\ &= \Psi_{\widetilde{\tau}_L(y_0)+\nu T_1(y_0,0)+\mathcal{O}(\nu^2),\nu}(y_0)\\ &= \Psi_{\widetilde{\tau}_L(y_0),\nu}(y_0) + \nu T_1(y_0,0)\,\frac{\partial}{\partial t}\Psi_{t,\nu}(y_0)\Big|_{t=\widetilde{\tau}_L(y_0)} + \mathcal{O}\big(\nu^2\big)\\ &= \Psi_{\widetilde{\tau}_L(y_0),0}(y_0) + \nu\,\frac{\partial}{\partial\nu}\Psi_{t,\nu}(y_0)\Big|_{\substack{t=\widetilde{\tau}_L(y_0)\\ \nu=0}}\\ &\qquad + \nu T_1(y_0,0)\,\frac{\partial}{\partial t}\Psi_{t,\nu}(y_0)\Big|_{\substack{t=\widetilde{\tau}_L(y_0)\\ \nu=0}} + \mathcal{O}\big(\nu^2\big)\\ &= \psi_L + \nu\left[\frac{\partial\Psi_{t,\nu}}{\partial\nu}(y_0) + \frac{\partial\widetilde{\tau}}{\partial\nu}(y_0,0)\frac{\partial\Psi_{t,\nu}}{\partial t}(y_0)\right]\Big|_{\substack{t=\widetilde{\tau}_L(y_0)\\ \nu=0}} + \mathcal{O}\big(\nu^2\big),\end{aligned}$$

and hence $|\psi - \psi_L| = \mathcal{O}(\nu)$. □

Theorem 2.1.3: $|\varphi - \varphi_L| = \mathcal{O}\big(\nu^2\big)$.

Proof: We know $x = \nu y$ so $\varphi(\nu y_0) = \nu\psi(y_0)$ and $\varphi_L(\nu y_0) = \nu\psi_L(y_0)$, thus giving

$$|\varphi(x_0) - \varphi_L(x_0)| = |\nu(\psi(y_0) - \psi_L(y_0))| = \mathcal{O}\big(\nu^2\big)$$

as required. □

Thus we have completed the derivation of the inside map, equation (2.8). Returning to the main theme, for the flow from Σ' back to Σ we linearize about

the homoclinic orbit to obtain a map $\varphi' : \Sigma' \to \Sigma$. If we write $x = x^H + y$ then y satisfies

$$\dot{y} = A_\Gamma(t)y + \mu\frac{\partial f}{\partial \mu}(x^H; 0) + G(t, y) \tag{2.14}$$

where $A_\Gamma(t) = Df(x^H(t), 0)$ and

$$G(t, y) = f(x^H(t) + y(t); \mu) - f(x^H(t); 0) - A_\Gamma(t)y - \mu\,\frac{\partial f}{\partial \mu}(x^H(t); 0).$$

We let $Y(t)$ be a fundamental matrix for the linear equation $\dot{y} = A_\Gamma(t)y$, and define the *heteroclinic matrix* H by

$$H(t) = e^{-tD_0}Y(t). \tag{2.15}$$

We now show that H tends to a constant matrix as $t \to \pm\infty$. Firstly, we adapt a theorem from Coddington & Levinson [1955] Ch. 3 Thm. 8.1.

Theorem 2.1.4: Suppose A is a constant diagonal matrix with eigenvalues μ_j; suppose that $R(t)$ is an integrable matrix such that

$$\int_0^\infty |R(t)|\, dt < \infty.$$

If e_k is the k-th standard basis vector, so that $Ae_k = \mu_k e_k$, then there is a solution φ_k of

$$\dot{x} = (A + R(t))x \tag{2.16}$$

and there exists $t_0 \in [0, \infty)$ such that

$$\lim_{t\to\infty} \varphi_k(t)e^{(t_0 - t)\mu_k} = e_k.$$

Proof: Choose t_0 large enough so that

$$\int_{t_0}^{\infty} |R(\tau)|\, d\tau < \frac{1}{2}, \tag{2.17}$$

then let $\Psi(t)$ be the diagonal matrix

$$\Psi(t) = e^{(t-t_0)A} \tag{2.18}$$

so that $\Psi' = A\Psi$. Now define

$$\psi_k(t) = \Psi(t)e_k = e^{(t-t_0)\mu_k} e_k \tag{2.19}$$

for $t \geqslant t_0$, where e_k is the k-th standard basis vector.

Now we split $\Psi = \Psi_1 + \Psi_2$ where the matrix Ψ_1 consists of those columns of Ψ that have index j such that Re $(\mu_k - \mu_j) > 0$ and Ψ_2 has columns with Re $(\mu_k - \mu_j) \leqslant 0$. We see that both Ψ_1 and Ψ_2 are diagonal and satisfy $\Psi_i' = A\Psi_i$. We now consider the equation

$$\begin{aligned} \varphi(t) = \psi_k(t) &+ \int_{t_0}^{t} \Psi_1(t)\Psi^{-1}(\tau)R(\tau)\varphi(\tau)\, d\tau \\ &- \int_{t}^{\infty} \Psi_2(t)\Psi^{-1}(\tau)R(\tau)\varphi(\tau)\, d\tau. \end{aligned} \tag{2.20}$$

If this equation has a solution, then we see that it will satisfy

$$\varphi' = (A + R(t))\varphi.$$

We solve (2.20) by the usual iterative methods; define $\varphi^0(t) = 0$ and recursively define

$$\begin{aligned} \varphi^{j+1}(t) = \psi_k(t) &+ \int_{t_0}^{t} \Psi_1(t)\Psi^{-1}(\tau)R(\tau)\varphi^j(\tau)\, d\tau \\ &- \int_{t}^{\infty} \Psi_2(t)\Psi^{-1}(\tau)R(\tau)\varphi^j(\tau)\, d\tau. \end{aligned} \tag{2.21}$$

Hence we see that $\varphi^1(t) = \psi_k(t)$ and

$$|\varphi^1(t) - \varphi^0(t)| = \left| e^{(t-t_0)\mathrm{Re}\ \mu_k} \right|. \tag{2.22}$$

The matrix $\Psi_1(t)\Psi^{-1}(\tau)$ is diagonal and has entries that are either zero, or are of form $h_l(t) = e^{(t-\tau)\mu_l}$ when Re $(\mu_k - \mu_l) > 0$. Hence $|h_l(t)| \leqslant e^{(t-\tau)\mathrm{Re}\ \mu_k}$ for $\tau < t$, and we thus obtain

$$|\Psi_1(t)\Psi^{-1}(\tau)R(\tau)| \leqslant |R(\tau)|\, e^{(t-\tau)\mathrm{Re}\ \mu_k} \tag{2.23}$$

on $\tau < t$. Similarly, we obtain

$$|\Psi_2(t)\Psi^{-1}(\tau)R(\tau)| \leqslant |R(\tau)|\, e^{(t-\tau)\mathrm{Re}\ \mu_k} \tag{2.24}$$

for $\tau > t$. Using these inequalities in (2.21) gives

$$|\varphi^{j+1}(t) - \varphi^j(t)|e^{(t_0-t)\mathrm{Re}\ \mu_k} \leqslant \int_{t_0}^{\infty} e^{(t_0-\tau)\mathrm{Re}\ \mu_k}|R(\tau)|\left|\varphi^j(\tau) - \varphi^{j-1}(\tau)\right| d\tau \tag{2.25}$$

and we see by induction from (2.22) and (2.17) that

$$|\varphi^{j+1}(t) - \varphi^j(t)| \leqslant \left(\frac{1}{2}\right)^j e^{(t-t_0)\mathrm{Re}\ \mu_k}, \tag{2.26}$$

which gives uniform convergence of $\{\varphi^j\}$ on any finite subinterval of $[t_0, \infty)$ to a continuous function φ that solves (2.20).

We now consider the asymptotic behaviour of this solution. From the iterative definition of φ we see that

$$|\varphi(t)| \leqslant 2e^{(t-t_0)\mathrm{Re}\ \mu_k}. \tag{2.27}$$

From this and (2.24) we obtain

$$\lim_{t\to 0} e^{(t_0-t)\mathrm{Re}\ \mu_k} \int_t^{\infty} \Psi_2(t)\Psi^{-1}(\tau)R(\tau)\varphi(\tau)\, d\tau = 0. \tag{2.28}$$

The definition of Ψ_1 gives

$$\lim_{t\to\infty} |\Psi_1(t)|\, e^{(t_0-t)\mathrm{Re}\ \mu_k} = 0. \tag{2.29}$$

For any $\epsilon > 0$, we can choose t_1 so that

$$\int_{t_1}^{\infty} |R(\tau)|\, d\tau < \frac{\epsilon}{2}$$

and we can then write

$$\left| e^{(t_0-t)\mathrm{Re}\ \mu_k} \int_{t_0}^{t} \Psi_1(t)\Psi^{-1}(\tau)R(\tau)\varphi(\tau)\, d\tau \right| \leqslant \epsilon + e^{(t_0-t)\mathrm{Re}\ \mu_k} |\Psi_1(t)| \int_{t_0}^{t_1} |\Psi^{-1}(\tau)R(\tau)\varphi(\tau)|\, d\tau$$

(where we have used (2.23)). As $t \to \infty$, it follows from (2.29) that

$$\lim_{t\to\infty} \sup \left| e^{(t_0-t)\mathrm{Re}\ \mu_k} \int_{t_0}^{t} \Psi_1(t)\Psi^{-1}(\tau)R(\tau)\varphi(\tau)\, d\tau \right| \leqslant \epsilon$$

and as ϵ was arbitrary, we have

$$\lim_{t\to\infty} e^{(t_0-t)\mathrm{Re}\ \mu_k} \int_{t_0}^{t} \Psi_1(t)\Psi^{-1}(\tau)R(\tau)\varphi(\tau)\, d\tau = 0. \tag{2.30}$$

Together, (2.28) and (2.30) give

$$\lim_{t\to\infty} \left[\varphi(t) e^{(t_0-t)\mu_k} - e_k \right] = 0 \tag{2.31}$$

as required (taking $\varphi_k = \varphi$). □

We now take $A = D_0$ and $R(t) = A_\Gamma(t) - D_0$, and to satisfy the hypotheses of the theorem we only need verify that

$$\int_0^{\infty} |A_\Gamma(t) - D_0|\, dt < \infty. \tag{2.32}$$

We know that

$$\begin{aligned} A_\Gamma(t) - D_0 &= Df(x^H(t);0) - Df(0;0) \\ &= D^2 f(0;0).x^H(t) + \mathcal{O}\big((x^H(t))^2\big) \end{aligned} \tag{2.33}$$

and that as $t \to \infty$, $x^H(t) \to 0$ in a manner

$$x^H(t) \sim e^{tD_0}\beta^H = \mathcal{O}\Big(\langle \beta^H, e^S\rangle e^{-\lambda^S t}\Big),$$

since $\beta^H_U = 0$. Hence $A_\Gamma(t) - D_0 = \mathcal{O}\Big(e^{-\lambda^S t}\Big)$ as $t \to \infty$, and the integral (2.32) is finite, as required. Application of Theorem 2.1.4 then tells us that there are solutions φ_k of $\dot{x} = (A + R(t))x$, that is, solutions of $\dot{x} = A_\Gamma(t)x$ with

$$\lim_{t\to\infty} \varphi_k(t)e^{-\mu_k t} = e_k e^{-\mu_k t_0}.$$

Such solutions must be linearly independent, and as $Y(t)$ was a fundamental matrix for $\dot{y} = A_\Gamma y$, we have shown that as $t \to \infty$, the heteroclinic matrix $H(t) = e^{-tD_0}Y(t) \to e^{-t_0 D_0}C$ for some constant matrix C.

The equivalent result as $t \to -\infty$ is produced in the same manner, showing that the integral

$$\int_0^\infty |D_0 - A_\Gamma(-t)|\, dt < \infty,$$

since $\alpha^H_S = 0$ gives

$$x^H(t) \sim e^{-tD_0}\alpha^H = \mathcal{O}\Big(e^{-\lambda^U t}\Big).$$

Notice also that the form of the heteroclinic matrix $H(-\infty)$ will be an invertible matrix (corresponding to change of basis to the φ_k's) multiplied by a diagonal matrix $e^{t_0 D_0}$, which is thus invertible.

We now let $M_0 = H(\infty)H^{-1}(-\infty)$. Then a solution of (2.14) with $y(t_0) = y_0$ can be written:

$$y(t) = Y(t)Y^{-1}(t_0)y_0 + Y(t)\int_{t_0}^t Y^{-1}(s)\left[G(s, y(s)) + \mu\frac{\partial f}{\partial \mu}(x^H(s); 0)\right] ds. \quad (2.34)$$

We now assume that the time of transit between Σ' and Σ is $t_U + t_S + \gamma$ (for some small γ) and put $t_0 = -t_U$ and $t = t_S + \gamma$ in equation (2.34), so that an initial

point on Σ' with α as in (2.6) gets mapped to a point x_0' on Σ with β' given by (2.6). Then, transforming to $y = x - x^H$, we have:

$$\begin{aligned}\beta' - \beta^H &= e^{\gamma D_0} H(t_S+\gamma) H^{-1}(-t_U)(\alpha - \alpha^H) \\ &\quad + e^{\gamma D_0} H(t_S+\gamma) \int_{-t_U}^{t_S+\gamma} H^{-1}(s) e^{-sD_0} \left[G + \mu \frac{\partial f}{\partial \mu}(x^H;0) \right] ds.\end{aligned} \tag{2.35}$$

We will restrict our attention to trajectories that remain within a neighbourhood of Γ of size ϵ; therefore $y = \mathcal{O}(\epsilon)$ and thus the ϵ dependence of the first term in the integral is

$$\int_{-t_U}^{t_S+\gamma} H^{-1}(s) e^{-sD_0} G(s, y(s))\, ds \sim \mathcal{O}\big(\epsilon^2\big). \tag{2.36}$$

We now wish to estimate the size of the second term in the integral (2.35). Since $f(x;\mu) = Dx + g(x;\mu)$, we put

$$\begin{aligned}\frac{\partial f}{\partial \mu}(x^H(t);0) &= \left.\frac{\partial D}{\partial \mu}\right|_{\mu=0} x^H(t) + \frac{\partial g}{\partial \mu}(x^H(t);0) \\ &= D_0' x^H(t) + \mathcal{O}\big((x^H(t))^2\big)\end{aligned} \tag{2.37}$$

and the second integral term becomes

$$\int_{-t_U}^{t_S+\gamma} \mu H^{-1}(s) e^{-sD_0} D_0' x^H(s)\, ds + \int_{-t_U}^{t_S+\gamma} \mu H^{-1}(s) e^{-sD_0} g_\mu(x^H(s);0)\, ds. \tag{2.38}$$

For both of these terms, we may split the range of integration into $(-t_U, -T] \cup (-T, T) \cup [T, t_S+\gamma)$ for large enough T, and use the asymptotic forms of $H(s)$ and x^H on the $(-t_U, -T]$ and $[T, t_S+\gamma)$ ranges. This shows that the first term is of size $\mu\mathcal{O}(t_U + t_S + \mathcal{O}(1))$, and the second term is of size $\mu\mathcal{O}(1) + \mu \exp[-\mathcal{O}(t_S, t_U)]$. Hence, overall the second term in the integral in (2.35) is of size $\mu\mathcal{O}(t_S + t_U + \mathcal{O}(1))$.

We know that $H(t)$ tends to a constant matrix as $t \to \pm\infty$. As $\nu \to 0$, we have that t_U and t_S tend to infinity in a manner $t_U, t_S \sim \log(1/\nu)$. Moreover, we can see that $t_S + \gamma$ must also tend to infinity as $\nu \to 0$, so we may write

$$H(t_S+\gamma) H^{-1}(-t_U) = M_0(I + o(1)) \qquad \text{as } \nu \to 0. \tag{2.39}$$

Finally, we Taylor expand γ as a function of y and μ, to give

$$\gamma(y,\mu) = (d\gamma)_{0,0}y + \mu\frac{\partial\gamma}{\partial\mu}(0,0) + \mathcal{O}\big(\mu y, y^2\big) \tag{2.40}$$

(where $(d\gamma)_{0,0}$ is the Jacobian matrix of the derivative of γ with respect to y evaluated at $y=0$, $\mu=0$) using the fact that $\gamma(0,0)=0$, by definition of t_S, t_U. As $y=\mathcal{O}(\epsilon)$, this gives $\gamma=\mathcal{O}(\epsilon,\mu)$ so that $e^{\gamma D_0} = I + \mathcal{O}(\epsilon)$ (presuming that $\mu \ll \epsilon$) for the pre-factor of the right hand side of (2.35).

Putting all this together, we find that we may write (2.35) as:

$$\beta' - \beta^H = M(\alpha - \alpha^H) + \mu c + \mathcal{O}(\epsilon) \tag{2.41}$$

where $c = \mathcal{O}(t_S + t_U + \mathcal{O}(1))$ and $M = H(t_S + \gamma|_{\mu=0})H^{-1}(-t_U) = M_0(1+o(1))$ as $\nu \to 0$. Thus, for fixed ν, for a specified μ value we must have

$$\epsilon \ll \mu \log \nu.$$

There may be potential problems in the order of these choices of parameters; however, we ignore them in the present work.

The composition of (2.41) with (2.8) thus defines our Poincaré map. This Poincaré map is of the standard form for analysis of homoclinic systems—a linear flow near the origin composed with an affine map near the homoclinic orbit. Depending on the eigenvalues of the matrix D_0, we may use the Poincaré map to prove equivalent results for higher dimensions. What is different in this formulation of the analysis is the scaling (2.6) of coordinates by the expansion and contraction rates in the linearized flow near to the fixed point at the origin.

2.2 Geometry of the Invariant Set

We have the approximate Poincaré map given by (2.41) and (2.8):

$$\alpha = e^{PD}\beta, \tag{2.42}$$

$$\beta' - \beta^H = M(\alpha - \alpha^H) + \mu c. \tag{2.43}$$

We know that P is large for small μ and ν. A neighbourhood of α^H in Σ' of size ϵ will be mapped by the affine map of equation (2.43) to a neighbourhood of β^H in Σ of size ϵ (provided $\mu \lesssim \epsilon$). Because of the stretching in the unstable components under the linearized flow near the origin, that portion of this neighbourhood of β^H that can be mapped back to the original neighbourhood of α^H must have an unstable component near the surface:

$$\beta_U = e^{-PD_U}\alpha_U^H. \tag{2.44}$$

Under the inside map φ, Σ is mapped to $\varphi(\Sigma)$, all of whose points must have a stable component near to the surface:

$$\alpha_S = e^{PD_S}\beta_S^H. \tag{2.45}$$

Note that both of these surfaces are one-dimensional, since we have free choice of the coordinate in the e^U and e^S directions respectively. This corresponds to varying the value of P in equation (2.45), and is illustrated in Figure 2.2.

Now we let:

$$\Lambda_0 = \{\beta \in \Sigma : \beta_U = e^{-PD_U}\alpha_U^H\},$$

$$\Sigma_0 = \{\beta \in \Sigma : \left|\beta_U - e^{-PD_U}\alpha_U^H\right| < \epsilon\},$$

$$\Lambda_0' = \{\alpha \in \Sigma' : \alpha_S = e^{PD_S}\beta_S^H\},$$

$$\Sigma_0' = \{\alpha \in \Sigma' : \left|\alpha_S - e^{PD_S}\beta_S^H\right| < \epsilon\}.$$

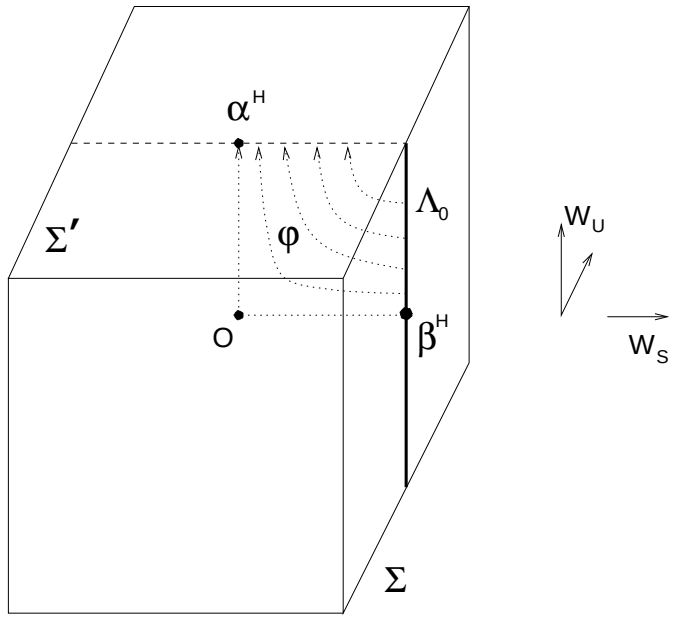

Figure 2.2 Schematic showing Λ_0 in the case that $n = 3$, $k = 2$.

Then Λ_0 is $(n-k)$-dimensional—one component in $\Sigma_U = \Sigma \cap W_U$, and $(n-k-1)$ components in $\Sigma_S = \Sigma \cap W_S$. Similarly, Λ_0' is k-dimensional with one component in $\Sigma_S' = \Sigma' \cap W_S$ and $(k-1)$ components in $\Sigma_U' = \Sigma' \cap W_U$. Now, both Σ_0 and Σ_0' are actually the $(n-1)$ dimensional sets that form the domains of φ and φ', but are close to the $(n-k)$-dimensional and k-dimensional sets Λ_0 and Λ_0' respectively. We thus refer to Σ_0 as "quasi-$(n-k)$-dimensional" and Σ_0' as "quasi-k-dimensional".

We now see that Λ_0 has codimension $k-1$ as a subset of the $(n-1)$-dimensional surface Σ, and similarly Λ_0' has codimension $n-k-1$ as a subset of Σ'. If we assume that φ' has no zero eigenvalues, then $\varphi'(\Lambda_0')$ also has codimension $n-k-1$ as a subset of Σ. Hence, by the transversality theorem (Guckenheimer & Holmes [1983] §3.1) we would expect $\Lambda_1 = \varphi'(\Lambda_0') \cap \Lambda_0$ to have codimension $n-2$ as a subset of Σ, and hence to be of dimension one. This gives a geometrical insight

into the method used in the next section to reduce the fixed point behaviour of the Poincaré map to a one-dimensional map in P.

We now attempt to justify some of the approximations involved. Suppose we have $\beta \in \Sigma$ such that $\varphi(\beta) = \alpha \in \Sigma'$ and $\varphi'(\alpha) = \beta'$. Then (2.42) implies that:

$$\begin{aligned} \beta_U &= e^{-PD_U}\alpha_U, \\ \alpha_S &= e^{PD_S}\beta_S. \end{aligned} \tag{2.46}$$

We now define

$$a_U = \alpha_U - \alpha_U^H, \quad b_S = \beta_S - \beta_S^H \tag{2.47}$$

so that we have

$$\begin{aligned} \beta_U &= e^{-PD_U}(\alpha_U^H + a_U), \\ \alpha_S &= e^{PD_S}(\beta_S^H + b_S). \end{aligned} \tag{2.48}$$

Hence we now convert our representation of points $\beta \in \Sigma$ to a representation in terms of P, a_U, and b_S. Firstly, note that since $\beta \in \Sigma$ we have $|\langle \beta, e^S \rangle| = 1$, which gives $\langle b_S, e^S \rangle = 0$ and similarly $|\langle \alpha, e^U \rangle| = 1$ implies that $\langle a_U, e^U \rangle = 0$. Hence b_S has $(n-k-1)$ independent components, and a_U has $(k-1)$ independent components, and together with the one component of P this gives $(n-1)$ components—enough to represent the $(n-1)$-dimensional hypersurface Σ.

So, given $\beta \in \Sigma$, we obtain its representation in terms of P, a_U, and b_S by:

$$\begin{aligned} \left|\langle (e^{PD_U}\beta_U, 0)^T, e^U \rangle\right| &= 1, \\ a_U &= e^{PD_U}\beta_U - \alpha_U^H, \\ b_S &= \beta_S - \beta_S^H \end{aligned}$$

so that $P = P(\beta)$, $a_U = a_U(\beta)$ and $b_S = b_S(\beta)$ are analytic everywhere that the map φ is defined. This map is not defined for those $\beta \in \Sigma$ such that the linear

flow does not carry them to Σ', which are those points with $\langle \beta_U, e^U \rangle = 0$. Given (P, a_U, b_S) we obtain the equivalent β from:

$$\beta_U = e^{-PD_U}(a_U + \alpha_U^H),$$
$$\beta_S = \beta_S^H + b_S$$

and we see that $\beta = \beta(P, a_U, b_S)$ is analytic. Now we express the Poincaré map $Y = \varphi' \circ \varphi$ in terms of this new representation. We have $Y(b_S, a_U, P) = (b_S', a_U', P')$ such that, if we write:

$$M = \begin{pmatrix} M_{UU} & M_{US} \\ M_{SU} & M_{SS} \end{pmatrix} \tag{2.49}$$

we have

$$b_S' = M_{SU} a_U + M_{SS} e^{PD_S}(\beta_S^H + b_S) + \mu c_S \tag{2.50}$$

and

$$e^{-P'D_U}(\alpha_U^H + a_U') = M_{UU} a_U + M_{US} e^{PD_S}(\beta_S^H + b_S) + \mu c_U, \tag{2.51}$$

and P' is given by the condition that points must actually return to Σ, that is $|\langle \beta', e^U \rangle| = 1$, which in the new representation is

$$\left| \left\langle (e^{P'D_U}[M_{UU} a_U + M_{US} e^{PD_S}(\beta_S^H + b_S) + \mu c_U], 0)^T, e^U \right\rangle \right| = 1. \tag{2.52}$$

We now consider $\dot{x}^H(t)$. Since $x^H(t)$ solves $\dot{x} = f(x, 0)$, then taking the derivative with respect to time gives $\ddot{x}^H(t) = Df(x^H, 0)\dot{x}^H$ and hence we see that $\dot{x}^H(t)$ solves

$$\dot{y}(t) = Df(x^H(t), 0)y(t) = A_\Gamma(t)y(t)$$

exactly. Now,

$$x^H \sim \begin{cases} e^{tD_0}\alpha^H & \text{as } t \to -\infty \\ e^{tD_0}\beta^H & \text{as } t \to +\infty \end{cases} \qquad \Rightarrow \qquad \dot{x}^H \sim \begin{cases} e^{tD_0} D_0 \alpha^H & \text{as } t \to -\infty \\ e^{tD_0} D_0 \beta^H & \text{as } t \to +\infty \end{cases}$$

We may now repeat the construction of the affine map (2.34) but with μ set to zero and with no error term $G(t, y)$. We then find $\dot{x}^H(t) = Y(t)Y^{-1}(t_0)\dot{x}^H(t_0)$. As we let $t \to \infty$ and $t_0 \to -\infty$ this gives

$$e^{tD_0} D_0 \beta^H = Y(t)Y^{-1}(t_0) e^{t_0 D_0} D_0 \alpha^H,$$

which by the definition (2.15) of H gives $D_0\beta^H = H(t)H^{-1}(t_0)D_0\alpha^H$. Taking the limit, we have $D_0\beta^H = MD_0\alpha^H$, that is:

$$D_0 \begin{pmatrix} 0 \\ \beta_S^H \end{pmatrix} = \begin{pmatrix} M_{UU} & M_{US} \\ M_{SU} & M_{SS} \end{pmatrix} \begin{pmatrix} D_{0_U}\alpha_U^H \\ 0 \end{pmatrix} = \begin{pmatrix} M_{UU} D_{0_U}\alpha_U^H \\ M_{SU} D_{0_U}\alpha_U^H \end{pmatrix}. \tag{2.53}$$

Hence $M_{UU} D_{0_U}\alpha_U^H = 0$ and as D_0 is hyperbolic, $D_{0_U}\alpha_U^H \neq 0$ and is thus a zero eigenvector of M_{UU}, so that rank $M_{UU} \leqslant k-1$. We will assume that rank $M_{UU} = k-1$ as the most generic case, since a lower rank implies the existence of further homoclinic orbits. This topic will be dealt with in the countably infinite dimensional case, together with its relationship to symmetry properties.

Now let η be the unique zero eigenvector of the adjoint of M_{UU}. Then, by (2.51), we have:

$$\langle \eta, e^{-P'D_U}\alpha_U^H \rangle = \langle \eta, M_{US} e^{PD_S}\beta_S^H \rangle + \langle \eta, \mu c_U \rangle + \langle \eta, M_{US} e^{PD_S} b_S - e^{-P'D_U} a_U' \rangle \tag{2.54}$$

in which the last term is small.

2.3 A One-Dimensional Map

We now write the Poincaré map given by (2.50), (2.51) and (2.54) in the form:

$$\begin{aligned}
\langle \eta, e^{-P' D_U} \alpha_U^H \rangle &= \langle \eta, M_{US} e^{P D_S} \beta_S^H \rangle + \langle \eta, \mu c_U \rangle + \varphi_1(P, P', a'_U, b_S), \\
a_U &= M_{UU}^{\perp -1} \left[e^{-P' D_U} \alpha_U^H - M_{US} e^{P D_S} \beta_S^H - \mu c_U \right] \\
&\quad + \varphi_2(P, P', a'_U, b_S) + \lambda D_{0_U} \alpha_U^H, \\
b'_S &= M_{SU} a_U + M_{SS} e^{P D_S} \beta_S^H + \mu c_S + \varphi_3(P, b_S)
\end{aligned} \tag{2.55}$$

where:

$$\begin{aligned}
\varphi_1(P, P', a'_U, b_S) &= \langle \eta, M_{US} e^{P D_S} b_S - e^{-P' D_U} a'_U \rangle, \\
\varphi_2(P, P', a'_U, b_S) &= M_{UU}^{\perp -1} \left[e^{-P' D_U} a'_U - M_{US} e^{P D_S} b_S \right], \\
\varphi_3(a_U, P, b_S) &= M_{SS} e^{P D_S} b_S
\end{aligned}$$

and where $M_{UU}^{\perp -1}$ is the inverse of M_{UU} on the space orthogonal to the zero eigenvector $D_U \alpha_U^H$, leaving the arbitrary component $\lambda D_U \alpha_U^H$ in the direction of the zero eigenvector. We may then determine λ from the condition $\langle a_U, e^U \rangle = 0$.

Here we have converted the Poincaré map $(P, a_U, b_S) \mapsto (P', a'_U, b'_S)$ to a mixed map $(P, a'_U, b_S) \mapsto (P', a_U, b'_S)$. This device should be compared to the mixed initial condition integral equation used in Shil'nikov [1967a] and Gaspard [1984b]. This conversion will not affect our search for fixed points of the map; however, it allows us to convert the expanding direction of the behaviour near the origin to a contracting direction, making the estimation of sizes of terms much simpler.

Equation (2.55) is defined in a neighbourhood of $a_U = 0 = b_S, P = \infty$; consider the specific neighbourhood $|a'_U| \lesssim \epsilon$, $|b_S| \lesssim \epsilon$, $|e^{-\sigma_m P}| \lesssim \epsilon$ where σ_m is the magnitude of the real part of the eigenvalue of D closest to zero. Then, taking $\mu \lesssim \epsilon$,

we have:

$$\varphi_1 = \mathcal{O}\big(\epsilon^2\big) + \mathcal{O}\Big(\epsilon e^{-P' D_U}\Big),$$
$$\varphi_2 = \mathcal{O}\big(\epsilon^2\big) + \mathcal{O}\Big(\epsilon e^{-P' D_U}\Big),$$
$$\varphi_3 = \mathcal{O}\big(\epsilon^2\big).$$

Equation $(2.55)_1$ then gives:

$$\langle \eta, e^{-P' D_U} \alpha_U^H \rangle = \mathcal{O}(\epsilon) + \mathcal{O}(\mu) + \mathcal{O}\big(\epsilon^2\big) + \mathcal{O}\Big(\epsilon e^{-P' D_U}\Big).$$

Hence we have $|e^{-\sigma_m P'}| = \mathcal{O}(\epsilon)$, giving:

$$\varphi_1 = \mathcal{O}\big(\epsilon^2\big), \qquad \varphi_2 = \mathcal{O}\big(\epsilon^2\big), \qquad \varphi_3 = \mathcal{O}\big(\epsilon^2\big).$$

Now consider the one-dimensional map $P \mapsto P'$ given by:

$$\langle \eta, e^{-P' D_U} \alpha_U^H \rangle = \langle \eta, M_{US} e^{P D_S} \beta_S^H \rangle + \langle \eta, \mu c_U \rangle. \tag{2.56}$$

If we have a fixed point $\widetilde{P}$ of this map (with $|e^{-\sigma_m \widetilde{P}}| \lesssim \epsilon$), then we define from it:

$$\widetilde{a}_U = M_{UU}^{\perp^{-1}} \left[e^{-\widetilde{P} D_U} \alpha_U^H - M_{US} e^{\widetilde{P} D_S} \beta_S^H - \mu c_U \right] + \widetilde{\lambda} D_U \alpha_U^H \tag{2.57}$$

with $\widetilde{\lambda}$ given by $\langle \widetilde{a}_U, e^U \rangle = 0$, and

$$\widetilde{b}_S = M_{SU} \widetilde{a}_U + M_{SS} e^{\widetilde{P} D_S} \beta_S^H + \mu c_S. \tag{2.58}$$

These are both of size $\mathcal{O}(\epsilon)$, hence we have a fixed point $(\widetilde{P}, \widetilde{a}_U, \widetilde{b}_S)$ of the Poincaré map (2.55) to within $\mathcal{O}\big(\epsilon^2\big)$. This argument may be made more precise by appealing to the implicit function theorem.

We now see that we have a one-dimensional map (2.56) that gives the behaviour of fixed points of the mixed map (2.55) under parameter changes. Fixed points of the mixed map are still fixed points of the original Poincaré map (2.42), (2.43) and thus correspond to periodic orbits of the flow, whose periods are thus governed by our one-dimensional map (2.56).

2.4 Applications

We now consider in turn each of the three possible cases mentioned in Chapter 1 for the eigenvalues of the linearization near the origin.

There are three generic cases for the two eigenvalues with real parts closest to zero, namely

$$\begin{aligned} &1)\ \sigma^U = \lambda^U, \sigma^S = -\lambda^S && \text{(saddle)} \\ &2)\ \sigma^U = \lambda^U, \sigma^S = -\lambda^S \pm i\omega^S && \text{(saddle-focus)} \\ &3)\ \sigma^U = \lambda^U \pm i\omega^U, \sigma^S = -\lambda^S \pm i\omega^S && \text{(bifocal)} \end{aligned}$$

and we note that the fourth possible case may be obtained by time reversal. We consider each of these cases in turn.

1) Saddle Case

Define $\xi = e^{-\lambda^U P}$ so that (2.56) can be approximately rescaled to

$$\xi' = a\xi^\delta + \mu, \tag{2.59}$$

where $\delta = \lambda^S/\lambda^U$. For $\xi > 0$, this has the form of the map derived for the Lorenz equations (Lorenz [1963], Sparrow [1982]). Equation (2.59) has a unique fixed point (for $\xi \ll 1$, $\mu \ll 1$), corresponding to the principal periodic orbit, on one side of $\mu = 0$, which is such that if $\delta > 1$ then $\xi \approx \mu$ and if $\delta < 1$ then $\xi \approx (-\mu/a)^{1/\delta}$. In either case, we have

$$\mu \sim e^{-\lambda_m P}$$

where $\lambda_m = \min\{\lambda^S, \lambda^U\}$, and this agrees with the result in Shil'nikov [1968].

2) Saddle-Focus Case

Taking $\sigma^U = \lambda^U$, $\sigma^S = -\lambda^S \pm i\omega^S$ (by time reversal if necessary), we approximate and rescale (2.56) to

$$e^{-\lambda^U P'} = ae^{-\lambda^S P}\cos(\omega^S P) + \mu \tag{2.60}$$

or

$$\xi' = a\,\xi^\delta \cos(\Omega \log \xi) + \mu, \tag{2.61}$$

with $\Omega = \omega^S/\lambda^U$ and ξ, δ as above. This map has the same form as the one-dimensional map derived in Arneodo *et al* [1985].

If $\delta > 1$, then equation (2.61) has a unique fixed point (for small ξ, μ) on one side of $\mu = 0$ with $\mu \sim e^{-\lambda_m P}$, as in the saddle case. However, when $\delta < 1$, there are multiple fixed points given by

$$\mu \sim \xi^\delta \cos(\Omega \log \xi). \tag{2.62}$$

As $\mu \to 0$, the period of the principal periodic orbit is thus given by

$$\mu \sim e^{-\lambda^S P}\cos\omega^S P, \tag{2.63}$$

giving Figure 2.3 which agrees with the results of Glendinning & Sparrow [1984], §3.1. The number of roots of (2.62) is given by $N \sim (\Omega/\pi)\log(1/\mu)$ as $\mu \to 0$, which gives the result of Shil'nikov [1965].

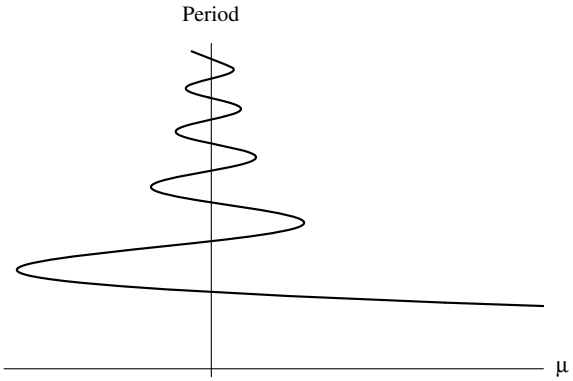

Figure 2.3 Principal periodic orbit in saddle-focus case

3) Bifocal Case

Similarly to above, approximation and rescaling of (2.56) yields

$$e^{-\lambda^U P'} \cos \omega^U P' = a e^{-\lambda^S P} \cos(\omega^S P + \theta) + \mu. \tag{2.64}$$

If we suppose that $\lambda^S < \lambda^U$, then fixed points corresponding to the principal periodic orbit have

$$\mu \sim e^{-\lambda^S P} \cos \omega^S P, \tag{2.65}$$

which gives behaviour as for the saddle-focus case. Equivalently, if $\lambda^U < \lambda^S$ then the principal periodic orbit has period satisfying

$$\mu \sim e^{-\lambda^U P} \cos \omega^U P. \tag{2.66}$$

2.5 Summary

In this chapter, we have derived a general method for analysing homoclinic bifurcations in ordinary differential equations. As has been the standard method since the first work in the subject, we constructed a Poincaré map on a surface near to the origin by splitting the flow into two sections. Near to the origin, we had near-linear behaviour, and we found error bounds on the difference between the linearized flow and the exact flow. Composed with this was the affine behaviour away from the origin, where the flow is linearized about the homoclinic orbit. Again, we maintained error estimates of the difference between the exact return map and the affine map.

Throughout the chapter, we have used the slightly unusual methods of representation introduced by Fowler [1990a]. These use the asymptotic behaviour of the homoclinic orbit to parameterize points by the time P taken for them to return to the Poincaré surface. The geometrical reasoning behind this representation was explained in Section 3.2, and involves the requirement that trajectories remain close to the homoclinic orbit.

The alternative representation allows us to see the map as having $(k-1)$ expanding directions, $(n-k-1)$ contracting directions and one other direction parameterized by the return time. By converting the return map $(P, a_U, b_S) \mapsto (P', a'_U, b'_S)$ into a mixed map $(P, a'_U, b_S) \mapsto (P', a_U, b'_S)$ we then created a map with $(n-2)$ contracting directions, and thus reduced the question of existence of fixed points of the Poincaré map to that of existence of fixed points of a one-dimensional map by using the implicit function theorem. From this one-dimensional map, we were able to reproduce the results of previous work that for sufficiently small μ, a periodic orbit of the flow always exists on at least one side of $\mu = 0$, and also to

predict that the behaviour of the period of this principal periodic orbit as $\mu \to 0$ is

$$\mu \sim e^{-\lambda_m P} \cos \omega_m P, \tag{2.67}$$

where $\lambda_m = \min\{\lambda^U, \lambda^S\}$, as has been found in previous work on each of the specific cases in low dimensions.

3 Homoclinic Bifurcations in Infinite Dimensions

In this chapter, we extend previous work by Fowler [1990b] on homoclinic bifurcations for partial differential equations on unbounded domains to vector-valued partial differential equations with symmetry. A finite-dimensional map of dimension equal to the number of independent symmetries of the system is derived, which map governs the bifurcation structure of periodic orbits of the system.

Other approaches to the problem of homoclinic bifurcations in partial differential equations have been considered by Blázquez [1986] and Chow & Deng [1989], in certain particular cases.

We will again utilize the standard methods of attack for homoclinic bifurcation problems. This consists of the construction of a Poincaré map on a surface near to the fixed point which is the α- and ω-limit of the homoclinic orbit. The map has two components—near the fixed point, the system may be approximated by the linearized behaviour. Away from the fixed point, the flow is taken to generate an affine map, for points sufficiently close to the homoclinic orbit and for parameter values sufficiently close to that at which the homoclinic orbit exists. Various aspects of behaviour are then deduced from this Poincaré map.

In the previous chapter, we saw that for ordinary differential equations this Poincaré map may be reduced to a one-dimensional map governing the asymptotic behaviour of periodic orbits of the system. We note that the generation of this one-dimensional map was related to the existence of an exact solution of the linearized equation, and this solution existed because of the time translation invariance of the system.

A previous paper by Fowler [1990b] attempted to extend formally this framework of analysis of homoclinic systems to scalar partial differential equations in one unbounded space variable, which were assumed to be space and time translation invariant. In this work, a Poincaré map was constructed in an analogous fashion to the finite dimensional case. The two translation invariances of the system gave two exact solutions of the linearized problem, which in turn led to a reduction of the Poincaré map to a two-dimensional map.

In this chapter, we extend this work to vector-valued PDEs, and moreover we deal with equations with an arbitrary number q of symmetries. In specific cases in Chapter 1, we found that the presence of discrete symmetries led to added complexity in the behaviours associated with the homoclinic bifurcations, although we could not deal with this generically. In this chapter, we will find that continuous groups of symmetries can be considered in a general context, and moreover we will find that these symmetries then lead to q exact solutions of the linearized problem, and to a q-dimensional map.

We will construct a Poincaré map on a surface near the origin in two parts, as before. Near to the origin (which is assumed to be our fixed point) we will have the flow governed by the linearization of the system, and solutions can be easily expressed in terms of Fourier transforms. Away from the origin, we will again only consider solutions remaining close to the homoclinic orbit and consider the linearization of the flow about this solution. The situation is made more complicated by the existence of symmetry properties; if we have q point symmetries of the system, we will have a q-parameter family of homoclinic orbits. We will pick one specific homoclinic orbit, so that for each orbit of the system that remains close to a representative of the family of homoclinic orbits, we will

have to take into account the symmetry shift required to make that orbit close to our specific homoclinic orbit on return to the Poincaré surface.

We consider a nonlinear PDE in one unbounded space dimension, for an n-dimensional vector-valued function $A(x,t) \in \mathbb{R}^n$ satisfying:

$$\frac{\partial A}{\partial t} = N[\partial_x](A;\mu) \tag{3.1}$$

where N is an autonomous differential operator. We will make the following assumptions:

1) the zero vector is a solution for all μ, that is $N(0;\mu) = 0$.
2) equation (3.1) is invariant under time and space translation, so that it has two one-parameter symmetry groups spanned by the vector fields ∂_t and ∂_x (see for example Olver [1986]) .
3) equation (3.1) is also invariant under $q-2$ additional one-parameter symmetries spanned by the vector fields $\mathbf{v}_3, \ldots, \mathbf{v}_q$. Furthermore, we assume that if these infinitesimal symmetries take $(x,t,A) \mapsto (\widetilde{x},\widetilde{t},\widetilde{A})$ then:
   a) each symmetry is *projectable*, that is $(\widetilde{x},\widetilde{t}) = \Xi(x,t)$ does not involve the dependent variables A.
   b) each symmetry does not transform time, that is $\widetilde{t} = t$.
4) at $\mu = 0$, there exists a q-parameter family of homoclinic orbits associated to the zero solution, generated by the q symmetries mentioned above.

We now pick one particular representative $A^H(x,t)$ of this family of homoclinic orbits, and we assume that the homoclinic orbit is localized, that is $A^H \to 0$ as $x \to \pm\infty$.

3.1 Derivation of a Poincaré Map

We denote the Fréchet derivative (Hutson & Pym [1980] §4.4) of the nonlinear operator N evaluated at the zero solution by $\mathcal{L}[0]$, and we then find that the solutions of the linearized problem are given by

$$A(x,t) = \int_{\mathbb{R}} e^{ikx} e^{S(k)t} f(k)\, dk, \tag{3.2}$$

where f is a complex vector-valued function given by:

$$f(k) = \frac{1}{2\pi} \mathcal{F}[A(x,0)](k) \tag{3.3}$$

and $\mathcal{F}[A(x)](k) = \int A(x) e^{-ikx}\, dx$ is the n-dimensional Fourier transform of A. The $n \times n$-dimensional dispersion relation matrix $S(k)$ is given by

$$S(k) = e^{-ikx} \mathcal{L}[0](e^{ikx} I), \tag{3.4}$$

which is independent of x by the space translation invariance of the system. Moreover, we will assume that a change of variables has been performed in order to diagonalize the matrix $S(k) = \mathrm{diag}\{\sigma_1(k), \ldots \sigma_n(k)\}$. We also define

$$U_j = \{k \in \mathbb{R} : \mathrm{Re}\ \sigma_j(k) > 0\},$$

$$S_j = \{k \in \mathbb{R} : \mathrm{Re}\ \sigma_j(k) < 0\},$$

so that if $k \in U_j$ then $e^{\sigma_j(k)t} \to 0$ as $t \to -\infty$ and if $k \in S_j$ then $e^{\sigma_j(k)t} \to 0$ as $t \to \infty$.

As $t \to \pm\infty$, $A^H \to 0$ and so approximately satisfies $A_t = \mathcal{L}[0]A$; hence we expect that there will exist complex vector-valued functions $\alpha^H(k)$ and $\beta^H(k)$ such that:

$$\begin{aligned} A^H &\sim \int_{\mathbb{R}} e^{ikx} e^{S(k)t} \alpha^H(k)\, dk \qquad \text{as} \quad t \to -\infty, \\ A^H &\sim \int_{\mathbb{R}} e^{ikx} e^{S(k)t} \beta^H(k)\, dk \qquad \text{as} \quad t \to +\infty \end{aligned} \tag{3.5}$$

and since $A^H \to 0$ as $t \to \pm\infty$, we have $\alpha_j^H(k) = 0$ for $k \in S_j$, $\beta_j^H(k) = 0$ for $k \in U_j$.

To construct our Poincaré map, we consider the surface of a ball $B = \{A(x) : \|A(x)\| = \nu\}$ about the origin, and make ν small enough so that $A^H(x,t)$ intersects B exactly twice—at $t = -t_U$ and $t = t_S$. We note that $t_U, t_S \to \infty$ as $\nu \to 0$. Recall that assumptions 2) and 3) tell us that the PDE we are studying has symmetries spanned by the q vector fields

$$\mathbf{v}_1 = \partial_t, \mathbf{v}_2 = \partial_x, \mathbf{v}_3, \ldots, \mathbf{v}_q.$$

If we suppose that the j-th symmetry sends a solution $A(x,t)$ of (3.1) to a new solution written as $G_j(\epsilon)(A(x,t))$, and we write:

$$G(\epsilon)(A(x,t)) = G_2(\epsilon_2)(\ldots G_q(\epsilon_q)(A(x,t))\ldots) \qquad \epsilon = (\epsilon_2, \ldots, \epsilon_q),$$

where we keep ϵ_1 separate, as it is the only symmetry involving time (by assumption 3b)). Moreover, we denote by $g(\epsilon)$ the induced transformation of the Fourier transform,

$$g(\epsilon)(\mathcal{F}[A(x,t)](k)) = \mathcal{F}[G(\epsilon)(A(x,t))](k). \tag{3.6}$$

For example, for the space translation symmetry generated by $\mathbf{v}_2 = \partial_x$, given by $G_2(\epsilon_2)(A(x,t)) = A(x+\epsilon_2, t)$, we find that this induces the transformation $g_2(\epsilon_2)(f(k)) = e^{ik\epsilon_2} If(k)$ in the Fourier transform.

We now specify our Poincaré surfaces Σ and Σ' by:

$$\begin{aligned} \Sigma &= \{A(x) \in B : \exists \epsilon \quad \|G(\epsilon)(A(x)) - A^H(x, t_S)\| \leqslant \delta\}, \\ \Sigma' &= \{A(x) \in B : \exists \epsilon \quad \|G(\epsilon)(A(x)) - A^H(x, -t_U)\| \leqslant \delta\}, \end{aligned} \tag{3.7}$$

where we choose the size ν of the ball B to be small enough that $\Sigma \cap \Sigma' = \emptyset$. For general $A(x)$ on Σ or Σ', we define complex vector-valued functions $\beta(k)$ and

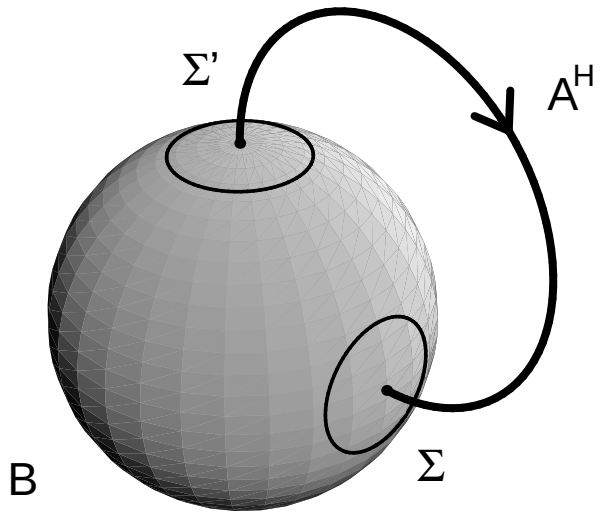

Figure 3.1 Schematic representation of the flow

$\alpha(k)$ respectively by:

$$\begin{aligned} A(x) &= \int_{\mathbb{R}} e^{ikx} e^{S(k)t_S} \beta(k)\, dk \qquad \text{on } \Sigma, \\ A(x) &= \int_{\mathbb{R}} e^{ikx} e^{-S(k)t_U} \alpha(k)\, dk \qquad \text{on } \Sigma'. \end{aligned} \tag{3.8}$$

In other words, we define:

$$\begin{aligned} \alpha(k) &= \frac{1}{2\pi} e^{S(k)t_U} \mathcal{F}[A](k) \qquad \text{for } A(x) \in \Sigma', \\ \beta(k) &= \frac{1}{2\pi} e^{-S(k)t_S} \mathcal{F}[A](k) \qquad \text{for } A(x) \in \Sigma, \end{aligned}$$

to give a representation of functions on Σ and Σ' in terms of scaled Fourier transforms.

Within the ball B, A satisfies $A_t = \mathcal{L}[0]A + g(A)$, where $g(A) = N(A;\mu) - \mathcal{L}[0]A$ is quadratic. Neglecting $g(A)$, we have an approximate solution

$$\alpha(k) = e^{S(k)P} \beta(k), \tag{3.9}$$

where $P = \widetilde{t} + t_U + t_S$, and $\widetilde{t}$ is the transit time between Σ and Σ', that is, P is given by the condition that we map onto Σ'.

For the return map, we consider solutions that remain close to the homoclinic orbit. A solution $A(x,t)$ is close to the homoclinic orbit if some symmetry transform of it is close to the homoclinic orbit; given such a solution, we change the origin of time (which sets ϵ_1), and then take values of the other symmetry parameters $\epsilon_2, \ldots, \epsilon_q$ (which may be non-unique) so that $G(\epsilon)(A(x,-t_U)) \in \Sigma'$ and so as to minimize $\|G(\epsilon)(A(x,-t_U)) - A^H(x,-t_U)\|$. Now we write

$$v(x,t) = G(\epsilon)(A(x,t)) - A^H(x,t)$$

so that $v(x,t)$ satisfies

$$v_t = \mathcal{L}[A^H]v + h(A^H, v) \tag{3.10}$$

where

$$h(A^H, v) = N(A^H + v; \mu) - N(A^H; 0) - \mathcal{L}[A^H]v \tag{3.11}$$

and $\mathcal{L}[A^H]$ is the Fréchet derivative of N at A^H and $\mu = 0$.

If we consider the fundamental solution $T(t,t_0)$ generated by the equation $v_t = \mathcal{L}[A^H]v$, which is an operator satisfying:

$$\begin{aligned} \frac{\partial T}{\partial t} &= \mathcal{L}[A^H]T \qquad t > t_0, \\ T(t_0,t_0) &= I, \end{aligned} \tag{3.12}$$

then the solution of the inhomogeneous equation (3.10) satisfies

$$v(x,t) = T(t,t_0)(v(x,t_0)) + \int_{t_0}^{t} T(t,\tau)(h(A^H(x,\tau), v(x,\tau)))\, d\tau. \tag{3.13}$$

Notice that under the application of the symmetry $G(\epsilon)$ to A, α and β do not necessarily transform according to (3.6). We will write the equivalent transformations as $g^\alpha(\epsilon)$ and $g^\beta(\epsilon)$, that is:

$$g^\alpha(\epsilon)(\alpha(k)) = \frac{1}{2\pi} e^{S(k)t_U} g(\epsilon)(\mathcal{F}[A](k)),$$
$$g^\beta(\epsilon)(\beta(k)) = \frac{1}{2\pi} e^{-S(k)t_S} g(\epsilon)(\mathcal{F}[A](k)).$$

For $A(x,t) \in \Sigma'$, we have by definition of Σ' and (3.8) that

$$\left\| \int_{\mathbb{R}} \left(e^{ikx} e^{-S(k)t_U} g^\alpha(\epsilon)(\alpha(k)) - e^{ikx} e^{-S(k)t_U} \alpha^H(k) \right) dk \right\| \leqslant \delta.$$

This motivates us to write

$$\widehat{\alpha} = g^\alpha(\epsilon)(\alpha) - \alpha^H. \tag{3.14}$$

Similarly, if the flow maps $A(x,t)$ to a point on Σ given by $\beta'(k)$, we write

$$\widehat{\beta} = g^\beta(\epsilon)(\beta') - \beta^H. \tag{3.15}$$

So, given $A(x,t) \in \Sigma'$, we change the origin of time and perform symmetry operations so that

$$\begin{aligned} v(x,-t_U) &= \int_{\mathbb{R}} e^{ikx} e^{-S(k)t_U} \widehat{\alpha}(k)\, dk \qquad \text{on } \Sigma', \\ v(x,t_S) &\approx \int_{\mathbb{R}} e^{ikx} e^{S(k)t_S} \widehat{\beta}(k)\, dk \qquad \text{on } \Sigma, \end{aligned} \tag{3.16}$$

where the second equation is only approximate because, given that $v(x,-t_U) \in \Sigma'$, we can only say that $v(x,t)$ hits Σ at approximately $t = t_S$ (although we can make this as close as we like by reducing δ). Note also that this approximate statement can only be made if there has been no rescaling of time, as assured by assumption 3b).

We can now use (3.13) to connect these two expressions:

$$\begin{aligned}\int_{\mathbb{R}} e^{ikx} e^{S(k)t_S}\,\widehat{\beta}(k)\,dk = T(t_S,-t_U)\int_{\mathbb{R}} e^{ikx}e^{-S(k)t_U}\,\widehat{\alpha}(k)\,dk \\ + \int_{-t_U}^{t_S} T(t_S,\tau)(h(A^H(x,\tau),v(x,\tau)))\,dk.\end{aligned} \tag{3.17}$$

If we can define a Green's function for $v_t = \mathcal{L}[A^H]v$ by

$$\begin{aligned}\frac{\partial K}{\partial t} = \mathcal{L}[A^H]K \qquad K = K(x,s,t,t_0) \qquad t > t_0, \\ K(x,s,t_0,t_0) = \delta(x-s)I,\end{aligned} \tag{3.18}$$

with the semiflow T given by

$$T(t,t_0)(v(x)) = \int_{\mathbb{R}} K(x,s,t,t_0)v(s)\,ds \tag{3.19}$$

then (3.17) becomes

$$\begin{aligned}\int_{\mathbb{R}} e^{ikx}e^{S(k)t_S}\,\widehat{\beta}(k)\,dk = \int_{\mathbb{R}} K(x,s,t_S,-t_U)\int_{\mathbb{R}} e^{ilx}e^{-S(l)t_U}\,\widehat{\alpha}(l)\,dl\,ds \\ + \int_{-t_U}^{t_S}\int_{\mathbb{R}} K(x,s,t_S,\tau)h(A^H(s,\tau),v(s,\tau))\,ds\,d\tau\end{aligned} \tag{3.20}$$

in terms of the Green's function K given by (3.18).

Equation (3.13) also gives an expression for v at $t = 0$:

$$\begin{aligned}v(x,0) &= T(0,-t_U)v(x,-t_U) + \int_{-t_U}^{0} T(0,\tau)(h(A^H(x,\tau),v(x,\tau)))\,d\tau \\ &= \int_{\mathbb{R}} K(x,s,0,-t_U)\int_{\mathbb{R}} e^{ilx}e^{-S(l)t_U}\,\widehat{\alpha}(l)\,dl\,ds \\ &\quad + \int_{-t_U}^{0}\int_{\mathbb{R}} K(x,s,0,\tau)(h(A^H(s,\tau),v(s,\tau)))\,ds\,d\tau,\end{aligned} \tag{3.21}$$

and we may also write $v(x,t_S)$ in terms of this as

$$\begin{aligned}v(x,t_S) &= \int_{\mathbb{R}} e^{ikx}e^{S(k)t_S}\,\widehat{\beta}(k)\,dk \\ &= T(t_S,0)v(x,0) + \int_0^{t_S} T(t_S,\tau)(h(A^H(x,\tau),v(x,\tau)))\,d\tau \\ &= \int_{\mathbb{R}} K(x,u,t_S,0)v(u,0)\,du \\ &\quad + \int_0^{t_S}\int_{\mathbb{R}} K(x,s,t_S,\tau)h(A^H(s,\tau),v(s,\tau))\,ds\,d\tau\end{aligned} \tag{3.22}$$

which will enable us to use the asymptotic form of K deduced below.

The semigroup property of T gives an equivalent semigroup property for the Green's function K:

$$\int_{\mathbb{R}} K(x,u,t,\tau)K(u,s,\tau,t_0)\,du = K(x,s,t,t_0) \tag{3.23}$$

for $t_0 < \tau < t$. From this, we formally extend the definition of K to $t < \tau$ by taking

$$\int_{\mathbb{R}} K(x,u,t_0,t)K(u,s,t,t_0)\,du = \delta(x-s)I, \tag{3.24}$$

which is equivalent to defining T^{-1}, and can only be done on a restricted domain. With this extended definition of K, we can invert the expression (3.21) for $v(x,0)$ to give

$$\begin{aligned}\int_{\mathbb{R}} e^{ilx}e^{-S(l)t_U}\widehat{\alpha}(l)\,dl &= \int_{\mathbb{R}} K(x,u,-t_U,0)v(u,0)\,du \\ &\quad - \int_{\mathbb{R}}\int_{-t_U}^{0}\int_{\mathbb{R}} K(x,u,-t_U,0)K(u,s,0,\tau)h(A^H(s,\tau),v(s,\tau))\,ds\,d\tau\,du.\end{aligned} \tag{3.25}$$

We now wish to find an asymptotic form of K. Since K satisfies (3.18) then as $t \to \pm\infty$, $A^H(x,t) \to 0$ and $\mathcal{L}[A^H] \to \mathcal{L}[0]$. We have already considered the solutions of $v_t = \mathcal{L}[0]v$ in (3.2), so

$$K(x,s,t,T) \approx \int_{\mathbb{R}} e^{ikx}e^{S(k)t}\widetilde{F}_{\pm}(s,k)\,dk \tag{3.26}$$

for some matrix $\widetilde{F}_{\pm}(s,k)$, and for sufficiently large T and with $t_0 > T$. By using (3.3) we find that in fact

$$\widetilde{F}_{\pm}(s,k) = \frac{1}{2\pi}e^{-iks}I. \tag{3.27}$$

Using the semigroup property (3.23) we find that

$$K(x,s,t,0) \approx \int_{\mathbb{R}}\int_{\mathbb{R}} e^{ikx}e^{S(k)t}\widetilde{F}_{\pm}(u,k)K(u,s,T,0)\,dk\,du$$

as $t \to \pm\infty$ so that we can write

$$K(x,s,t,0) \approx \int_{\mathbb{R}} e^{ikx} e^{S(k)t} F_{\pm}(s,k)\, dk \qquad \text{as } t \to \pm\infty, \tag{3.28}$$

where

$$F_{\pm}(s,k) = \frac{1}{2\pi} \int_{\mathbb{R}} e^{-iku} K(u,s,T,0)\, du. \tag{3.29}$$

From this, as $\nu \to 0$, we find $t_S, t_U \to \infty$, and hence (3.25) further inverts to

$$\begin{aligned} \widehat{\alpha}(k) = &\int_{\mathbb{R}} F_-(u,k) v(u,0)\, du \\ &- \int_{\mathbb{R}} \int_{-t_U}^{0} \int_{\mathbb{R}} F_-(u,k) K(u,s,0,\tau) h(A^H(s,\tau), v(s,\tau))\, ds\, d\tau\, du. \end{aligned} \tag{3.30}$$

If we now take $G_-(x,k)$ to be such that

$$\int G_-(x,k) F_-(s,k)\, dk = \delta(x-s) I \tag{3.31}$$

then we can re-invert (3.30) to

$$v(x,0) = \int_{\mathbb{R}} G_-(x,k) \widehat{\alpha}(k)\, dk + \int_{-t_U}^{0} \int_{\mathbb{R}} K(x,s,0,\tau) h(A^H(s,\tau), v(s,\tau))\, ds\, d\tau. \tag{3.32}$$

Comparing this expression to the original expression (3.21) we see that the net result of the inversion and re-inversion process is to have:

$$G_-(x,k) = \lim_{t_U \to \infty} \int_{\mathbb{R}} K(x,s,0,-t_U) e^{iks} e^{-S(k)t_U}\, ds.$$

We also use the semigroup property (3.23) of K and the asymptotic form (3.28) of K in (3.22) to obtain

$$\begin{aligned} \int_{\mathbb{R}} e^{ikx} e^{S(k)t_S} \widehat{\beta}(k)\, dk = &\int_{\mathbb{R}} \int_{\mathbb{R}} e^{ikx} e^{S(k)t_S} F_+(u,k) v(u,0)\, dk\, du \\ + &\int_0^{t_S} \int_{\mathbb{R}} \int_{\mathbb{R}} \int_{\mathbb{R}} e^{ikx} e^{S(k)t_S} F_+(u,k) K(u,s,0,\tau) h(A^H(s,\tau), v(s,\tau))\, dk\, du\, ds\, d\tau, \end{aligned} \tag{3.33}$$

which we invert to

$$\widehat{\beta}(k) = \int_{\mathbb{R}} F_+(u,k)v(u,0)\,du + \int_0^{t_S}\int_{\mathbb{R}}\int_{\mathbb{R}} F_+(u,k)K(u,s,0,\tau)h(A^H(s,\tau),v(s,\tau))\,du\,ds\,d\tau.$$

Finally, we substitute the expression (3.32) for $v(x,0)$ to give

$$\widehat{\beta}(k) = \int_{\mathbb{R}}\left[\int_{\mathbb{R}} F_+(u,k)G_-(u,l)\,du\right]\widehat{\alpha}(l)\,dl + I'(k) \tag{3.34}$$

where

$$I'(k) = \int_{-t_U}^{t_S}\int_{\mathbb{R}}\int_{\mathbb{R}} F_+(u,k)K(u,s,0,\tau)h(A^H(s,\tau),v(s,\tau))\,du\,ds\,d\tau, \tag{3.35}$$

and we will write

$$M(k,l) = \int_{\mathbb{R}} F_+(u,k)G_-(u,l)\,du. \tag{3.36}$$

We can expand I' as

$$I'(k) = I'(k)\big|_{\substack{\mu=0\\ \nu=0}} + \mu\frac{\partial I'}{\partial\mu}\bigg|_{\substack{\mu=0\\ \nu=0}} + \mathcal{O}\big(\nu,\nu\mu,\mu^2\big) \tag{3.37}$$

and then write

$$c(k) = \frac{\partial I'}{\partial\mu}\bigg|_{\substack{\mu=0\\ \nu=0}}.$$

Now, by the definition (3.11) of h, we find that

$$h(A^H,v)\big|_{\mu=0} = N(A^H+v,0) - N(A^H,0) - \mathcal{L}[A^H]v = \mathcal{O}\big(\|v\|^2\big),$$

where $v(x,t) = G(\epsilon)(A(x,t)) - A^H(x,t)$. By considering only those trajectories that remain within a distance ν of A^H, we may take $\|v\| = \mathcal{O}(\nu)$ and hence

$$h(A^H,v)\big|_{\substack{\mu=0\\ \nu=0}} = 0,$$

so that equation (3.37) above becomes

$$I'(k) = \mu c(k) + \mathcal{O}\big(\nu,\nu\mu,\mu^2\big). \tag{3.38}$$

We also note, from the definitions of h, F_+ (in (3.28)) and K (in (3.18)), that I' is independent of P and ϵ.

This leaves us with two technical questions to address. Firstly, is it actually possible to find a solution K of (3.18); that is, can we write T as (3.19)? Secondly, under what conditions can we formally extend the domain of $K(x, s, t, t_0)$ to $t < t_0$? These questions cannot be answered in the general case; however, we may indicate suitable properties of $\mathcal{L}[A^H]$ which will, for instance, guarantee existence of solutions of (3.18).

Suppose we have Hilbert spaces V and H, with V dense in H, and we define the bilinear operator

$$a(t; u, v) = \langle -\mathcal{L}[A^H]u, v\rangle \qquad u, v \in V$$

We can use, for example, Temam [1988] Thm. II.3.4 to prove the existence of a solution K of (3.18). Taking one column of K at a time, and denoting it $u(t)$, we seek solutions of

$$\frac{du(t)}{dt} + A(t)u(t) = 0 \qquad u(0) = u_0 \tag{3.39}$$

for $A(t) = -\mathcal{L}[A^H(t)]$, which is the first variation of (3.1). Provided $u_0 \in H$, then if

a) $t \mapsto a(t; u, v)$ is measurable,

b) $\exists M < \infty$ such that $|a(t; u, v)| \leqslant M\|u\|.\|v\|$ for almost all t, and

c) $\exists \alpha > 0$ such that $a(t; u, u) \geqslant \alpha\|u\|^2$ for almost all t (i.e. a is *coercive*),

then there is a unique solution $u(t)$ of equation (3.39)with

$$u(t) \in L^2(\mathbb{R}; V) \cap \mathcal{C}(\mathbb{R}; H),$$

$$u'(t) \in L^2(\mathbb{R}; V).$$

A suitable choice of spaces will often be $H = L^2(\mathbb{R}^2)$ and $V = H_0^m(\mathbb{R}^2)$. For the example of the complex Ginzburg-Landau equation studied in Chapter 6,

suitable choices of spaces turn out to be the complexified spaces $H = \mathbb{L}^2(\mathbb{R}^2)$ and $V = \mathbb{H}^1_0(\mathbb{R}^2)$; see Temam [1988] §IV.5.1.

The problem of backward uniqueness of solutions of (3.18) is more technical; we will in general have to restrict the domain in some way. We take the following lemma from Temam [1988] §III.6:

Lemma 3.1.1: Let H be a Hilbert space with norm $|\cdot|$, and let A be a linear positive self-adjoint operator in H, and denote $V = D(A^{1/2})$ equipped with the norm

$$\|v\| = \begin{cases} |A^{1/2}v| & \forall v \in D(A^{1/2}) \\ \{(Av, v)\}^{(1/2)} & \forall v \in D(A) \end{cases}$$

If we consider a function w

$$w \in L^\infty(0, T; V) \cap L^2(0, T; D(A))$$

that satisfies

$$\frac{dw(t)}{dt} + Aw(t) = h(t, w(t)) \qquad t \in (0, T), \tag{3.40}$$

where we have, for any w satisfying equation (3.40),

$$|h(t, w(t))| \leqslant k(t)\|w(t)\| \quad \text{for a.e.} \quad t \in (0, T) \tag{3.41}$$

with $k \in L^2(0, T)$, then if

$$w(T) = 0$$

then

$$w(t) = 0 \qquad t \in [0, T].$$

If we have two solutions K_1 and K_2 of (3.18) that agree at time T, we now set

$$w = K_1(x, s, t, t_0) - K_2(x, s, t, t_0)$$

and we can see that the majorization conditions (3.40), (3.41) of the lemma are satisfied, since $\mathcal{L}[A^H]$ is a linear operator. Hence it will suffice to show, in individual cases, that

$$w = K_1(x,s,t,t_0) - K_2(x,s,t,t_0) \in L^\infty(0,T;V) \cap L^2(0,T;D(A)).$$

3.2 A Finite-Dimensional Map

We have our approximate Poincaré map given by

$$\begin{aligned} \alpha(k) &= e^{S(k)P}\beta(k), \\ g^\beta(\epsilon)(\beta'(k)) - \beta^H(k) &= \int_{\mathbb{R}} M(k,l)\left[g^\alpha(\epsilon)(\alpha(l)) - \alpha^H(l)\right]\, dl + \mu c(k). \end{aligned} \tag{3.42}$$

We will now concentrate on the latter of these two equations, and change variables by writing

$$\begin{aligned} A(k) &= g^\alpha(\epsilon)(\alpha(k)), & B(k) &= g^\beta(\epsilon)(\beta(k)), \\ a_U(k) &= A_U(k) - \alpha_U^H(k), & b_S(k) &= B_S(k) - \beta_S^H(k), \end{aligned} \tag{3.43}$$

where a subscript S or U denotes that if $f(k) = (f_1(k), \ldots, f_n(k))$ then $f_U = (f_{U_1}, \ldots, f_{U_n})$ and $f_S = (f_{S_1}, \ldots, f_{S_n})$ with

$$f_{U_j}(k) = \begin{cases} f_j(k) & \text{if } k \in U_j \\ 0 & \text{if } k \in S_j \end{cases} \qquad f_{S_j}(k) = \begin{cases} 0 & \text{if } k \in U_j \\ f_j(k) & \text{if } k \in S_j \end{cases}$$

We then write $(3.42)_2$ as

$$\begin{aligned} \left[g^\beta(\epsilon)(\beta'(k))\right]_S - \beta_S^H(k) &= \int_U M_S(k,l)a_U(l)\, dl + \int_S M_S(k,l)A_S(l)\, dl + \mu c_S(k), \\ \left[g^\beta(\epsilon)(\beta'(k))\right]_U &= \int_U M_U(k,l)a_U(l)\, dl + \int_S M_U(k,l)A_S(l)\, dl + \mu c_U(k), \end{aligned} \tag{3.44}$$

where $(M_S(k,l))_{ij}$ and $(M_U(k,l))_{ij}$ are zero for $k \in U_i$ and $k \in S_i$ respectively. Define the operator $\mathcal{M}_{UU}$ by

$$\mathcal{M}_{UU} f(k) = \int_U M_U(k,l) f(l)\, dl,$$

so that the last part of equation (3.44) gives

$$\mathcal{M}_{UU} a_U(k) = \left[g^\beta(\epsilon)(\beta'(k))\right]_U - \left\{ \int_S M_U(k,l) A_S(l)\, dl + \mu c_U(k) \right\}. \tag{3.45}$$

We now turn to a consideration of the equation $u_t = \mathcal{L}[A^H]u$, and its behaviour under the symmetries of the original equation. For each of the q symmetries in turn, we consider

$$\begin{aligned} &\frac{\partial}{\partial t}\left(G_j(\epsilon_j)(A^H(x,t))\right) = N(G_j(\epsilon_j)(A^H(x,t))) \\ \Rightarrow &\frac{\partial}{\partial \epsilon_j}\frac{\partial}{\partial t}\left(G_j(\epsilon_j)(A^H(x,t))\right) = \mathcal{L}[G_j(\epsilon_j)(A^H(x,t))]\left(\frac{\partial}{\partial \epsilon_j}(G_j(\epsilon_j)(A^H(x,t)))\right), \end{aligned} \tag{3.46}$$

and by exchanging the order of derivatives and evaluating at $\epsilon_j = 0$ we find that $\partial_t v_j(x,t) = \mathcal{L}[A^H]v_j(x,t)$, where

$$v_j(x,t) = \left.\frac{\partial}{\partial \epsilon_j}\left(G_j(\epsilon_j)(A^H(x,t))\right)\right|_{\epsilon_j=0}. \tag{3.47}$$

From the asymptotic form (3.5) of A^H, we see that

$$\begin{aligned} v_j(x,t) &\sim \int_{\mathbb{R}} e^{ikx} e^{S(k)t} \left.\frac{\partial}{\partial \epsilon_j}\left(g_j^\alpha(\epsilon_j)(\alpha^H(k))\right)\right|_{\epsilon_j=0} dk \qquad \text{as } t \to -\infty, \\ v_j(x,t) &\sim \int_{\mathbb{R}} e^{ikx} e^{S(k)t} \left.\frac{\partial}{\partial \epsilon_j}\left(g_j^\beta(\epsilon_j)(\beta^H(k))\right)\right|_{\epsilon_j=0} dk \qquad \text{as } t \to \infty, \end{aligned}$$

so that we can take

$$\widehat{\alpha}(k) = \left.\frac{\partial}{\partial \epsilon_j}\left(g_j^\alpha(\epsilon_j)(\alpha^H(k))\right)\right|_{\epsilon_j=0} \qquad \widehat{\beta}(k) = \left.\frac{\partial}{\partial \epsilon_j}\left(g_j^\beta(\epsilon_j)(\beta^H(k))\right)\right|_{\epsilon_j=0}$$

in the expression (3.16) for the start and end of the external flow. We then obtain from the Poincaré map (3.42) with $I' = 0$ (as we are dealing with exact solutions) that $\widehat{\beta}(k) = \int M(k,l)\widehat{\alpha}(l)\,dl$, that is

$$\frac{\partial}{\partial\epsilon_j}\left(g_j^\beta(\epsilon_j)(\beta^H(k))\right)\Big|_{\epsilon_j=0} = \int_{\mathbb{R}} M(k,l)\ \frac{\partial}{\partial\epsilon_j}\left(g_j^\alpha(\epsilon_j)(\alpha^H(l))\right)\Big|_{\epsilon_j=0} dl. \tag{3.48}$$

We know that $\beta_U^H = 0$ and $\alpha_S^H = 0$; if we now consider only systems that have symmetries of form such that

$$\begin{aligned} \left[g_j^\alpha(\epsilon_j)(f(k))\right]_S &= g_j^\alpha(\epsilon_j)(f_S(k)), \qquad & \left[g_j^\alpha(\epsilon_j)(f(k))\right]_U &= g_j^\alpha(\epsilon_j)(f_U(k)), \\ \left[g_j^\beta(\epsilon_j)(f(k))\right]_S &= g_j^\beta(\epsilon_j)(f_S(k)), \qquad & \left[g_j^\beta(\epsilon_j)(f(k))\right]_U &= g_j^\beta(\epsilon_j)(f_U(k)), \end{aligned} \tag{3.49}$$

then we can split (3.48) to obtain:

$$\int_U M_U(k,l)\ \frac{\partial}{\partial\epsilon_j}\left(g_j^\alpha(\epsilon_j)(\alpha_U^H(l))\right)\Big|_{\epsilon_j=0} dl = 0. \tag{3.50}$$

By way of example, the space translation symmetry generated by ∂_x induces a transformation $g_2(\epsilon_2) = e^{ik\epsilon_2}I$, which certainly obeys (3.49). Moreover, the change of phase symmetry for complex scalar systems mentioned later also obeys (3.49).

As this holds for $j = 1,\ldots,q$, the operator $\mathcal{M}_{UU}$ has a null space of dimension at least q. We will assume, as the most generic case, that the null space has dimension exactly q, and we let $\eta_1,\ldots,\eta_q$ span the null space of the Hilbert adjoint operator $\mathcal{M}_{UU}^*$ (Kreyszig [1978] §3.9); then (3.45) can only be inverted if its right hand side is orthogonal to all the η_j. That is, we require

$$\begin{aligned} \int_U \left[g^\beta(\epsilon)(\beta'(k))\right]_U .\overline{\eta}_j(k)\,dk = &\int_U\int_S M_U(k,l)A_S(l).\overline{\eta}_j(k)\,dl\,dk \\ &+ \mu\int_U c_U(k).\overline{\eta}_j(k)\,dk \end{aligned} \tag{3.51}$$

for $j = 1, \ldots, q$. In this equation, we now write

$$\begin{aligned}\beta'(k) &= e^{-S(k)P'}\alpha'(k) = e^{-S(k)P'}g^{\alpha}(-\epsilon')(A'(k)),\\ A_S(k) &= [g^{\alpha}(\epsilon)(\alpha(k))]_S = \left[g^{\alpha}(\epsilon)\left(e^{S_S(k)P}\beta(k)\right)\right]_S\\ &= \left[g^{\alpha}(\epsilon)\left(e^{S_S(k)P}g^{\beta}(-\epsilon)(B(k))\right)\right]_S,\end{aligned}$$

and use (3.49) to give

$$\begin{aligned}\int_U g^{\beta}(\epsilon)\circ e^{-S_U(k)P'}I\circ g^{\alpha}(-\epsilon')(A'_U(k)).\overline{\eta}_j(k)\,dk &= \mu\int_U c_U(k).\overline{\eta}_j(k)\,dk\\ + \int_U\int_S M_U(k,l)\,g^{\alpha}(\epsilon)\circ e^{S_S(l)P}I\circ g^{\beta}(-\epsilon)(B_S(l)).\overline{\eta}_j(k)\,dl\,dk,&\end{aligned}$$

which we approximate by

$$\begin{aligned}\int_{k\in U} g^{\beta}(\epsilon)\circ e^{-S_U(k)P'}I\circ g^{\alpha}(-\epsilon')(\alpha^H_U(k)).\overline{\eta}_j(k)\,dk &= \mu\int_{k\in U} c_U(k).\overline{\eta}_j(k)\,dk\\ + \int_{k\in U}\int_{l\in S} M_U(k,l)\,g^{\alpha}(\epsilon)\circ e^{S_S(l)P}I\circ g^{\beta}(-\epsilon)(\beta^H_S(l)).\overline{\eta}_j(k)\,dk\,dl&\end{aligned} \tag{3.52}$$

for $j = 1, \ldots, q$. This has the form of a finite-dimensional map from (P, ϵ) to (P', ϵ'); this is analogous to the one-dimensional map derived in the previous chapter for homoclinic bifurcations in ordinary differential equations.

We can now seek solutions of this finite dimensional map with $P = P'$; given such a solution, and under the assumption that a_U and b_S are small, then we may approximately define a_U from (3.45) together with the condition of return to Σ. From this, we can then approximately define b_S from $(3.44)_1$, and we have an approximate fixed point of the full Poincaré map and hence a (quasi-)periodic orbit of the full system. Examples of specific cases of this map are given and explored in detail in the next chapter.

3.3 Summary

In this chapter we have attempted to extend the methods of previous work on homoclinic bifurcations in ordinary differential equations to a class of partial differential equations in one space dimension of form

$$\frac{\partial A}{\partial t} = N[\partial_x](A;\mu),$$

for a n-dimensional vector-valued function $A(x,t)$, where N is an autonomous differential operator. We have assumed that the equation is invariant under space and time translation, together with $(q-2)$ other one-parameter symmetries. Under the assumption that this system admits a homoclinic orbit, we produced a Poincaré map in two parts. This map was defined on neighbourhoods of the intersections of the homoclinic orbit with a ball of size ν around the origin.

Based on the standard procedure for ordinary differential equations (as in Glendinning & Sparrow [1984], Wiggins [1988], Fowler [1990a]) and following the method of Fowler [1990b], this Poincaré map consisted of the composition of a near-linear part close to the origin, and a map close to the homoclinic orbit for the return part. This return part of the Poincaré map was considerably more complicated to produce than in the case of ordinary differential equations, involving several stages of construction and some further assumptions, most notably the restriction of the domain of the Poincaré map to those functions for which the inverse flow is defined.

We have used a Fourier transform representation of functions in this chapter which enables us to see more clearly the dependence of the Poincaré map on the return time P; moreover, we have made explicit the dependence on the values of the

symmetry parameters $\epsilon_2, \ldots, \epsilon_q$ that transform a function as close as possible to the homoclinic orbit. In a similar manner to the derivation of a one-dimensional map in Fowler [1990a], we have used this to derive a finite-dimensional map, (3.52), relating the values of P and $\epsilon_2, \ldots, \epsilon_q$ between successive visits to the Poincaré surface. In the next chapter, we will examine particular examples of this finite-dimensional map, relating to real and complex equations with minimal symmetries, and in Chapter 6 we will explore the form of this map for the complex Ginzburg-Landau equation.

4 Finite-Dimensional Map Behaviour

In the current chapter we examine in more detail the finite-dimensional map (3.52) derived at the end of the previous chapter. In the first section, we consider the form of the map for real or complex scalar partial differential equations. In this case, we find that we can approximate the map and provide a simpler form of (3.52).

In the second section, we consider two particular cases of this new finite-dimensional map. The first case is the simplest possible example, and the second case is only slightly more complicated. In both cases, we discuss the behaviour of the finite-dimensional map considered purely as a map, in isolation from any considerations of application to the PDE systems it may be derived from. In doing this, we discover a varied array of bifurcation behaviours in the first case, and an even richer set of possible behaviours in the second case.

4.1 Scalar PDEs

For a real scalar PDE with just the symmetries spanned by ∂_t, ∂_x we find that $g_2^\alpha(\epsilon_2) = g_2^\beta(\epsilon_2) = g_2(\epsilon_2) = e^{ik\epsilon_2} I$ and hence (3.52) becomes

$$\begin{aligned}\int_{k\in U} e^{ikQ} e^{-S_U(k)P'} e^{-ikQ'} \alpha_U^H(k)\overline{\eta}_j(k)\,dk = \mu \int_{k\in U} c_U(k)\overline{\eta}_j(k)\,dk \\ + \int_{k\in U}\int_{l\in S} M_U(k,l)\, e^{S_S(l)P} \beta_S^H(l)\overline{\eta}_j(k)\,dk\,dl\end{aligned} \tag{4.1}$$

for $j = 1, 2$, where we have written $Q = \epsilon_2$. Note that in this case $S(k) = e^{-ikx}\mathcal{L}[0]e^{ikx}$.

If we have a complex scalar PDE, converted into two vector (u, v) form, with symmetries generated by $\partial_t, \partial_x, u\partial_v - v\partial_u$ (where the last of these generates the change of phase symmetry $A(x,t) \mapsto e^{i\epsilon_3}A(x,t)$), then we find the extra symmetry gives $g_3(\epsilon_3) = e^{i\epsilon_3}I$ and hence (3.52) is now

$$\begin{aligned}\int_{k\in U} e^{ikQ+i\theta}e^{-S_U(k)P'}e^{-ikQ'-i\theta'}\alpha_U^H(k).\overline{\eta}_j(k)\,dk = \mu\int_{k\in U} c_U(k).\overline{\eta}_j(k)\,dk \\ + \int_{k\in U}\int_{l\in S} M_U(k,l)\,e^{S_S(l)P}\beta_S^H(l).\overline{\eta}_j(k)\,dk\,dl\end{aligned} \tag{4.2}$$

for $j = 1, 2, 3$, where we have written $\theta = \epsilon_3$. Since this 2-vector equation is originally derived from a complex equation, we find that

$$\begin{pmatrix}\alpha_1^H\\ \alpha_2^H\end{pmatrix} = \begin{pmatrix}\alpha_c^H\\ i\,\overline{\alpha}_c^H\end{pmatrix}, \qquad e^{S(k)t} = e^{\mathrm{Re}\ \sigma(k)t}\begin{pmatrix}\cos\omega(k)t & -\sin\omega(k)t\\ \sin\omega(k)t & \cos\omega(k)t\end{pmatrix}$$

for $\omega(k) = \mathrm{Im}\ \sigma(k)$, $\sigma(k) = e^{-ikx}\mathcal{L}[0]e^{ikx}$. Hence we can write equation (4.2) in complex form as

$$\begin{aligned}\int_{k\in U} e^{-\sigma_U(k)P'-ik(Q'-Q)-i(\theta'-\theta)}\alpha_U^H(k)\overline{\eta}_j(k)\,dk = \mu\int_{k\in U} c_U(k)\overline{\eta}_j(k)\,dk \\ + \int_{k\in U}\int_{l\in S} M_U(k,l)\,e^{\sigma_S(l)P}\beta_S^H(l)\overline{\eta}_j(k)\,dk\,dl\end{aligned} \tag{4.3}$$

for $j = 1, 2, 3$.

In either of the real or complex scalar cases, we may write thus the finite-dimensional map (3.52) as

$$\int_{k\in U} e^{-\sigma_U(k)P'-ik(Q'-Q)-i(\theta'-\theta)}w_j(k)\,dk = \int_{l\in S} e^{\sigma_S(l)P}y_j(l)\,dl + \mu, \tag{4.4}$$

where $j = 1, 2$ in the real case (and also the θ terms disappear) and $j = 1, 2, 3$ in the complex case, and where

$$\begin{aligned}w_j(k) &= \frac{\alpha_U^H(k)\overline{\eta}_j(k)}{\int_U c_U(l)\overline{\eta}_j(l)\,dl},\\ y_j(l) &= \frac{\beta_S^H(l)\int_U M_U(k,l)\overline{\eta}_j(k)\,dk}{\int_U c_U(k)\overline{\eta}_j(k)\,dk}.\end{aligned} \tag{4.5}$$

As we are dealing with a homoclinic system at $\mu = 0$, we expect to encounter periodic orbits of high period. Hence we will consider asymptotic behaviour as $P \to \infty$; we use the method of steepest descents to approximate the integrals in (4.4) (Carrier *et al* [1966] §6.2, Bender & Orszag [1978] §6.6). This method relies heavily on Watson's Lemma:

Lemma 4.1.1: Consider

$$f(P) = \int_0^T e^{-Pt} t^\lambda g(t)\, dt$$

for $\lambda > -1$ and where $g(t)$ is such that there exist constants C, b such that $|g(t)| < Ce^{bt}$ for $t \in (0, T)$. Suppose also that

$$g(t) = \sum_{i=0}^{m} a_i t^i + R_{m+1}(t), \qquad |R_{m+1}(t)| < Dt^{m+1}$$

for $t \in (0, A)$, with D a constant. Then as $P \to \infty$ we have

$$f(P) \sim \sum_{i=0}^{m} a_i \frac{\Gamma(\lambda + 1 + i)}{P^{\lambda+1+i}} + \mathcal{O}\left(\frac{1}{P^{\lambda+m+2}}\right). \tag{4.6}$$

We will assume that Re $\sigma(k)$ changes sign at zeros $k_1 < k_2 < \ldots < k_N$, so that U and S consist of the union of segments (k_m, k_{m+1}), which we split further into $(k_m, \widetilde{k}) \cup (\widetilde{k}, k_{m+1})$. We expect that the main contributions to each of the integrals in (4.4) will be from the neighbourhoods of the points k_m, where $e^{-\sigma_U(k)P'}$ or $e^{\sigma_S(l)P}$ are largest. Moreover, we will assume that $\sigma'(k_m) \neq 0$ for $m = 1, \ldots, N$ as the most general case.

For the right hand side of (4.4), considering one segment $l \in (k_m, \widetilde{k})$, we deform this into a contour C in the complex l plane on which Im $(\sigma_S(l)P)$ is constant

near to the start k_m of the contour. Thus for the first part of this contour, Im $[\sigma_S(k_m) - \sigma_S(l)] = 0$ and thus we may parameterize the first part of the contour by $u = \sigma_S(k_m) - \sigma_S(l)$ and write it as

$$\int_{k_m}^{\widetilde{k}} e^{\sigma_S(l)P} y_j(l)\, dl = e^{\sigma_S(k_m)P} \int_{u=0}^{u=T} e^{-uP} y_j(l(u)) \frac{dl}{du}\, du + R. \tag{4.7}$$

We neglect the remainder term R, consisting as it does of contributions from the second part of the contour where $e^{\sigma_S(l)P}$ will be small.

We apply Watson's Lemma to this integral to obtain

$$\int_{k_m}^{\widetilde{k}} e^{\sigma_S(l)P} y_j(l)\, dl \sim e^{\sigma_S(k_m)P} \frac{y_j(k_m)}{-\sigma_S'(k_m)P} + \mathcal{O}\big(P^{-2}\big),$$

and then combine all of the contributions of this form to find that

$$\int_{l\in S} e^{\sigma_S(l)P} y_j(l)\, dl \sim \sum_m \pm \frac{y_j(k_m) e^{i\omega_m P}}{\sigma'(k_m)P} \qquad \text{as } P \to \infty, \tag{4.8}$$

where $\sigma(k_m) = i\omega_m$ and the upper sign is taken if $(k_m, k_{m+1}) \subset U$.

Similarly for the other integral in (4.4), we deform the contours into the complex k plane so that Im $(-\sigma_U(k)P')$ is constant, to obtain

$$\int_{k\in U} e^{-\sigma_U(k)P' - ik(Q'-Q) - i(\theta'-\theta)} w_j(k)\, dk \sim \sum_m \pm \frac{w_j(k_m) e^{-i\omega_m P' - ik_m L - i(\theta'-\theta)}}{\sigma'(k_m)P'} \tag{4.9}$$

as $P \to \infty$, where $L = Q' - Q$ and we take the upper sign if $(k_m, k_{m+1}) \subset U$. If we assume that there are no saddle point contributions to the integrals, then the map has the form

$$\sum_m \frac{c_{jm} e^{-i\omega_m P' - ik_m L - i(\theta'-\theta)}}{P'} = \sum_m \frac{d_{jm} e^{i\omega_m P}}{P} + \mu \tag{4.10}$$

for $j = 1, 2, 3$ in the complex case, and for $j = 1, 2$ with $\theta = \theta' = 0$ in the real case, where

$$d_{jm} = \pm \frac{y_j(k_m)}{\sigma'(k_m)}, \qquad c_{jm} = \pm \frac{w_j(k_m)}{\sigma'(k_m)}, \tag{4.11}$$

and the upper sign is taken if $(k_m, k_{m+1}) \subset U$.

4.2 Symmetric Quadratic Real Systems

If the system $A_t = N(A)$ is real, then $\sigma(k) = e^{-ikx}\mathcal{L}[0]e^{ikx}$, and by taking complex conjugates we find that roots of Re $\sigma(k) = 0$ occur in pairs $\pm k_m$ with corresponding frequency Im $\sigma(\pm k_m) = \pm\omega_m$.

We consider the case when the system is *symmetric*; this implies that $\langle\mathcal{L}[0]f, g\rangle = \langle f, \mathcal{L}[0]g\rangle$ for any f, g. Take $f = g = e^{ikx}$ on a suitably restricted domain to give

$$\begin{aligned} \langle\mathcal{L}[0]e^{ikx}, e^{ikx}\rangle &= \langle e^{ikx}, \mathcal{L}[0]e^{ikx}\rangle \\ \Rightarrow \quad \sigma(k)\langle e^{ikx}, e^{ikx}\rangle &= \overline{\sigma(k)}\langle e^{ikx}, e^{ikx}\rangle \\ \Rightarrow (\sigma(k) - \overline{\sigma(k)})\langle e^{ikx}, e^{ikx}\rangle &= 0. \end{aligned}$$

Hence $\sigma(k) \in \mathbb{R}$.

The simplest symmetric case is when the dispersion relation is quadratic, $\sigma(k) = C(k_0^2 - k^2)$, so that we have $k_m = \pm k_0$, $\omega_m = 0$. Returning to definitions in the previous chapter, we initially find from (3.8) that

$$\alpha^H(-k) = \overline{\alpha^H(k)}, \qquad \beta^H(-k) = \overline{\beta^H(k)}$$

and from (3.28) and (3.31) we obtain

$$F_+(s,-k) = \overline{F_+(s,k)}, \qquad F_-(s,-k) = \overline{F_-(s,k)},$$
$$G_-(x,-k) = \overline{G_-(x,k)}.$$

The definition (3.36) of M then gives $M(-k,-l) = \overline{M(k,l)}$, which in turn gives $\eta_j(-k) = \overline{\eta_j(k)}$, using the fact that U is symmetrical about 0. Thus from (4.5) we obtain

$$w_j(-k) = \overline{w_j(k)}.\left(\frac{\overline{K}_j}{K_j}\right), \qquad y_j(-k) = \overline{y_j(k)}.\left(\frac{\overline{K}_j}{K_j}\right),$$

where $K_j = \int_U c_U(l)\overline{\eta_j(l)}\,dl$. We find that $c_U(-l) = \overline{c_U(l)}$ and hence $K_j \in \mathbb{R}$, so we find $c_{j2} = \overline{c}_{j1}$, $d_{j2} = \overline{d}_{j1}$. We can then write (4.10) as

$$\begin{aligned} c_1\zeta + \overline{c}_1\overline{\zeta} &= \mu + \frac{d_1}{P}, \\ c_2\zeta + \overline{c}_2\overline{\zeta} &= \mu + \frac{d_2}{P} \end{aligned} \tag{4.12}$$

with $d_j \in \mathbb{R}$ and

$$\zeta = \frac{e^{-ik_0L}}{P'}.$$

We may solve this for ζ to obtain

$$\frac{e^{-ik_0L}}{P'} = \frac{A}{P} + \mu B \tag{4.13}$$

with

$$A = \frac{d_1\overline{c}_2 - d_2\overline{c}_1}{c_1\overline{c}_2 - c_2\overline{c}_1}, \qquad B = \frac{\overline{c}_2 - \overline{c}_1}{c_1\overline{c}_2 - c_2\overline{c}_1}.$$

Firstly, we consider the bifurcation behaviour of this map. In general, there will be no fixed point solutions with $P' = P$, $L = 0$; however, solutions with $P' = P$, $L \neq 0$ may exist. We see that $|A + \mu PB| = 1$ is the equivalent condition, which has solutions

$$\mu P = \frac{-(A\overline{B} + B\overline{A}) \pm \sqrt{4|B|^2 + (A\overline{B} - B\overline{A})^2}}{2|B|^2}. \tag{4.14}$$

This has a reality condition

$$|B| > |A_RB_I - A_IB_R|. \tag{4.15}$$

Note that if $|A| < 1$, then this reality condition is automatically satisfied. Returning to (4.14) for the form of the reality condition, we have

$$\begin{aligned} (4.15) \quad &\Leftrightarrow \qquad 4|B|^2 + (A\overline{B} - B\overline{A})^2 > 0 \\ &\Leftrightarrow \qquad 4|B|^2 + (A\overline{B} + B\overline{A})^2 > 4|A|^2|B|^2 \\ &\Leftrightarrow \qquad (A\overline{B} + B\overline{A})^2 > 4|B|^2\left(|A|^2 - 1\right), \end{aligned}$$

and we see that if $|A| < 1$, the right hand side is < 0, and the condition is satisfied.

Equation (4.14) has two solutions; if these are of the same sign, we will find solutions with positive P values only on one side of $\mu = 0$, and if they are of different sign, we find positive P solutions on both sides of $\mu = 0$. The solutions of (4.14) will have different signs if and only if

$$\begin{aligned} & (A\overline{B} + B\overline{A})^2 < 4|B|^2 + (A\overline{B} - B\overline{A})^2 \\ \Leftrightarrow \qquad & (A\overline{B} + B\overline{A})^2 - (A\overline{B} - B\overline{A})^2 < 4|B|^2 \\ \Leftrightarrow \qquad & 4AB\overline{AB} < 4|B|^2 \\ \Leftrightarrow \qquad & |A|^2 < 1. \end{aligned}$$

So the determining condition is that there will be solutions on both sides of $\mu = 0$ if and only if $|A| < 1$.

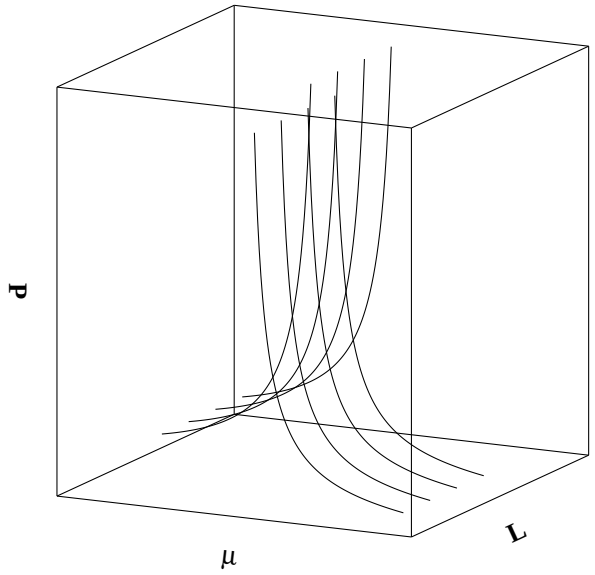

Figure 4.1 Bifurcation diagram for symmetric, quadratic, real scalar system, as described by (4.14) and equation (4.16), when there are solutions on both sides of $\mu = 0$, that is when $|A| < 1$.

Note that in either case, these solutions will thus have $P \sim 1/\mu$ as $\mu \to 0$. For such solutions P, we then obtain L from

$$L = \frac{2n\pi}{k_0} - \frac{1}{k_0}\arg(A + \mu PB), \tag{4.16}$$

which we note is constant since μP is constant. These solutions then correspond to modulated travelling waves moving with wave speed $L/P \sim 2\mu n\pi/k_0$.

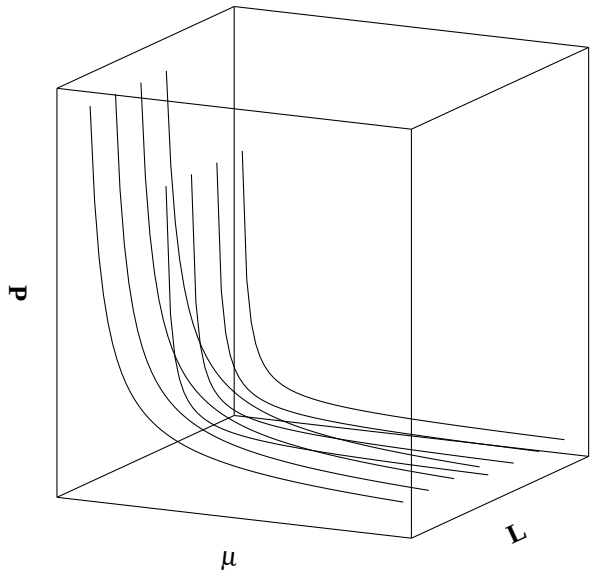

Figure 4.2 Bifurcation diagram for symmetric, quadratic, real scalar system, as described by (4.14) and (4.16), when there are solutions only on sides of $\mu = 0$, that is when $|A| > 1$.

We now explore the general behaviour of the finite-dimensional map (4.13), without any reference to the systems it is obtained from. We consider the map $P \mapsto P'$

which is given by

$$\begin{aligned} P' = f(P) &= \left| \frac{A}{P} + \mu B \right|^{-1} \\ &= \frac{|P|}{\sqrt{|A|^2 + \mu P(A\overline{B} + B\overline{A}) + \mu^2 P^2 |B|^2}} \end{aligned} \tag{4.17}$$

for $P > 0$. To fill in the details of the shape of this function, we firstly notice that as $P \to \infty$, we have $f(P) \to (1/|\mu B|)$ and $f'(P) \to 0$. Also, we can see that $f(0) = 0$ and that the slope at $P = 0$ is $f'(0) = 1/|A|$. If we now examine

$$f'(P) = \frac{2|A|^2 + \mu P(A\overline{B} + B\overline{A})}{2\left(|A|^2 + \mu P(A\overline{B} + B\overline{A}) + \mu^2 P^2 |B|^2\right)^{(3/2)}} \tag{4.18}$$

in order to look for local extrema, we find there will be exactly one local extremum, at

$$\widetilde{P} = \frac{-2|A|^2}{\mu c}, \tag{4.19}$$

where we have written

$$c = (A\overline{B} + B\overline{A}) = 2(A_R B_R + A_I B_I).$$

Another important factor is whether this extremum is above the line $P' = P$, that is, whether $|f(\widetilde{P})| > |\widetilde{P}|$? To examine this more closely, we find

$$\begin{aligned} |f(\widetilde{P})| = \frac{2|A|}{\mu\sqrt{4|A|^2|B|^2 - c^2}} &> |\widetilde{P}| = \frac{2|A|^2}{\mu|c|} \\ \Leftrightarrow \quad 4|A|^4|B|^2 &< c^2(1 + |A|^2) \quad (\text{for } \mu > 0). \end{aligned} \tag{4.20}$$

Taking these factors in order, we can deduce most of the shape of the function from:

1) Is the slope at 0 greater or less than one? That is, is $f'(0) = 1/|A|$ greater or less than one? If $|A| < 1$, the graph of $f(P)$ initially starts above the line $P' = P$; otherwise, it starts below.

2) Is the local extremum $\widetilde{P}$ in the range $[0, \infty)$? Whether it is or it is not, the other situation will hold if the sign of μ is changed.
3) Is the local extremum above the line $P' = P$? That is, does $f(\widetilde{P}) > \widetilde{P}$ hold?

However, these alternatives do not completely exhaust the possibilities. The graph of $f(P)$ may have inflexion points, and consequently cross the line $P' = P$. The condition for an inflexion point is that $f''(P) = 0$, in other words:

$$f''(P) = 0 = \frac{-\mu\left(4|A|^2 + 12|A|^2|B|^2\mu P + c^2\mu P + 4|B|^2 c\mu^2 P^2\right)}{4\left(|A|^2 + \mu c P + |B|^2\mu^2 P^2\right)^{(5/2)}}$$
$$\Leftrightarrow \qquad 4|B|^2 c\,(\mu P)^2 + (c^2 + 12|A|^2|B|^2)(\mu P) + 4c|A|^2 = 0.$$

Hence we see that there can be at most two inflexion points, and in general there will be either two or zero inflexion points. If there are a pair of inflexion points, and these inflexion points cause the graph of $f(P)$ to cross the line $P' = P$, this will generate two more solutions of $f(P) = P$.

If we assume that there are no inflexion points, then the different possibilities for 1) – 3) above generate the graphs shown in Figure 4.3. If we examine the number of solutions of $f(P) = P$ in each of these cases, we have Table 4.1.

In addition to this table, if we have a pair of inflexion points, we may add an additional two non-zero solutions of $f(P) = P$. However, we have previously shown that there at most two non-zero solutions of $f(P) = P$, and hence only the cases in the table with no solutions can have inflexion points that cause crossings of $P' = P$. These possibilities, namely that $|A| > 1, \widetilde{P} < 0$ or $|A| > 1, \widetilde{P} > 0, f(\widetilde{P}) < \widetilde{P}$, are shown in Figure 4.4.

We may also consider the possibility of the existence of periodic solutions of this finite-dimensional map. This is unfortunately quite subtle; if we seek solutions of

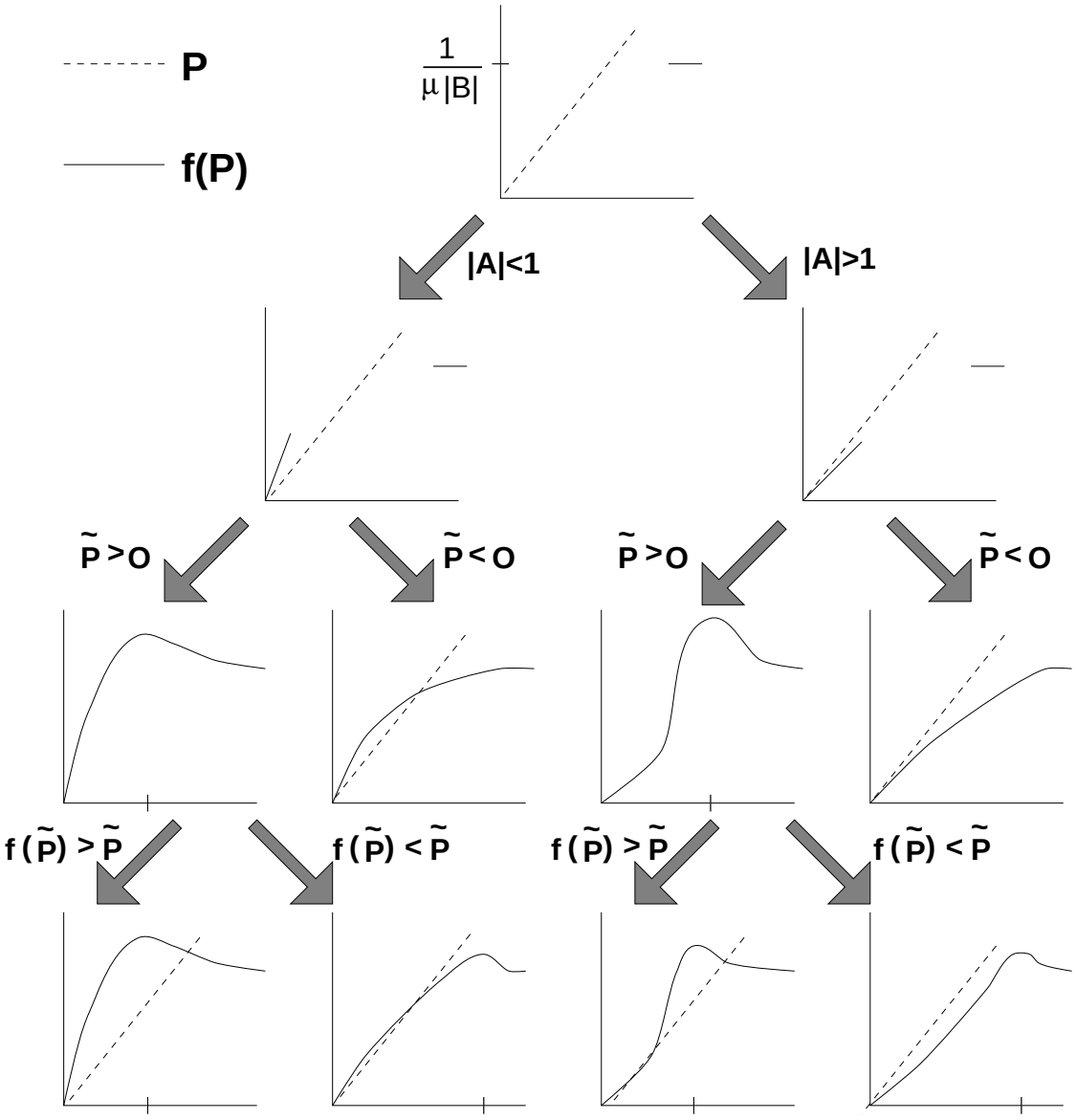

Figure 4.3 Different possibilities for the shape of the map (4.17), depending on the conditions $|A| < 1$, $\widetilde{P} > 0$ and $f(\widetilde{P}) > \widetilde{P}$, under the assumption that there are no inflexion points.

$\lvert A\rvert$	$\widetilde{P}$	$f(\widetilde{P})$	No. of solns of $P = f(P)$
< 1	> 0	$> \widetilde{P}$	1
< 1	> 0	$< \widetilde{P}$	1
< 1	< 0	$> \widetilde{P}$	1
< 1	< 0	$< \widetilde{P}$	1
> 1	> 0	$> \widetilde{P}$	2
> 1	> 0	$< \widetilde{P}$	0
> 1	< 0	$> \widetilde{P}$	0
> 1	< 0	$< \widetilde{P}$	0

Table 4.1 Numbers of solutions of $f(P) = P$ under various conditions, assuming no inflexion points.

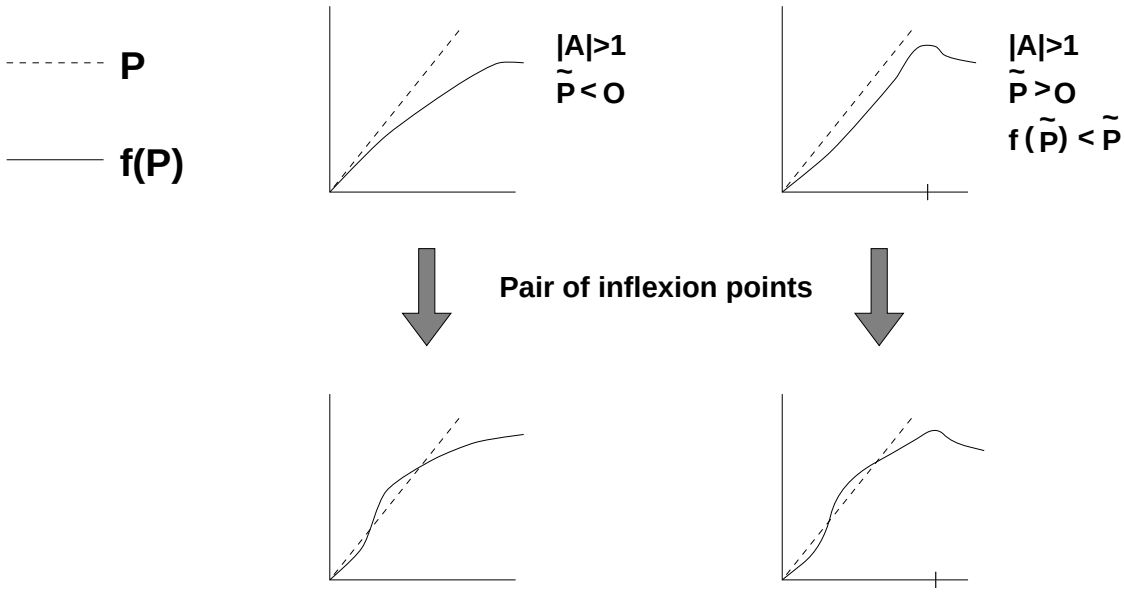

Figure 4.4 Inflexion point possibilities for the map (4.17)

$f(f(P)) = P$ by trusting manipulation via *Mathematica* (Wolfram [1991]), then we find two new solutions other than the solutions (4.14) of $f(P) = P$, given by

$$\mu P = \frac{c\left(1-|A|^4\right) \pm \left[\left(|A|^2-1\right)\left(|A|^2+1\right)^2\left(c^2(3+|A|^2) - 4|B|^2\left(1+|A|^2\right)^2\right)\right]^{\frac{1}{2}}}{2\left(|B|^2+2|A|^2|B|^2+|A|^4|B|^2-c^2\right)} \tag{4.21}$$

However, applying this formula in particular cases quickly reveals that these apparent solutions may not actually solve $f(f(P)) = P$! These solutions are such that $P \mapsto P' \mapsto P'' \neq P$, but $P \mapsto P'$, and $-P' \mapsto P$. During the algebraic manipulation of $f(f(P)) = P$, the square roots are squared out, and this later allows for incorrect solutions. More careful manipulation reveals that P solves $f(f(P)) = P$ if and only if

$$-c\mu|P|\sqrt{|A|^2 + c\mu P + |B|^2\mu^2P^2} = (1+|A|^2)|B|^2\mu^2P^2 + |A|^2c\mu P + (1-|A|^4). \tag{4.22}$$

(A solution of $f(-f(P)) = P$ will have the opposite sign on the left hand side). Hence (4.21) only gives solutions of $f(f(P)) = P$ if also

$$\text{sign}(-c\mu) = \text{sign}((1+|A|^2)|B|^2\mu^2P^2 + |A|^2c\mu P + (1-|A|^4)). \tag{4.23}$$

By inspection, when $|A| < 1$ and $\widetilde{P} < 0$, we have $\text{sign}(-c\mu) = -1$ and the right hand side of equation (4.23) is positive, so there can be no period two solutions in this case.

In addition to (4.23), there is also a reality condition for the roots of (4.21), given by

$$c^2(3+|A|^2) > 4|B|^2\left(1+|A|^2\right)^2$$

when $|A| > 1$ and

$$c^2(3+|A|^2) < 4|B|^2\left(1+|A|^2\right)^2$$

when $|A| < 1$.

In Figure 4.5, we show an example of (4.17) with parameter values such that a period two solution exists. The uniterated map has the form of a *unimodal map* (Devaney [1989] §1.18); hence, depending on the values of the parameters A and B, iteration of the map (4.17) may display any of the complicated behaviours (such as stable period n orbits or chaotic sequences, see Feigenbaum [1980], Devaney [1989] §1.8) associated with such unimodal maps.

However, we do not observe the changes in behaviour with changing parameter values associated to such unimodal maps (such as period-doubling cascades). This is because our parameter μ does not actually control the steepness of the "hump" in $f(P)$. If we examine the scaling of the map (4.17) with μ we see that

$$\lambda f(\lambda^{-1}P;\lambda\mu) \equiv \lambda \left| \frac{A}{\lambda^{-1}P} + \lambda\mu B \right|^{-1} \equiv \left| \frac{A}{P} + \mu B \right|^{-1} \equiv f(P;\mu).$$

This tells us that the shape of the map does not change with μ, only with A and B (which are fixed for a particular system). Hence we will not observe any qualitative change in the behaviour of the iteration of (4.17) with μ, only a rescaling. In particular we will not observe any period-doubling cascades with changing μ.

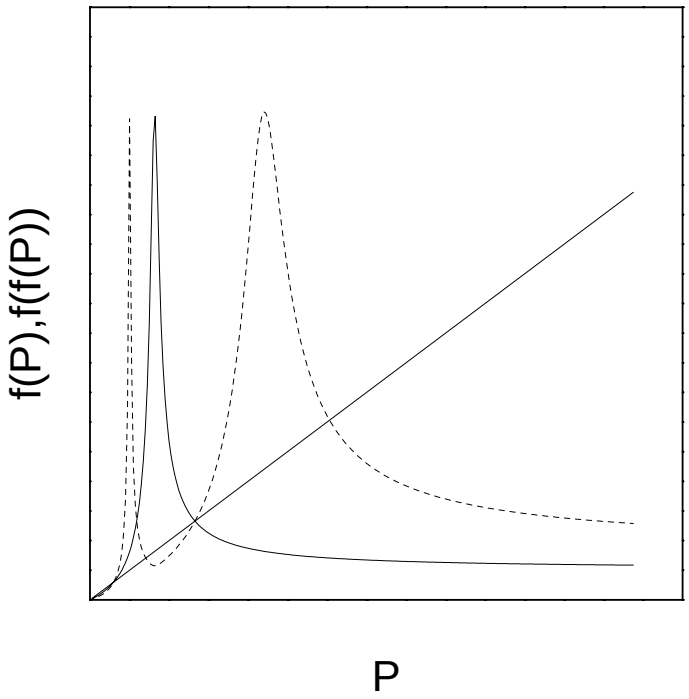

Figure 4.5 Iteration of the finite-dimensional map (4.17) with $A = -1.3 - 0.9i$, $B = 1.9 + 1.5i$ so that $|A| > 1$, $\widetilde{P} > 0$ and $f(\widetilde{P}) > \widetilde{P}$, and so that a period two orbit exists.

4.3 Non-Symmetric Quadratic Real Systems

If we relax the assumption that the system is symmetric, but keep a quadratic dispersion relation then we will have corresponding frequencies $\pm\omega_0 = \text{Im } \sigma(\pm k_0)$, and the map (4.10) becomes

$$\begin{aligned} c_1\zeta + \overline{c}_1\overline{\zeta} &= d_1\chi + \overline{d}_1\overline{\chi} + \mu \\ c_2\zeta + \overline{c}_2\overline{\zeta} &= d_2\chi + \overline{d}_2\overline{\chi} + \mu \end{aligned} \tag{4.24}$$

with

$$\zeta = \frac{e^{-ik_0L - i\omega_0 P'}}{P'}, \qquad \chi = \frac{e^{i\omega_0 P}}{P}.$$

From this we obtain

$$\frac{e^{-ik_0L - i\omega_0 P'}}{P'} = \frac{A}{P}\cos(\omega_0 P - \theta) + \mu B \tag{4.25}$$

for $A, B \in \mathbb{C}$, $\theta \in \mathbb{R}$, where

$$\begin{aligned} A\cos\theta &= \frac{2\overline{c}_2 d_{1R} - 2\overline{c}_1 d_{2R}}{c_1\overline{c}_2 - \overline{c}_1 c_2}, \\ A\sin\theta &= \frac{2\overline{c}_2 d_{1I} - 2\overline{c}_1 d_{2I}}{c_1\overline{c}_2 - \overline{c}_1 c_2}, \\ B &= \frac{\overline{c}_2 - \overline{c}_1}{c_1\overline{c}_2 - \overline{c}_1 c_2}. \end{aligned}$$

Again, for solutions with $P' = P$, we need to solve

$$|A\cos(\omega_0 P - \theta) + \mu BP| = 1 \tag{4.26}$$

for P, given μ. As this equation is transcendental, this can no longer be done in closed form, but we see that as $\mu \to 0$ we will have

$$\mu \sim \frac{1}{P}\cos(\omega_0 P - \theta).$$

L is obtained from

$$k_0 L + \omega_0 P = 2n\pi + \arg(A\cos(\omega_0 P - \theta) + \mu BP) \tag{4.27}$$

and we then see that the wave speed is

$$\frac{L}{P} \sim -\frac{\omega_0}{k_0} + \mu\frac{2n\pi}{k_0}.$$

As in the previous case, we attempt to explore the behaviour of the finite-dimensional map (4.25), considered as a map $P \mapsto P'$:

$$\begin{aligned} P' = f(P) &= \left|\frac{A}{P}\cos(\omega_0 P - \theta) + \mu B\right|^{-1} \\ &= \frac{P}{\sqrt{|A|^2\cos^2(\omega_0 P - \theta) + \mu c P\cos(\omega_0 P - \theta) + \mu^2|B|^2P^2}}, \end{aligned} \tag{4.28}$$

where $c = A\overline{B} + B\overline{A}$ as before. We initially make some observations about the possible shape of this function. Firstly, we can see that $f(0) = 0$ and that, as

in the symmetric case, $f(P) \to \pm(1/\mu|B|)$ as $P \to \pm\infty$. The first derivative of $f(P)$ is

$$f'(P) = \frac{\left(c\mu P + 2|A|^2\cos(\omega_0 P - \theta)\right)\left(\cos(\omega_0 P - \theta) - \omega_0 P \sin(\omega_0 P - \theta)\right)}{2\left[|A|^2\cos^2(\omega_0 P - \theta) + \mu c P \cos(\omega_0 P - \theta) + \mu^2|B|^2P^2\right]^{\frac{3}{2}}}, \tag{4.29}$$

so that the slope at $P = 0$ is $f'(0) = (1/|A|\cos\theta)$. However, we cannot find a limit for $f'(P)$ as $P \to \pm\infty$; this is because the shape of the function remains oscillatory about $\pm(1/\mu|B|)$ with decreasing amplitude as $P \to \pm\infty$; example diagrams illustrating this are shown later in the chapter.

Local extrema of the map (4.28) are much more common than in the symmetric case. We find that $\widetilde{P}$ is a local extremum of $f(P)$, that is $f'(\widetilde{P}) = 0$ if and only if

$$\cos(\omega_0\widetilde{P} - \theta) = \frac{-c\mu\widetilde{P}}{2|A|^2}$$

or

$$\tan(\omega_0\widetilde{P} - \theta) = \frac{1}{\omega_0\widetilde{P}}.$$

The second of these conditions will certainly provide a infinite number of local extrema.

Although equations (4.26) or (4.28) may not be solved analytically, we can choose values for A, B, ω_0 and θ and solve them numerically. To do this, we initially find a solution (μ_0, P_0) of (4.26) with a one-dimensional search using Brent's method (Press *et al* [1992] §9.3)[1]. With this solution, we then attempt continuation, using the techniques described in Doedel [1986] and Parker & Chua [1989]. We seek a path $(\mu(s), P(s))$ of solutions of $g(P;\mu) = f(P;\mu) - P$, so that $g(P(s);\mu(s)) \equiv 0$. Differentiating this with respect to s, we find

$$\frac{dP}{ds} = \frac{\frac{-\partial g}{\partial \mu}}{\frac{\partial g}{\partial P}} \cdot \frac{d\mu}{ds}.$$

[1] Specifically, we use the `C` routine `zbrent` from Press *et al.*

This then gives us the direction of the unit tangent vector $(\dot{\mu}_0, \dot{P}_0)$ to the solution curve $(\mu(s), P(s))$ at (μ_0, P_0). To continue the branch, we take a small step along the tangent, to

$$(\mu_1, P_1) = (\mu_0, P_0) + \Delta s(\dot{\mu}_0, \dot{P}_0).$$

As we still want (μ_1, P_1) to be a solution, we actually solve

$$\begin{aligned} g(P_1; \mu_1) &= 0, \\ (P_1 - P_0)\dot{P}_0 + (\mu_1 - \mu_0)\dot{\mu}_0 - \Delta s &= 0. \end{aligned} \tag{4.30}$$

This is a two-dimensional root finding problem; to solve it, we use a globally convergent multi-dimensional Newton's method, as described[2] in Press *et al* [1992] §9.7. Note that the Jacobian of the system is

$$\begin{pmatrix} \frac{\partial g}{\partial P}(P_1; \mu_1) & \frac{\partial g}{\partial \mu}(P_1; \mu_1) \\ \dot{P}_0 & \dot{\mu}_0 \end{pmatrix} \tag{4.31}$$

and is nonsingular at regular solution points and at simple turning points of $g(P(s); \mu(s)) = 0$. The determinant of this Jacobian is monitored along the solution branch, so that a change of sign of the determinant will indicate the existence of a zero of the determinant, which in turn may indicate the existence of a local bifurcation point.

By choosing values for A, B, ω_0 and θ at random and observing the bifurcation diagrams resulting, we see an interesting variety of shapes of bifurcation diagrams. One clear characteristic between different examples of these bifurcation diagrams is whether the oscillations of a branch of solutions that is tending to $P = \infty$ as $\mu \to 0$ cross the $\mu = 0$ axis. Examining (4.26), we see that we will have solutions at $\mu = 0$ if

$$\begin{aligned} & |A\cos(\omega_0 P - \theta)| = 1 \\ \Leftrightarrow \qquad & \cos(\omega_0 P - \theta) = \pm\frac{1}{|A|}, \end{aligned}$$

[2] Specifically, we use the `C` routine `newt` from Press *et al.*

so that there will be solutions at $\mu = 0$ if and only if $|A| \geqslant 1$.

We now show three examples of bifurcation diagrams produced for different values of A and B, with $\theta = 0$ and $\omega_0 = 1$. These particular examples are culled from a selection of several hundred bifurcation diagrams produced with different random values for A and B; the range of different shapes of bifurcation curves observed is covered by these examples.

In each case, as described above, we find an initial solution and then perform continuation to give a (μ, P) bifurcation diagram. The first case is shown in Figure 4.6, and has $|A| < 1$ and hence no solutions at $\mu = 0$. In this case, we also plot the L component, and note that the $2n\pi$ term in (4.27) means that the L coordinate can be taken to be periodic on $2\pi/k_0$, so that we obtain a full bifurcation picture as in Figure 4.7.

The second and third cases both have $|A| > 1$ and hence solutions at $\mu = 0$. However, these solutions are connected on two bifurcation branches in Figure 4.8, and are disconnected isolas in Figure 4.9.

In each case, the monitoring of the sign of the Jacobian reveals that the turning points of $(\mu(s), P(s))$ are the only local bifurcations of $f(P) = P$ produced by the system. This is to be expected, since in general we will only observe codimension one bifurcations in a system with a one-dimensional parameterization. The only codimension one local bifurcation of fixed points of a one-dimensional map is the *saddle-node bifurcation* (Wiggins [1990] §3.2), which is just another name for a turning point of $(\mu(s), P(s))$.

However, there is another possibility for codimension one bifurcations—that of a *period doubling bifurcation.* At such a bifurcation, a pair of branches of solutions of

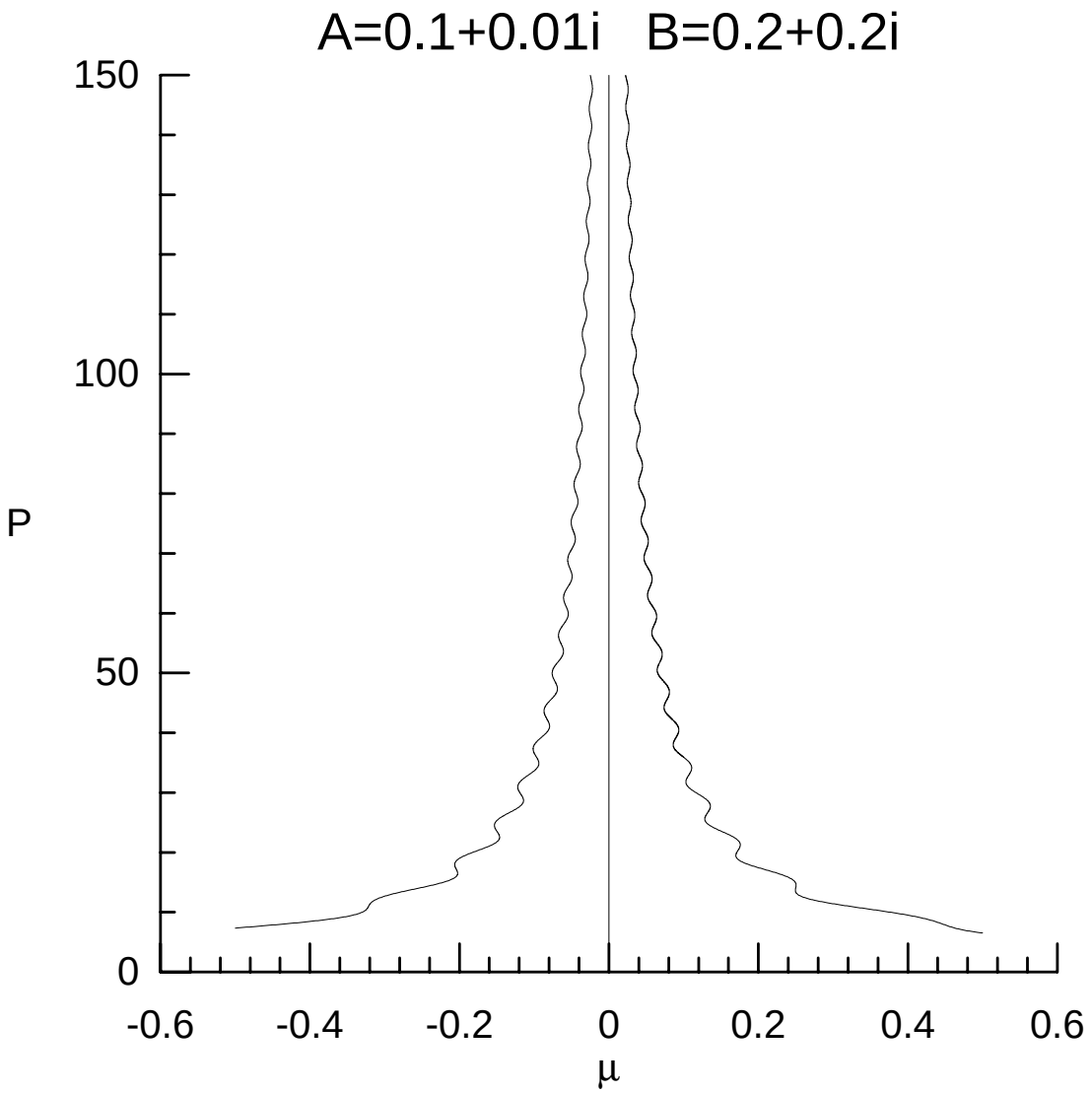

Figure 4.6 Bifurcation diagram for non-symmetric, quadratic, real scalar system, as described by equations (4.26) and (4.27). In this case, there are no solutions at $\mu = 0$.

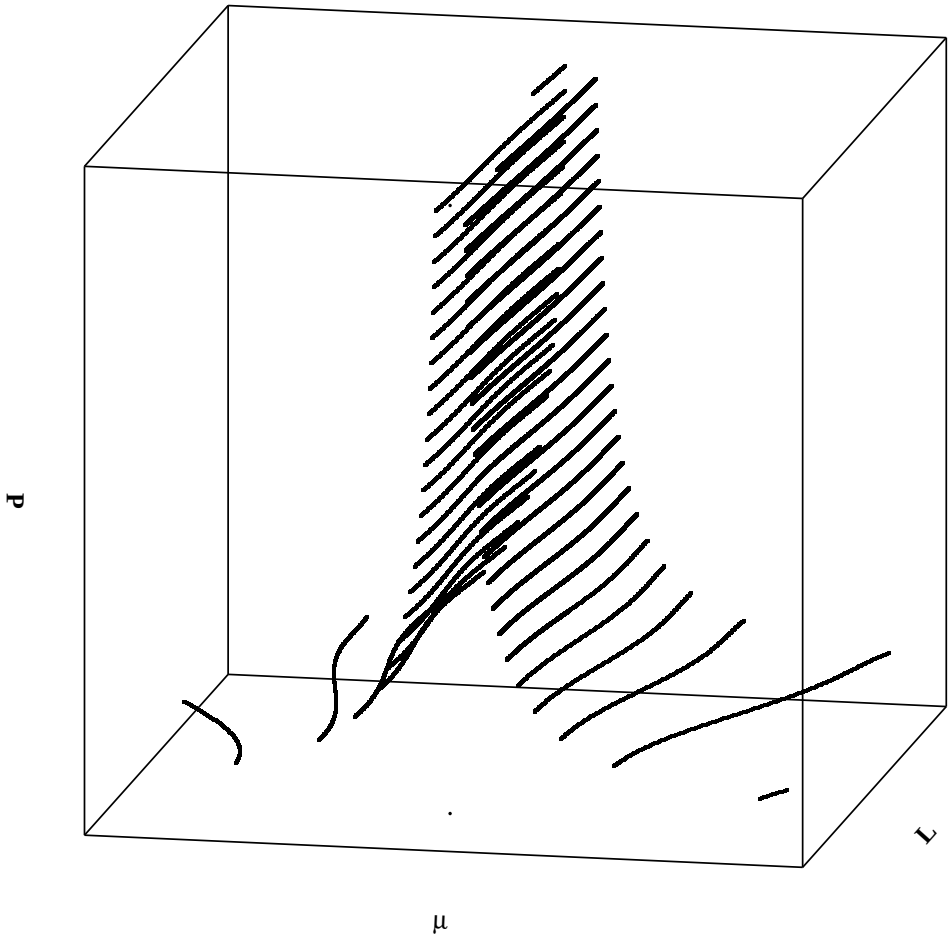

Figure 4.7 Full bifurcation diagram for non-symmetric, quadratic, real scalar system, as described by equations (4.26) and (4.27). The L component is plotted modulo $2\pi/k_0$, because of the $2n\pi$ term in (4.27). In this case, there are no solutions at $\mu = 0$.

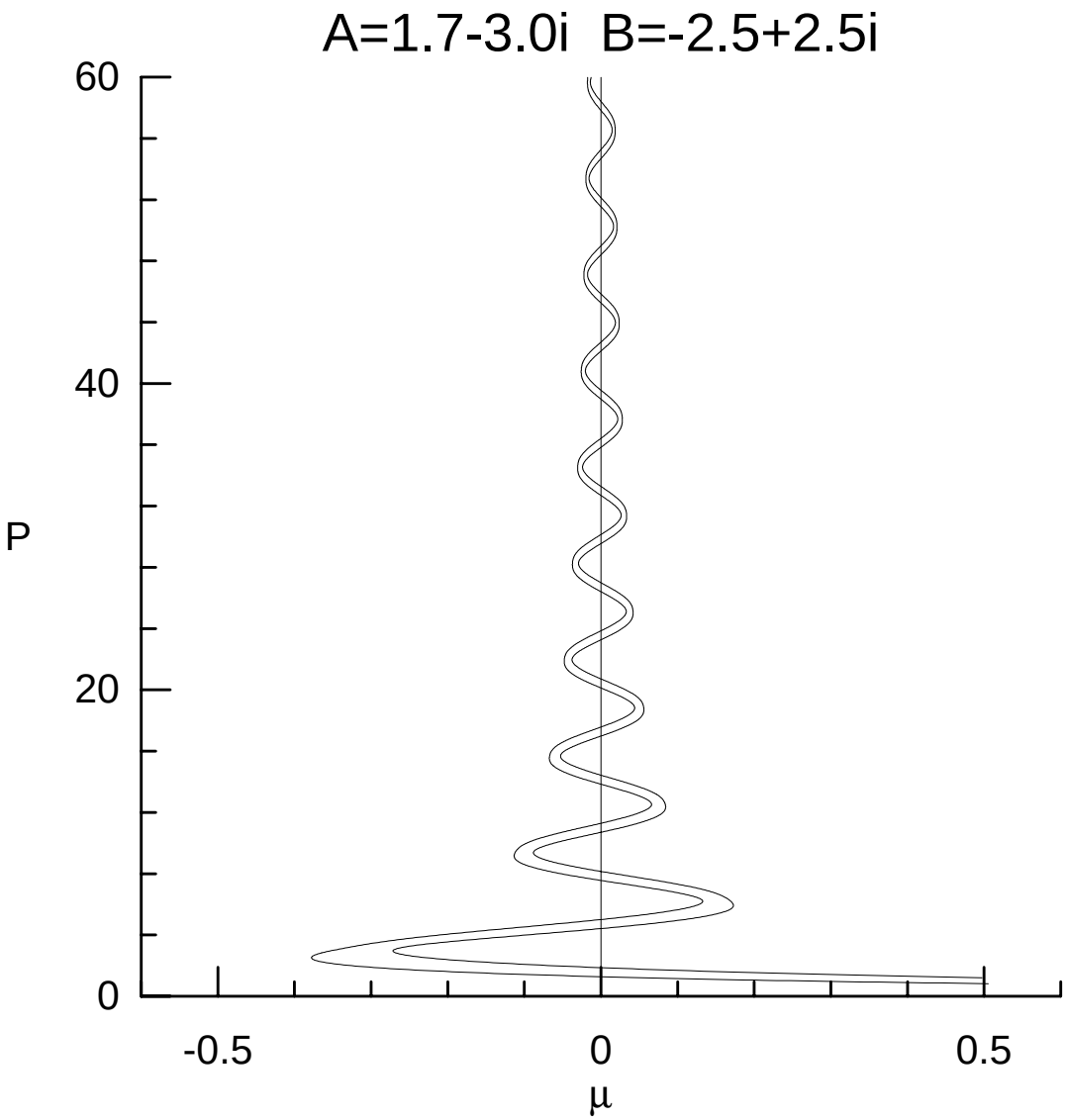

Figure 4.8 Bifurcation diagram for non-symmetric, quadratic, real scalar system, as described by equations (4.26) and (4.27). In this case, there are solutions at $\mu = 0$, which are all connected on two bifurcation branches.

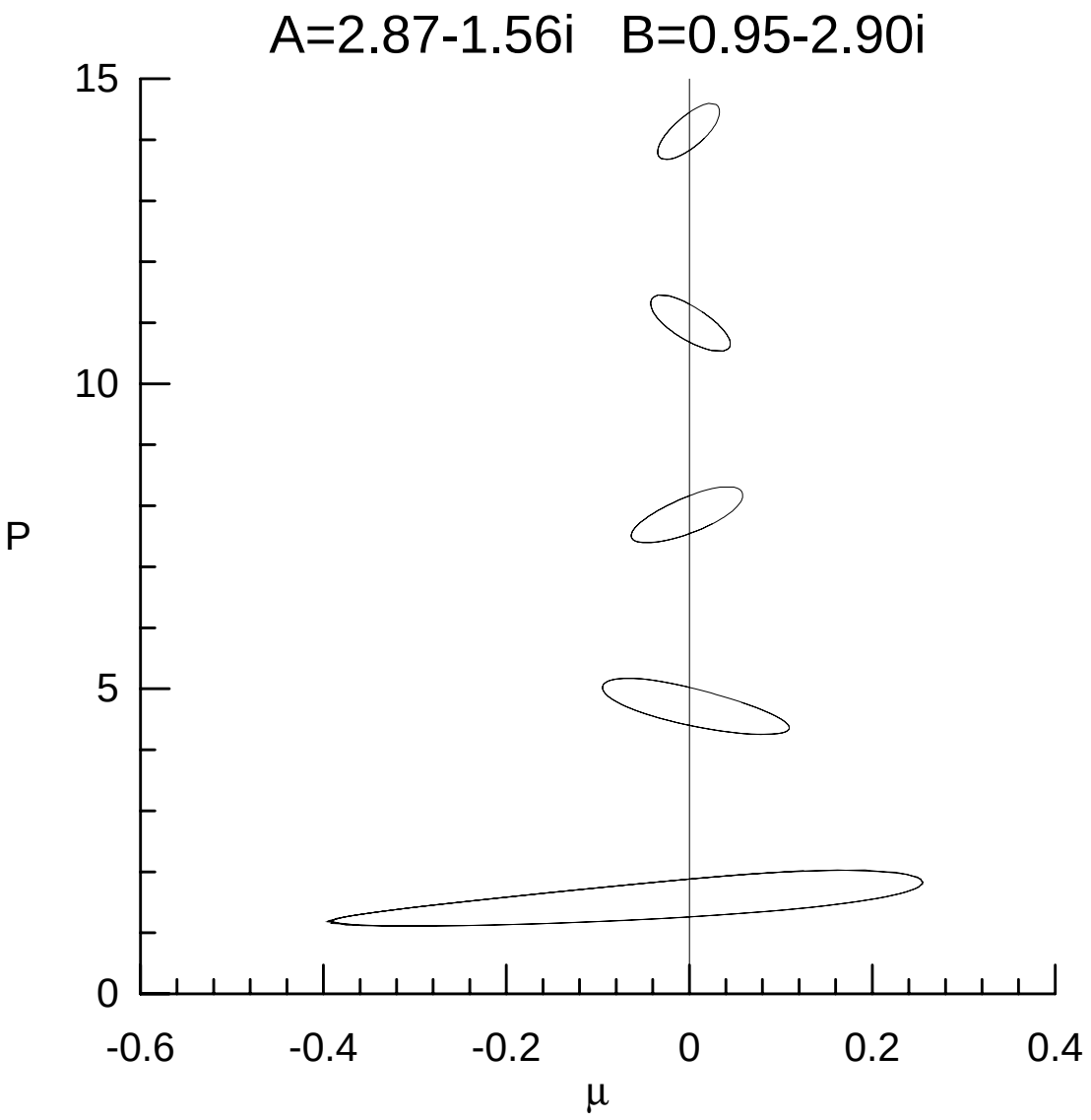

Figure 4.9 Bifurcation diagram for non-symmetric, quadratic, real scalar system, as described by equations (4.26) and (4.27). In this case, there are solutions at $\mu = 0$, which are only connected in pairs.

$f(f(P)) = P$ bifurcates from the solution branch. Because there are no new solutions of the equation $g(P) = f(P) - P = 0$, these bifurcations cannot be detected by monitoring the sign of the determinant of the Jacobian (4.31). The condition for such bifurcations is that $f'(P;\mu) = -1$ (Guckenheimer & Holmes [1983] §3.5, Wiggins [1990] §3.2); examining the derivative $f'(P)$ from (4.29) at a solution of $f(P) = P$ (so that the denominator is 2), we see that such bifurcations are likely to be common, occurring at (μ, P) such that

$$\left(c\mu P + 2|A|^2 \cos(\omega_0 P - \theta)\right)\left(\cos(\omega_0 P - \theta) - \omega_0 P \sin(\omega_0 P - \theta)\right) = -2.$$

Indeed, a numerical search for such period-doubling bifurcations in the three cases previously shown produces too many for them to be added to the diagrams without obscuring the rest of the bifurcation diagram.

To see this from another angle, if we take some example values for A, B, ω_0 and θ and plot $f(P)$ against P in Figure 4.10, we see that for large P the form of $f(P)$ involves rapid oscillations about $P = |\mu B|^{-1}$. In Figure 4.11, we look more closely at the intersections of the line $P' = P$ with this function, and we find that sections of it have the form of a unimodal map (Devaney [1989] §1.18).

In contrast to the symmetric case, the function $f(P)$ no longer scales with μ, and hence as μ changes we may observe the cascades of period doubling associated with such unimodal maps. In Figure 4.12 we draw an *orbit diagram* for the map (4.28) with example values for A, B, ω_0 and θ. An orbit diagram is a picture of the asymptotic behaviour of orbits under iteration of f for varying μ values. For each μ value, we pick a collection of initial conditions at random, iterate them with f to eliminate transient behaviour, and then plot a number of later points from the orbit. If we examine sections of Figure 4.12 more closely, as in Figure 4.13, we do indeed observe the characteristic period doubling cascades of

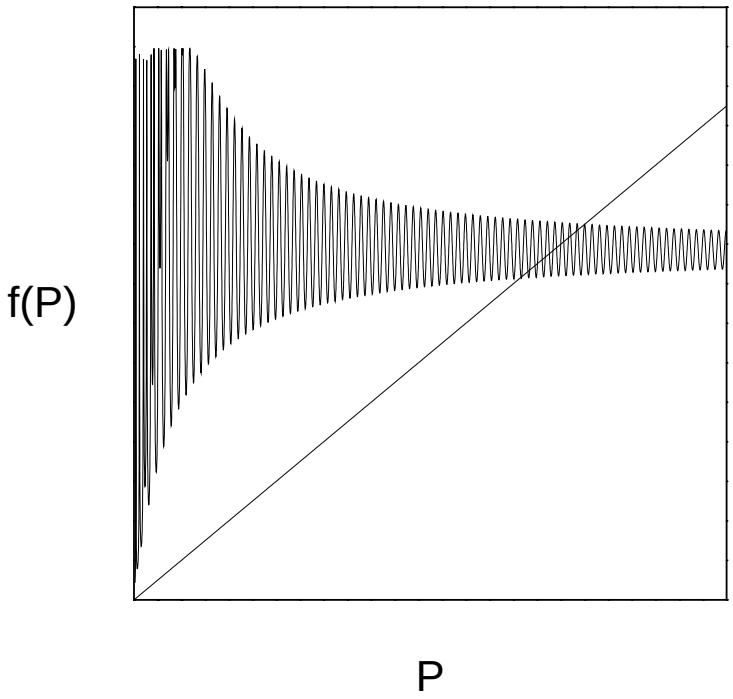

Figure 4.10 The finite-dimensional map (4.28) with $A = 0.1 + 0.01i$, $B = 0.2 + 0.2i$, $\omega_0 = 1$ and $\theta = 0$

unimodal maps. Hence we can see that as $\mu \to 0$, we will get a countable infinity of μ values accumulating at 0 at each of which the map has all of the complexity associated with universality theory in one dimensional maps (Feigenbaum [1978], [1979], Lanford [1982]).

4.4 Discussion

In this chapter we have derived a simple form (4.10) of the finite-dimensional map (3.52) from the previous chapter. We then proceeded to examine two of the simplest possible examples of this map. In the first example, taken from a real quadratic symmetric system, we found essentially simple bifurcation behaviour,

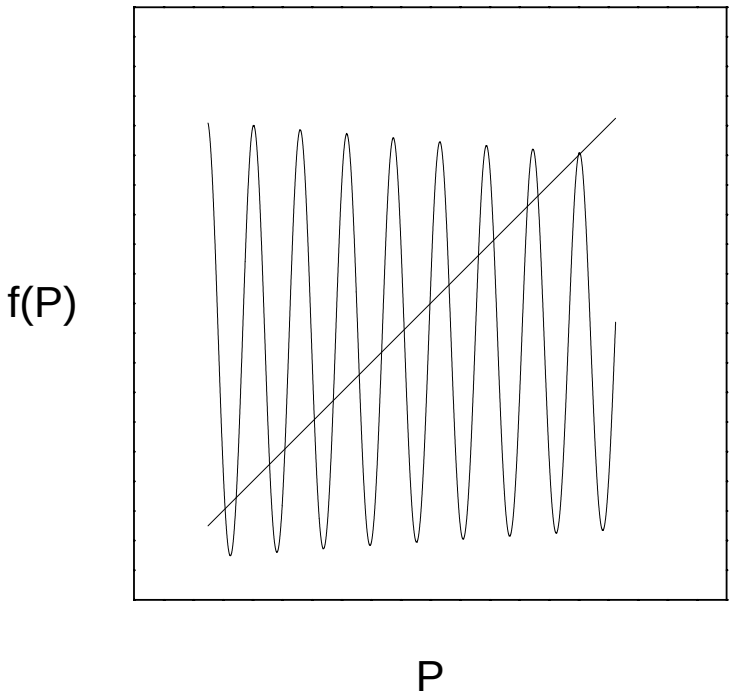

Figure 4.11 Closer examination of the intersections of the previous diagram

but with a multitude of different cases depending upon the coefficients A and B of the map. In all cases, bifurcation branches approached $P = \infty$ as $\mu \to 0$ in a manner $\mu \sim P^{-1}$. In some cases, branches existed on either side of $\mu = 0$, and in others only on one side. Moreover, in some cases period two solutions could be found, although no period-doubling bifurcations or other bifurcations could occur with varying μ.

The second example was slightly more complicated, relaxing the assumption of symmetry in the dispersion relation to consider a real quadratic system. In this case, analytical solution of fixed point condition of the map (4.10) was no longer possible, and numerical continuation methods were employed instead. A variety of possible bifurcation behaviours were observed for particular instances of the map, characterized by oscillatory behaviour of solution branches. In all instances, both saddle-node and period-doubling bifurcations were observed on the solution

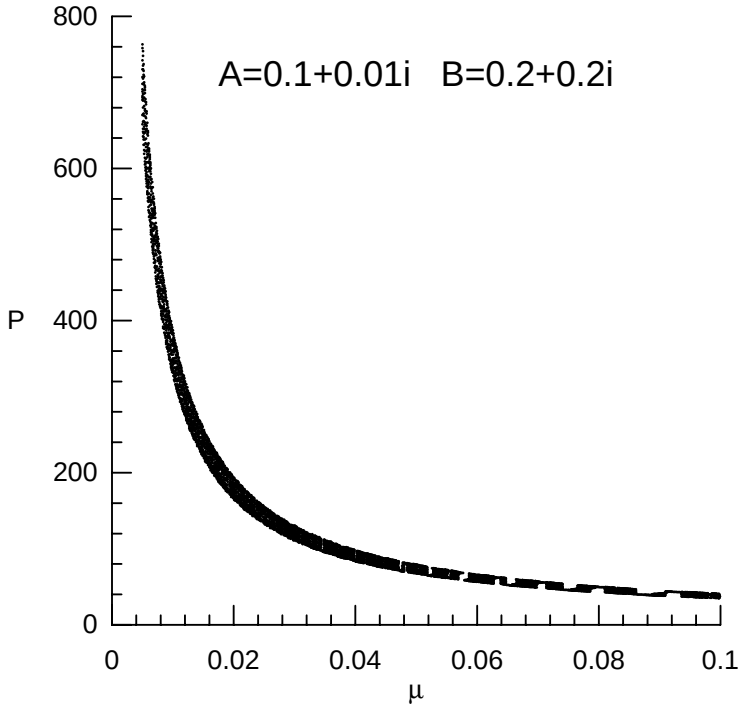

Figure 4.12 Orbit diagram for the finite-dimensional map (4.28) with $A = 0.1 + 0.01i$, $B = 0.2 + 0.2i$, $\omega_0 = 1$ and $\theta = 0$

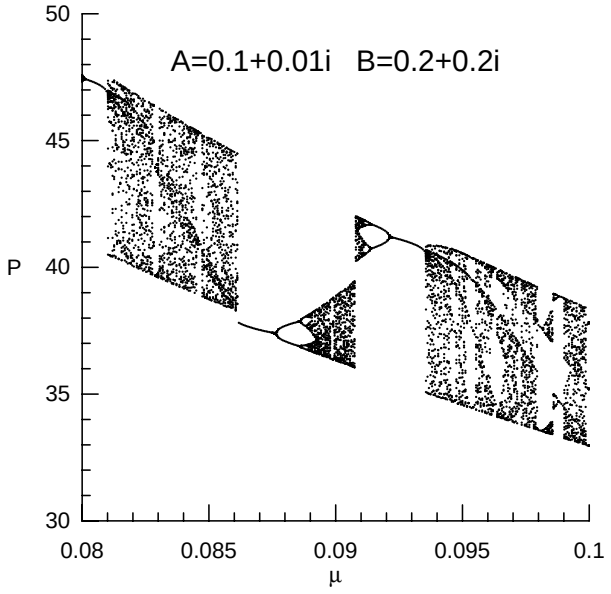

Figure 4.13 Closer examination of a section of the previous diagram, showing a cascade of period doubling.

branches of $f(P) = P$.

In both cases, the L component of the finite-dimensional map (4.10) could be separated out from the P behaviour, leading to simpler bifurcation analysis. Also, in both cases this $P \mapsto P'$ behaviour was considered purely as a bifurcation problem in a one-dimensional map, without reference to the possible partial differential equations that these maps have originally been derived from. The hope is then that these fixed points of the finite-dimensional maps will correspond to solutions of the original partial differential equations via some form of shadowing. If such is the case, then a fixed point $P' = P$, $L \neq 0$ of the finite-dimensional map will correspond to a modulated travelling wave solution of the PDE. If we have finite periodic sequences

$$P_0 \mapsto (P_1, L_1) \mapsto \ldots (P_q, L_q) = (P_0, L_q),$$

then these will correspond to travelling wave solutions of the PDE with periodic modulation. We cannot extend this correspondence to infinite sequences of P, but such sequences still remain indicative of the level of complexity of behaviour possible in such systems.

5 Homoclinic Bifurcations in Countably Infinite Dimensions

In Chapter 2 we considered the general case of an n-dimensional ordinary differential equation system, and in Chapter 3 we considered the case of a partial differential equation on an unbounded domain. In this chapter we consider partial differential equations on a bounded domain, having a countably infinite set of eigenfunctions. This case is very much an extension of the finite dimensional case given in Chapter 2; however, here we consider the effects of symmetry (as in the case of partial differential equations on unbounded domains). Moreover, we consider the limit as the domain size tends to infinity, and thus the relationship between the finite-dimensional maps derived in chapters 2 and 3.

This situation is extremely important for numerical applications, since any integration of a partial differential equation will have to be performed on a finite domain, in a manner that is in general equivalent to an integration of a (large) set of ordinary differential equations.

We consider a system

$$u_t(x,t) = F(u(x,t);\mu) \tag{5.1}$$

for x on a bounded domain D, and where F is a nonlinear differential operator. In general we will expect periodic boundary conditions. We assume that:

1) the origin is a fixed point for all values of μ, that is $F(0;\mu) = 0$.
2) equation (5.1) is invariant under $q-1$ one-parameter symmetries spanned by the vector fields $v_2,\ldots,v_q$, generating transformations $A(x,t) \mapsto G_j(\epsilon_j)A(x,t)$ such that each transformation is projectable and also does not involve the time variable t.

3) at $\mu = 0$ an orbit $A^H(x,t)$ homoclinic to the origin exists.

Note that we select one of the q-parameter family of possible homoclinic orbits existing at $\mu = 0$ that are related by these symmetry transforms, and denote it by $u^H(t)$.

Moreover, we assume that $L = DF(0;0)$ has a countably infinite, complete orthonormal set of eigenfunctions such that:

1) there are no zero eigenvalues.
2) there is a unique eigenvalue with largest negative real part, and a unique eigenvalue with smallest positive real part.

5.1 Derivation of a Poincaré Map

We write the eigenvalues of L as $\{\lambda_k\}_{k\in K}$, with corresponding eigenfunctions $\{v_k(x)\}_{k\in K}$ where $K = I \cup J$, $I \cap J = \emptyset$ and Re $\lambda_i > 0$ $(i \in I)$, Re $\lambda_j < 0$ $(j \in J)$. Thus I corresponds to an unstable eigenspace, and J corresponds to a stable eigenspace.

We then see that the general solution of the linearized equation

$$u_t = Lu \tag{5.2}$$

is

$$u(x,t) = \sum_{k\in K} f_k e^{\lambda_k t} v_k(x), \tag{5.3}$$

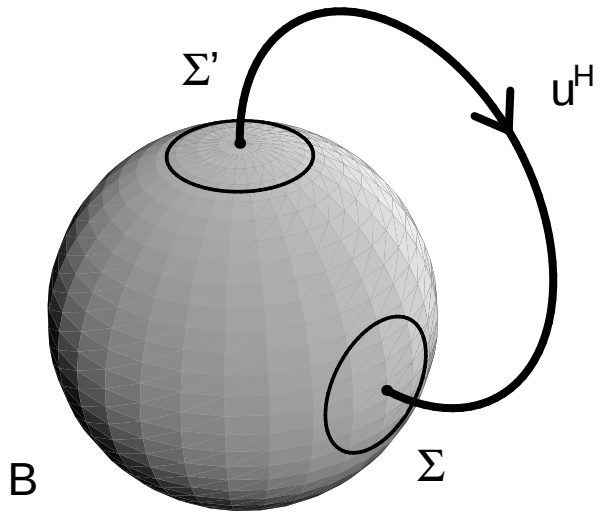

Figure 5.1 Schematic representation of the flow

where $f_k = \langle u(x,0), v_k \rangle$.

We now define suitable surfaces for our Poincaré map to pass through. Firstly, let

$$B = \{u : \|u\| = \nu\}.$$

The homoclinic orbit must pass through B on its way to the origin as $t \to \pm\infty$. We define $-t_U < t_S$ as times such that $u^H(-t_U), u^H(t_S) \in B$. Note that as $\nu \to 0$, $t_U, t_S \to \infty$, and we let ν be small enough that t_U and t_S are unique. We now define our Poincaré surfaces to be neighbourhoods of size δ of these intersections. However, as we actually have a continuous family of homoclinic orbits, we will define the surfaces as consisting of those points that may be shifted into a neighbourhood of the homoclinic orbit by symmetry transforms, that is

$$\begin{aligned} \Sigma &= \{u \in B : \|G(\epsilon)u - u^H(t_S)\| \leqslant \delta\}, \\ \Sigma' &= \{u \in B : \|G(\epsilon)u - u^H(-t_U)\| \leqslant \delta\}. \end{aligned} \tag{5.4}$$

The function $u^H(t_S) \in \Sigma$ may be decomposed as $u^H(t_S) = \sum_K f_k^+ v_k$, and we write this in a rescaled form as $\beta_k^H = e^{-\lambda_k t_S} f_k^+$; similarly $u^H(-t_U) = \sum_K f_k^- v_k$

and we write $\alpha_k^H = e^{\lambda_k t_U} f_k^-$ so that

$$u^H(t_S) = \sum_K \beta_k^H e^{\lambda_k t_S} v_k, \qquad u^H(-t_U) = \sum_K \alpha_k^H e^{-\lambda_k t_U} v_k.$$

In fact, for any $v \in \Sigma$ we decompose v into the form

$$v = \sum_K \beta_k e^{\lambda_k t_S} v_k, \tag{5.5}$$

and for any $v \in \Sigma'$ we decompose v into the form

$$v = \sum_K \alpha_k e^{-\lambda_k t_U} v_k. \tag{5.6}$$

If we consider a point $v_0 \in \Sigma$ sufficiently close to the homoclinic orbit, it is mapped through to Σ'. We let $\widetilde{t}$ be the time taken to reach Σ', so there is an orbit $v(t)$ of the system with $v(0) = v_0 \in \Sigma$, $v(\widetilde{t}) \in \Sigma'$. If we now decompose $v(0)$ and $v(\widetilde{t})$ in the above form, and moreover assume that within the ball B we may approximate the system with the linear system (5.2), then the general solution (5.3) will give

$$\alpha_k = e^{\lambda_k P} \beta_k, \qquad P = t_S + t_U + \widetilde{t} \tag{5.7}$$

for $k \in K$.

We now construct a return map outside the ball B in a similar manner to previous chapters by linearizing about the homoclinic orbit. We write

$$w = G(\epsilon)u - u^H$$

for an ϵ that minimizes the distance $\|w\|$ on Σ'. The system then becomes

$$w = \mathcal{L}[u^H]w + h(u^H, w),$$

where $h(u^H, w) = F(u^H + w; \mu) - F(u^H; 0) - \mathcal{L}[u^H]w$. We start from a point on Σ', which we write in the form

$$w = \sum_K e^{-\lambda_k t_U} (g(\epsilon)\alpha_k - \alpha_k^H) v_k = \sum_K e^{-\lambda_k t_U} \widehat{\alpha}_k v_k, \tag{5.8}$$

with

$$\widehat{\alpha}_k = g(\epsilon)\alpha_k - \alpha_k^H. \tag{5.9}$$

For points remaining sufficiently close to the homoclinic orbit, these will be mapped to Σ by the flow, to a point that we will represent as

$$w = \sum_K e^{\lambda_k t_S}(g(\epsilon)\beta_k' - \beta_k^H)v_k = \sum_K e^{\lambda_k t_S}\widehat{\beta}_k v_k, \tag{5.10}$$

with

$$\widehat{\beta}_k = g(\epsilon)\beta_k' - \beta_k^H. \tag{5.11}$$

Here we have taken $g(\epsilon)$ to be the transformation in the coefficients of the v_k induced by the symmetry transform $G(\epsilon)$, that is, if $A = \sum_K f_k v_k$ then $G(\epsilon)A = \sum_K g(\epsilon) f_k v_k$. Note also that we are abusing notation; the transformation $g(\epsilon)$ will almost certainly mix up different α_k, and hence should be written

$$g(\epsilon)\alpha_k = \left[g(\epsilon)\left(\{\alpha_l\}_{l\in K}\right)\right]_k.$$

For example, if we have a standard set of sine and cosine basis functions for functions periodic on $[-L, L]$, and

$$f(x) = a_0 + \sum_1^\infty a_n \cos\frac{n\pi x}{L} + \sum_1^\infty b_n \sin\frac{n\pi x}{L}$$

(so that $\{\alpha_k\}_{k\in K} = \{a_0, b_1, a_1, b_2, a_2, \ldots\}$), then we find that

$$f(x+\epsilon) = \widetilde{a}_0 + \sum_1^\infty \widetilde{a}_n \cos\frac{n\pi x}{L} + \sum_1^\infty \widetilde{b}_n \sin\frac{n\pi x}{L}$$

with

$$\widetilde{a}_0 = a_0, \quad \widetilde{a}_n = a_n\cos\frac{n\pi\epsilon}{L} + b_n\sin\frac{n\pi\epsilon}{L}, \qquad \widetilde{b}_n = b_n\cos\frac{n\pi\epsilon}{L} - a_n\sin\frac{n\pi\epsilon}{L}, \tag{5.12}$$

which thus shuffles pairs of α_ks. We will, however, make the assumption that the symmetry transform $g(\epsilon)$ will not mix up α_k between I and J. This is analogous to the assumption (3.49) made in Chapter 3.

By definition, the homoclinic orbit takes a time $t_U + t_S$ to flow from Σ' to Σ; we will assume that for points sufficiently close to the homoclinic orbit, the time taken to flow from Σ' to Σ will also be approximately $t_U + t_S$. By the autonomous nature of the equation, we shift the origin of time so that

$$w(x, -t_U) = \sum_K \widehat{\alpha}_k e^{-\lambda_k t_U} v_k(x),$$
$$w(x, t_S) = \sum_K \widehat{\beta}_k e^{\lambda_k t_S} v_k(x).$$

We can thus obtain an affine map of the form

$$\widehat{\beta}_k = \sum_{l \in K} m_{kl} \widehat{\alpha}_k + \mu c_k, \tag{5.13}$$

which we combine with (5.7) to give our Poincaré map

$$\alpha_k = e^{\lambda_k P} \beta_k, \qquad g(\epsilon)\beta'_k = \beta_k^H + \sum_{l \in K} m_{kl}(g(\epsilon)\alpha_l - \alpha_l^H) + \mu c_k. \tag{5.14}$$

5.2 Reduction to a Finite-Dimensional Map

We now derive a finite-dimensional map from this Poincaré map, in an analogous manner to the method used in Chapter 2. Firstly, we note that the homoclinic orbit must approach the origin along the stable manifold as $t \to \infty$, and along the unstable manifold as $t \to -\infty$. This implies that

$$\beta_i^H = 0 \quad i \in I, \qquad \alpha_j^H = 0 \quad j \in J.$$

We now split the Poincaré map for $i \in I$, $j \in J$ recalling that $K = I \cup J$.

$$\begin{aligned}
\alpha_i &= e^{\lambda_i P}\beta_i, \\
\alpha_j &= e^{\lambda_j P}\beta_j, \\
g(\epsilon)\beta_i' &= \sum_{l\in I} m_{il}(g(\epsilon)\alpha_l - \alpha_l^H) + \sum_{l\in J} m_{il}g(\epsilon)\alpha_l + \mu c_i, \quad i \in I, \\
g(\epsilon)\beta_j' &= \beta_j^H + \sum_{l\in I} m_{jl}(g(\epsilon)\alpha_l - \alpha_l^H) + \sum_{l\in J} m_{jl}g(\epsilon)\alpha_l + \mu c_j, \quad j \in J.
\end{aligned} \tag{5.15}$$

We consider the third of these equations in the form

$$\sum_{l\in I} m_{il}(g(\epsilon)\alpha_l - \alpha_l^H) = g(\epsilon)\beta_i' - \left\{\sum_{l\in J} m_{il}g(\epsilon)\alpha_l + \mu c_i\right\}, \quad i \in I. \tag{5.16}$$

We also consider $\widetilde{w} = u_t^H$, which is an exact solution of the linearized equation $w_t = Df(u^H;0)w$. Since u^H has asymptotic behaviour

$$\begin{aligned}
u^H &\sim \sum_I \alpha_i^H e^{\lambda_i t} v_i \qquad \text{as } t \to -\infty \\
u^H &\sim \sum_J \beta_j^H e^{-\lambda_j t} v_j \qquad \text{as } t \to \infty
\end{aligned}$$

we find that

$$\begin{aligned}
\widetilde{w} &\sim \sum_I \alpha_i^H \lambda_i e^{\lambda_i t} v_i \qquad \text{as } t \to -\infty \\
\widetilde{w} &\sim \sum_J -\beta_j^H \lambda_j e^{-\lambda_j t} v_j \qquad \text{as } t \to \infty
\end{aligned}$$

As in previous cases, we can work through the derivation of the outside return map, but working with an exact solution, to find that on taking $\widehat{\alpha}_i = \lambda_i \alpha_i^H$, equation (5.16) turns out to be

$$\sum_{l\in I} m_{il}\lambda_l \alpha_l^H = 0 \qquad \forall i \in I.$$

We now consider the space of I-tuples, and define M_{II} to be an operator on that space given by $M_{II}(\{\alpha_i\}_{i\in I}) = \{\alpha_i'\}_{i\in I}$ with

$$\alpha_i' = \sum_{l\in I} m_{il}\alpha_l,$$

which we see is a linear operator with a zero eigenvector $w^1 = \{\lambda_i \alpha_i^H\}_{i \in I}$.

This zero eigenvector exists because of the autonomous nature of the equation, so that it is a consequence of the invariance of equation (5.1) under the symmetry generated by ∂_t. The other symmetries of the equation will also produce similar results. As in Chapter 3, if we consider

$$\frac{\partial}{\partial \epsilon_j} G_j(\epsilon_j) A^H(x,t) \Big|_{\epsilon_j = 0}$$

for $j = 2, \ldots, q$, then we find that this is also an exact solution of the equation linearized about the homoclinic orbit. In the same manner as in Chapter 3, we then find that, under the assumption that each of the symmetries does not mix components in the stable and unstable directions, we have

$$w^j = \left\{ \frac{\partial}{\partial \epsilon_j} g_j(\epsilon) \alpha_i^H \Big|_{\epsilon_j = 0} \right\}_{i \in I}$$

as a zero eigenvector of M_{II}. Hence we have at least q zero eigenvectors of M_{II}; we will assume (in the generic case) that there are no other zero eigenvectors, for otherwise other homoclinic orbits must exist. As promised in Chapter 2, we now consider the effects of the existence of multiple zero eigenvectors of M_{II}.

Lemma 5.2.1: If M_{II} has $s \geqslant 2$ zero eigenvectors, then there is an $(s-1)$-parameter family of homoclinic orbits associated to the origin at $\mu = 0$.

Proof: A homoclinic orbit exists at $\mu = 0$ if and only if we can find a point on Σ' of form (5.6) with $\alpha_j = 0$ for $j \in J$, which is mapped around to a point on Σ of form (5.5) with β_i for $i \in I$.

Suppose that the s zero eigenvectors of M_{II} are $\{w_i^1\}_{i \in I}, \ldots, \{w_i^s\}_{i \in I}$; then we let

$$\begin{aligned} \alpha_i &= \alpha_i^H + \Lambda_1 w_i^1 + \ldots \Lambda_s w_i^s, \\ \alpha_j &= 0, \end{aligned} \tag{5.17}$$

where we have free choice of $s-1$ of the Λ_i (provided that they are suitably small), and the last is constrained by the condition that the point be on Σ', that is by

$$\left\| \sum_I \alpha_i e^{-\lambda_i t_U} v_i \right\| = \nu. \tag{5.18}$$

With this choice of α_i, we clearly see that $M_{II}(\{\alpha_i - \alpha_i^H\}_{i\in I}) = 0$. Hence at $\mu = 0$, our approximate affine map (5.13) for the outside flow will map this point onto Σ with decomposition (5.5) such that $\beta_i = 0$ for $i \in I$—in other words, a point on the stable eigenspace of the origin.

We now use the implicit function theorem to show that this approximate solution implies the existence of an equivalent homoclinic orbit. Firstly we restrict our attention to the subspace of Σ' where the components in the directions of each of the zero eigenvectors of M_{II} are specified (thus enabling us to invert the operator M_{II} on the subspace), that is the space

$$S = \left\{ \{\alpha_i\}_{i\in I} : \langle \{\alpha_i\}, \{w_i^j\} \rangle = \Lambda_j, \left\| \sum_I \alpha_i e^{-\lambda_i t_U} v_i \right\| = \nu \right\}. \tag{5.19}$$

We now consider the function

$$f(X;\delta) = M_{II}.X + \frac{1}{\delta} E(\delta X, \delta)$$

on this space, where $E(x,\delta)$ is the error term in the original affine map, and is of size

$$E(x,\delta) = \mathcal{O}\big(x^2\big) + \mathcal{O}(\delta).$$

We thus find that

$$\lim_{\delta\to 0} \frac{1}{\delta} E(\delta X, \delta) = E_0 < \infty,$$

so we take $X_0 = -(M_{II}|_S)^{-1} E_0 + \sum_{l=1}^{s} \Lambda_l w^l$; hence $f(X_0;0) = 0$. The derivative of the function f at X_0 is $M_{II}|_S$, which is invertible, so by the implicit function

theorem, for all sufficiently small δ, we have a solution $X(\delta)$ of $f(X;\delta) = 0$. Writing $x(\delta) = \delta X(\delta)$, we now have a solution of

$$M_{II}x(\delta) + E(x(\delta), \delta) = 0$$

for sufficiently small δ, which is thus an exact homoclinic orbit. Since we have free choice of $s-1$ of the parameters $\Lambda_1, \ldots \Lambda_s$ used in the definition of S, we have thus shown the existence of an $s-1$ parameter family of homoclinic orbits, defined for sufficiently small δ, that is defined in a neighbourhood of the original homoclinic orbit. □

Thus we see that a q parameter family of homoclinic orbits leads to q zero eigenvectors of M_{II}, and s zero eigenvectors of M_{II} lead to an $s-1$ parameter family of homoclinic orbits, each of which may be time translated, giving an s parameter family of homoclinic orbits.

Using the standard l^2 inner product on the space of I-tuples, we let $\{\eta_i^j\}_{i\in I}$ for $j = 1, \ldots, q$ be the zero eigenvectors of the adjoint operator of M_{II}. Then, taking the inner product of equation (5.16) with $\{\eta_i^j\}_{i\in I}$ gives

$$\sum_I g(\epsilon)\beta_i'\eta_i^j = \sum_I \sum_J m_{ij} g(\epsilon)\alpha_j \eta_i^j + \sum_I \mu c_i \eta_i^j.$$

We now write $\beta_k' = e^{-\lambda_k P'}\alpha_k'$ for $k \in K$ and write $\alpha_j = e^{\lambda_j P}\beta_j$ for $j \in J$ to give

$$\sum_I g(\epsilon)\left(e^{-\lambda_i P'}\alpha_i'\right)\eta_i^j = \sum_I \sum_J m_{ij} g(\epsilon)\left(e^{\lambda_j P}\beta_j\right)\eta_i^j + \sum_I \mu c_i \eta_i^j,$$

and approximate $\alpha' \approx g(-\epsilon')\alpha^H$, $\beta \approx g(-\epsilon)\beta^H$ to give

$$\sum_I g(\epsilon)\left(e^{-\lambda_i P'}g(-\epsilon')\alpha_i^H\right)\eta_i^j \approx \sum_I \sum_{l\in J} m_{ij} g(\epsilon)\left(e^{\lambda_l P}g(-\epsilon)\beta_l^H\right)\eta_i^j + \sum_I \mu c_i \eta_i^j. \tag{5.20}$$

In exactly the same manner as in Chapter 2, this map is dominated by those eigenvalues closest to zero; in fact, the results of Chapter 2 extend exactly to this case. However, in this case we may also have symmetry effects modifying the behaviour of the map—one example of such a modification is given later in this chapter.

We may also approximately revert from this finite-dimensional map to a solution of the full Poincaré map. Given a solution $P = P' = \widetilde{P}$ of (5.20) we define

$$\widetilde{\alpha}_i = \alpha_i^H + M_{II}^{\perp^{-1}}\{e^{-\lambda_i \widetilde{P}}\alpha_i^H - \mu c_i - \sum_J m_{ij} e^{\lambda_j \widetilde{P}}\beta_j^H\} + \sum_{l=1}^{q} \Lambda_l w_i^l,$$

where $M_{II}^{\perp^{-1}}$ is the inverse of M_{II} on the space orthogonal to its zero eigenspace, and where $\Lambda_l w^l$ is the component in the direction of the zero eigenvector w^l. We have free choice of $q-1$ of these Λ_l, and the last is determined by the condition that $\{\widetilde{\alpha}_k\}_{k\in K}$ is on the surface Σ. From this we define

$$\widetilde{\beta}_j = \beta_j^H + \sum_{i\in I} m_{ji}(\widetilde{\alpha}_i - \alpha_i^H) + \sum_{l\in J} m_{jl} e^{\lambda_l \widetilde{P}}\beta_l^H + \mu c_j$$

to give an approximate solution $(\widetilde{P}, \{\widetilde{\alpha}_i\}_{i\in I}, \{\widetilde{\beta}_j\}_{j\in J})$ of the full Poincaré map (5.14).

5.3 Moving from Bounded to Unbounded Domains

In this section we consider the relationship between the results of this chapter and those of Chapter 3. We are essentially considering the limit as domain size tends to infinity; we will see that this corresponds to the limit as a Fourier series becomes a Fourier transform.

This limit is very important in practical applications. Any numerical simulation of a partial differential equation system will perforce be a finite-dimensional approximation to that system. Hence, we must consider the difference in expected behaviours between the two, and the conditions under which numerical results should simulate the full system.

We will compare the equation $A_t = N(A;\mu)$ on $[-L,L]$ and on $(-\infty,\infty)$ for scalar (possibly complex) $A(x,t)$ under the assumption that both cases possess the same symmetries. In practice, for the required impulse symmetry, this will usually mean the imposition of periodic boundary conditions on the finite domain case. We shall briefly work through the derivations of the finite dimensional maps in both cases, trying to maintain the structural similarity between expressions in the two cases.

The Poincaré map in the finite domain case was found above to be

$$\begin{aligned} \alpha_k &= e^{\lambda_k P}\beta_k, \\ g(\epsilon)\beta_k' - \beta_k^H &= \sum_{l\in K} m_{kl}(g(\epsilon)\alpha_l - \alpha_l^H) + \mu c_k, \end{aligned} \tag{5.21}$$

and the equivalent infinite domain map (3.42) from Chapter 3 was

$$\begin{aligned} \alpha(k) &= e^{S(k)P}\beta(k), \\ g^\beta(\epsilon)(\beta'(k)) - \beta^H(k) &= \int_{\mathbb{R}} M(k,l)\left[g^\alpha(\epsilon)(\alpha(l)) - \alpha^H(l)\right]\,dl + \mu c(k). \end{aligned} \tag{5.22}$$

In both cases, these maps were split in parts according to the stable and unstable eigenspaces of the linearization of the system at the origin. In the finite domain case, we defined an operator M_{II} on the space of I-tuples $\{\alpha_i\}_{i\in I}$; in the infinite domain case we defined an operator $\mathcal{M}_{UU}$ on the space of functions $f(k)$ defined for $k \in U$. A necessary condition for satisfaction of the Poincaré map was then shown to be

$$M_{II}\{g(\epsilon)\alpha_l - \alpha_l^H\}_{l\in I} = \left\{ g(\epsilon)\beta_i' - \sum_{l\in J} m_{il}g(\epsilon)\alpha_l - \mu c_i \right\}_{i\in I} \tag{5.23}$$

in the finite domain case and

$$\mathcal{M}_{UU}\left(g^{\alpha}(\epsilon)(\alpha(k))_U - \alpha_U^H(k)\right) = \left[g^{\beta}(\epsilon)(\beta'(k))\right]_U - \left\{\int_S M_U(k,l)g^{\alpha}(\epsilon)(\alpha(k))_U\,dl + \mu c_U(k)\right\} \tag{5.24}$$

in the infinite domain case.

In both cases we showed that the existence of q symmetries implies the existence of q exact solutions of the system linearized about the homoclinic orbit. In turn, these exact solutions corresponded to zero eigenfunctions of the operator M_{II} or $\mathcal{M}_{UU}$, and we let $\{\eta_i^j\}_{i\in I}$ and η_j for $j = 1,\ldots,q$ be the corresponding zero eigenvectors of the adjoint operators M_{II}^* and $\mathcal{M}_{UU}^*$ respectively.

By taking inner products in a suitable space, the previous two equations imply that

$$\sum_I g(\epsilon)\beta_i'\eta_i^j = \sum_I \sum_{l\in J} m_{il}g(\epsilon)\alpha_l\eta_i^j + \sum_I \mu c_i\eta_i^j \tag{5.25}$$

in the finite domain case, and

$$\int_U \left[g^{\beta}(\epsilon)(\beta'(k))\right]_U .\overline{\eta}_j(k)\,dk = \int_U\int_S M_U(k,l)g^{\alpha}(\epsilon)(\alpha_S(k)).\overline{\eta}_j(k)\,dl\,dk + \mu\int_U c_U(k).\overline{\eta}_j(k)\,dk \tag{5.26}$$

in the infinite domain case, for $j = 1,\ldots,q$ in both cases. Writing:

$$\beta_k' = e^{-\lambda_k P'}\alpha_k' \approx e^{-\lambda_k P'}g(-\epsilon')\alpha_k^H,$$
$$\alpha_j = e^{\lambda_j P}\beta_j \approx e^{\lambda_j P}g(-\epsilon)\beta_j^H \quad \text{for } j\in J$$

and

$$\beta'(k) = e^{-S(k)P'}\alpha'(k) \approx e^{-S(k)P'}g^{\alpha}(-\epsilon')\alpha^H(k),$$
$$\alpha_S(k) = e^{S(k)P}\beta_S(k) \approx e^{S(k)P}g^{\beta}(-\epsilon)\beta_S^H(k),$$

these become

$$\sum_I g(\epsilon)\left(e^{-\lambda_i P'} g(-\epsilon')\alpha_i^H\right)\eta_i^j = \sum_I \mu c_i \eta_i^j + \sum_I \sum_{l\in J} m_{il} g(\epsilon)\left(e^{\lambda_l P} g(-\epsilon)\beta_l^H\right)\eta_i^j$$

and

$$\int_{k\in U} g^\beta(\epsilon)\circ e^{-S(k)P'} I \circ g^\alpha(-\epsilon')(\alpha_U^H(k)).\overline{\eta}_j(k)\,dk = \mu\int_{k\in U} c_U(k).\overline{\eta}_j(k)\,dk + \int_{k\in U}\int_{l\in S} M_U(k,l)\, g^\alpha(\epsilon)\circ e^{S(l)P} I\circ g^\beta(-\epsilon)(\beta_S^H(l)).\overline{\eta}_j(k)\,dk\,dl \tag{5.27}$$

for $j = 1,\ldots,q$. These are now both in the form of finite-dimensional maps from (P,ϵ) to (P',ϵ'); we can clearly see the structural similarity between the finite and infinite domain cases.

We will now proceed to consider the asymptotic behaviours of these maps as the period P increases towards infinity; here, we will discover that the two alternatives produce different results. In order to do this, we must take a more specific example of each type.

We will assume that the system is one dimensional, has only two symmetries (namely time and space translation invariance) and that the finite domain system has a countable set of eigenfunctions given by $\{\sin(n\pi x/L)\}_{n=1}^\infty$, $\{\cos(n\pi x/L)\}_{n=0}^\infty$. Recalling that $\sigma(k)e^{ikx} = \mathcal{L}[0]e^{ikx}$, we then see that the corresponding eigenvalues for these eigenfunctions are $\sigma(n\pi/L)$ for both $\sin(n\pi x/L)$ and $\cos(n\pi x/L)$. These are arranged in the form

$$\{\lambda_k\}_0^\infty = \{\quad \sigma(0),\quad \sigma(\pi/L),\quad \sigma(\pi/L),\quad \sigma(2\pi/L),\quad \sigma(2\pi/L),\quad \ldots\},$$

$$\{v_k\}_0^\infty = \{\quad 1,\quad \sin(\pi x/L),\quad \cos(\pi x/L),\quad \sin(2\pi x/L),\quad \cos(2\pi x/L),\quad \ldots\},$$

and we see that the unstable and stable eigenspaces are

$$I = \left\{ i \in \mathbb{N} : \text{Re } \lambda_i = \text{Re } \sigma \left(\left\lfloor \frac{i+1}{2} \right\rfloor \pi/L \right) > 0 \right\},$$
$$J = \left\{ j \in \mathbb{N} : \text{Re } \lambda_j = \text{Re } \sigma \left(\left\lfloor \frac{j+1}{2} \right\rfloor \pi/L \right) < 0 \right\}$$

(where $\lfloor x \rfloor$ denotes the largest integer less than or equal to x), so that $2n \in I \Leftrightarrow (2n-1) \in I$ and $2m \in J \Leftrightarrow (2m-1) \in J$.

Recalling the form of the transformation of coefficients under the spatial translation symmetry as given in (5.12), we write the finite domain map as

$$\begin{aligned}
&\sum_{2n \in I} e^{-\sigma(n\pi/L)P'} \left\{ \left[\cos\left(\frac{n\pi(Q-Q')}{L} \right) \alpha^H_{2n-1} + \sin\left(\frac{n\pi(Q-Q')}{L} \right) \alpha^H_{2n} \right] \eta^j_{2n-1} \right. \\
&\quad \left. + \left[\cos\left(\frac{n\pi(Q-Q')}{L} \right) \alpha^H_{2n} - \sin\left(\frac{n\pi(Q-Q')}{L} \right) \alpha^H_{2n-1} \right] \eta^j_{2n} \right\} = \\
&\quad \mu \sum_I c_i \eta^j_i + \\
&\quad \sum_{2n \in I} \sum_{2m \in J} e^{\sigma(m\pi/L)P} \begin{pmatrix} m_{2n-1\ 2m-1} & m_{2n-1\ 2m} \\ m_{2n\ 2m-1} & m_{2n\ 2m} \end{pmatrix} \begin{pmatrix} \beta^H_{2m-1} \\ \beta^H_{2m} \end{pmatrix} . \begin{pmatrix} \eta^j_{2n-1} \\ \eta^j_{2n} \end{pmatrix}
\end{aligned} \tag{5.28}$$

for $j = 1, 2$, with $Q = \epsilon_2$. Under these conditions, we find that

$$g^\alpha(\epsilon) = g^\beta(\epsilon) = e^{ikQ}.$$

Writing $\sigma(k) = S(k)$ as before, we find that the infinite domain equation is

$$\begin{aligned}
\int_{k \in U} e^{-\sigma(k)P'} e^{ik(Q-Q')} \alpha^H_U(k) . \overline{\eta}_j(k)\, dk &= \mu \int_{k \in U} c_U(k) . \overline{\eta}_j(k)\, dk \\
&+ \int_{k \in U} \int_{l \in S} M_U(k,l)\, e^{\sigma(l)P} \beta^H_S(l) . \overline{\eta}_j(k)\, dk\, dl
\end{aligned} \tag{5.29}$$

for $j = 1, 2$. In both cases we now make approximations appropriate to the limit $P \to \infty$. For the finite domain case, as noted earlier, the map is dominated by those eigenvalues that are closest to zero. We let $N \in I$, $M \in J$ be such that

$\sigma(N\pi/L), \sigma(M\pi/L)$ are the eigenvalues with real parts closest to zero; then we approximate (5.28) by

$$e^{-\sigma_N P'}\left[a_j \cos\left(\frac{N\pi(Q-Q')}{L}\right) + b_j \sin\left(\frac{N\pi(Q-Q')}{L}\right)\right] = \mu + d_j e^{\sigma_M P}, \quad (5.30)$$

where we have written $\sigma_N = \sigma(N\pi/L)$, $\sigma_M = \sigma(M\pi/L)$.

The steepest descent approximations introduced in Chapter 4 are now applied to the map in the infinite domain case to yield

$$\sum_m \frac{c_{jm} e^{-i\omega_m P' + ik_m(Q-Q')}}{P'} = \sum_m \frac{d_{jm} e^{i\omega_m P}}{P} + \mu, \quad (5.31)$$

where we recall that $\sigma(k_m) = i\omega_m \in i\mathbb{R}$. If we assume for simplicity that the dispersion relation has only one root (although this assumption is unrealistic), we have

$$\frac{c_j e^{-i\omega_0 P'} e^{ik_0(Q-Q')}}{P'} = \mu + \frac{d_j e^{i\omega_0 P}}{P} \quad (5.32)$$

for $j = 1, 2$. The eigenvalues in the finite domain case are those with real parts closest to zero—we find that

$$N, M = \left\lfloor \frac{k_0 L}{\pi} \right\rfloor, \left\lceil \frac{k_0 L}{\pi} \right\rceil,$$

where $\lfloor x \rfloor$ denotes the largest integer less than or equal to x, and $\lceil x \rceil$ denotes the smallest integer greater than or equal to x. Hence for large L, we find that $\sigma_N \to 0_+ + i\omega_0$ and $\sigma_M \to 0_- + i\omega_0$ and we may approximate the finite domain map as

$$e^{-i\omega_0 P'}\left[a_j \cos\left(k_0(Q-Q')\right) + b_j \sin\left(k_0(Q-Q')\right)\right] = \mu + d_j e^{i\omega_0 P}. \quad (5.33)$$

The two maps given by equation (5.33) and equation (5.32) clearly have considerable structural similarity, as we might expect. However, we notice that the infinite domain case has the $1/P$ and $1/P'$ factors.

The presence of these factors is the fundamental difference between the finite-dimensional maps in the finite and infinite domain cases. This difference is caused by the different orders of the limits $L \to \infty$ and $P \to \infty$. In the finite domain case, for a fixed L however large, in the limit of $P \to \infty$ the sums over the eigenvalues will be dominated by the single eigenvalue with real part closest to zero. If we could hold P fixed and increase L then more of the eigenvalues would provide a contribution, tending to a continuous dispersion relation in the limit. In the infinite domain case we have already taken the limit $L \to \infty$ and so when we make approximations in the limit $P \to \infty$ we have a continuous dispersion relation whose integral is evaluated using the method of steepest descents, leading to the extra $1/P$ factor.

In any numerical simulation, we are perforce restricted to simulations of finite systems. It is worthwhile considering the conditions under which we may hope that such simulations provide a useful insight into the behaviour of equivalent infinite systems. Naïvely, we might expect that, if the spatial recurrence distance $Q - Q'$ is small compared to the domain size, edge effects would be reduced and that behaviour appropriate to the infinite domain case might appear. To make this insight more precise, we consider the left hand side of (5.28) in the form

$$S = \sum_{2n \in I} e^{-\sigma(n\pi/L)P'} e^{in\pi(Q-Q')/L} \chi_n. \tag{5.34}$$

We need to consider the conditions for large P' and L when the approximation

$$\lim_{P' \to \infty} S = e^{-\sigma(N\pi/L)P'} e^{iN\pi(Q-Q')/L} \chi_N$$

of S by just the dominant term becomes inappropriate. In this case, more terms of the sum contribute, and as $L \to \infty$ the sum becomes an approximation (Bender & Orszag [1978] §6.7) of the Riemann integral

$$\lim_{L \to \infty} S = \int_{k \in U} e^{-\sigma(k)P'} e^{ik(Q-Q')} \chi(k)\, dk,$$

which is the left hand side of (5.29). Continuing the limits, we see that

$$\lim_{L\to\infty}\lim_{P'\to\infty} S = \chi_N e^{-\sigma(k_0)P'} e^{ik_0(Q-Q')},$$
$$\lim_{P'\to\infty}\lim_{L\to\infty} S = \frac{\chi(k_0) e^{-\sigma(k_0)P'} e^{ik_0(Q-Q')}}{P'}.$$

The distinguishing feature between the two cases is the comparative size of the term $\sigma(n\pi/L)P'$. This in turn will depend upon the form of the dispersion relation $\sigma(k)$. If we assume that this dispersion relation is polynomial in k with highest power k^d, then the condition for multiple terms to contribute towards the sum S is that

$$P' \ll L^d, \tag{5.35}$$

which gives us a practical test to apply to numerical simulations.

5.4 Summary

In this chapter we have formally extended the finite dimensional results of Chapter 2 to countably infinite dimensional systems, namely partial differential equations on bounded domains. As usual, this study involved the creation of a Poincaré map in two parts, on surfaces near to the homoclinic point.

However, unlike the finite dimensional case, in this chapter we were able to examine the effects of symmetry considerations, in a similar manner to that of Chapter 3.

Having obtained this Poincaré map, we then reduced it to a finite-dimensional map in the same way as in chapters 2 and 3 for ordinary differential equations and

partial differential equations on unbounded domains respectively. As in Chapter 3, this finite-dimensional map had dimension equal to the number of continuous one-parameter symmetries of the system.

In Section 5.3, we directly compared the results of chapter 3 with those of this chapter, comparing the infinite domain case with the finite domain case in the limit as domain size tends to infinity. This yielded two maps with considerable structural similarity, but nonetheless with significant differences. On examination, this difference was found to stem from the order in which the limits of large domain size and large recurrence time were taken; this examination also yielded a practical criterion to apply to numerical results in order to determine which results are likely to be appropriate.

6 The Ginzburg-Landau Equation

In this chapter we consider the behaviour of one particular system, the Ginzburg-Landau equation. This equation arises in many different contexts, for example in hydrodynamic instability theory (Bretherton & Spiegel [1983]), chemical systems governed by reaction-diffusion systems (Kuramoto & Tsuzuki [1975]), as an example of a $\lambda - \omega$ system (Sherratt [1994]), in models of superconductivity (Tinkham [1975]) and in the nonlinear growth of convection rolls in the Rayleigh-Bénard problem. The equation is thus very general, and we will study it in isolation, without reference to any underlying physical system.

The Ginzburg-Landau equation is

$$A_t = \alpha A + \beta |A|^2 A + \gamma A_{xx} \tag{6.1}$$

for $A(x,t) \in \mathbb{C}$ with $\alpha, \beta, \gamma \in \mathbb{C}$. We find[1] that it has symmetries spanned by the vector fields ∂_x, ∂_t and $v\partial_u - u\partial_v$ for $A = u + iv$. In other words, we have time and space translation invariance together with a phase shift invariance. This phase shift invariance enables us to assume that $\alpha \in \mathbb{R}$ by replacing $A \mapsto e^{-\mathrm{Im}\ \alpha t} A$.

This equation is studied in Temam [1988] IV.5.1 and VI.7.1, where existence results for both the equation itself and the first variation equation used at (3.18) are shown. Results from particular parameter regimes of the system, taken with periodic boundary conditions, demonstrate finite dimensional behaviour (Doering *et al* [1988]), period doubling cascade behaviour (Keefe [1985]) and bifurcations to 2- and 3-tori (Takáč [1991]), thus displaying a wide range of the properties

[1] Using `MULIE`, Head [1991]

exhibited by nonlinear and chaotic systems. In this chapter, we study a parameterization of the system as given in Bretherton & Spiegel [1983], under the condition of large domain length.

In the first section, we calculate the form of the finite-dimensional map derived in chapters 3 and 4. This will leave us with several undetermined coefficients; in the second section, we examine numerical results from integrations of the system, in order to demonstrate the possibility of the existence of a homoclinic orbit, and in order to collate a set of data appropriate to fitting these undetermined coefficients. The third section will then discuss the method used to fit these coefficients, and the fourth section will use the values obtained to generate a bifurcation picture from the finite-dimensional map that may be compared to the actual numerical results.

6.1 Form of the Finite-Dimensional Map

We first apply the results of Chapter 3 to this equation, in order to determine the form of the finite-dimensional map that will govern the behaviour of periodic orbits of the system near to homoclinicity. The linearization of (6.1) at the origin is

$$\mathcal{L}[0]A = \alpha A + \gamma A_{xx}, \tag{6.2}$$

which gives the dispersion relation $\sigma(k) = \alpha - \gamma k^2$. Hence, provided $k_0^2 = \alpha/\gamma_R > 0$ we have

$$S = (-\infty, -k_0) \cup (k_0, \infty),$$

$$U = (-k_0, k_0).$$

We also notice that

$$\sigma(\pm k_0) = -i\frac{\gamma_I \alpha}{\gamma_R}$$

and as $\sigma'(k) = -2\gamma k$ we have

$$\sigma'(\pm k_0) = \mp 2\gamma \left(\frac{\alpha}{\gamma_R}\right)^{\frac{1}{2}}.$$

In the previous chapter, we applied the method of steepest descents to various integrals. This required us to deform the subsection S of the k-axis into a contour in a complex k-plane given by Im $\sigma(k) =$ constant. In this case, this is given by the hyperbola

$$k_R^2 + 2\frac{\gamma_R}{\gamma_I} k_R k_I - k_I^2 = \frac{\alpha}{\gamma_R}. \tag{6.3}$$

We thus deform $(-\infty, -k_0)$ into the lower section of the left half of this hyperbola (as indicated by AB on Figure 6.1), and deform (k_0, ∞) into the upper section of the right half of this hyperbola (indicated by ED).

Similarly, we want to deform U into a contour on which Im $\sigma(k) =$ constant, which is again the hyperbola (6.3). In this case we have the two sections marked BC and FE, together with the asymptote COF linking them, given by

$$\frac{k_I}{k_R} = \frac{\gamma_R}{\gamma_I} - \left(1 + \frac{\gamma_R^2}{\gamma_I^2}\right)^{\frac{1}{2}}.$$

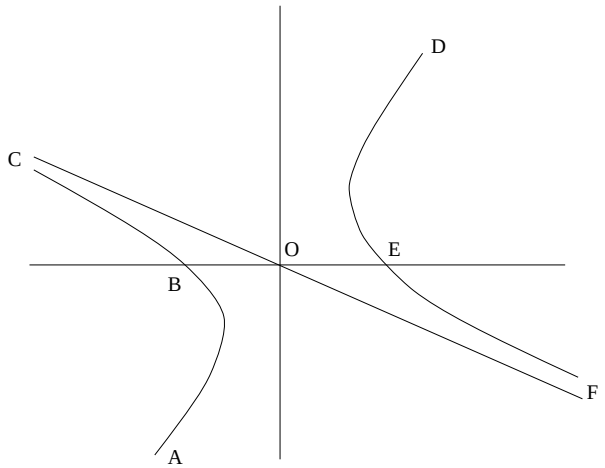

Figure 6.1 Steepest descent contours for the complex Ginzburg-Landau equation

As in Bretherton & Spiegel [1983], we consider the one parameter subfamily of the complex Ginzburg-Landau equation derived as a model of overstable two-dimensional thermohaline convection, with

$$\alpha = 1, \qquad \beta = i, \qquad \gamma = 1 + i(\mu + \mu_0) \tag{6.4}$$

(which has no additional point symmetries to those in the general case). The parameter μ_0 is included to allow us to shift μ so that the homoclinic orbit exists at $\mu = 0$. In this case, equation (6.1) becomes

$$A_t = A + i|A|^2 A + (1 + i(\mu + \mu_0))A_{xx}. \tag{6.5}$$

If we now consider the form of the finite-dimensional map derived in Chapter 4, we find that (4.10) becomes

$$\begin{aligned} \frac{c_{j1}e^{i\mu_0 P'}e^{ik_0 L - i(\theta' - \theta)}}{P'} + \frac{c_{j2}e^{i\mu_0 P'}e^{-ik_0 L - i(\theta' - \theta)}}{P'} = \\ \frac{d_{j1}e^{-i\mu_0 P}}{P} + \frac{d_{j2}e^{-i\mu_0 P}}{P} + \mu \end{aligned} \tag{6.6}$$

for $j = 1, 2, 3$, where

$$\begin{aligned} c_{j1} &= \frac{-w_j(k_0)}{2(1 + i\mu_0)}, \qquad & c_{j2} &= \frac{w_j(-k_0)}{-2(1 + i\mu_0)}, \\ d_{j1} &= \frac{y_j(k_0)}{2(1 + i\mu_0)}, \qquad & d_{j2} &= \frac{-y_j(-k_0)}{-2(1 + i\mu_0)}, \end{aligned} \tag{6.7}$$

and w_j, y_j are as in (4.5). We recall that $k_0 = 1$ here, and write $\Delta = \theta' - \theta$ and $D_j = d_{j1} + d_{j2}$ to obtain

$$\frac{c_{j1}e^{i\mu_0 P'}e^{i(L - \Delta)}}{P'} + \frac{c_{j2}e^{i\mu_0 P'}e^{-i(L + \Delta)}}{P'} = \frac{D_j e^{-i\mu_0 P}}{P} + \mu \tag{6.8}$$

for $j = 1, 2, 3$.

Recalling the results for non-symmetric, quadratic, real systems in Chapter 4, we see that the values of the coefficients c_{j1}, c_{j2}, D_j for $j = 1, 2, 3$ and μ_0 may well

have a significant effect on the bifurcation structure of the system. As such, we defer numerical investigation of the bifurcation structure of this map until we can provide some actual values for these coefficients.

6.2 Numerical Results

We have not so far shown any evidence of the existence of a homoclinic orbit for this system. An analytical proof of the existence of such an orbit would be very difficult; however, numerical results do provide some evidence of homoclinic behaviour. However, there are some difficulties associated with numerical integration of these equations.

We have performed multiple numerical simulations of the system with parameters as at (6.4), initially using a fixed timestep Crank-Nicholson method implemented by the present author in `C++`. The discretized version of (6.1) reads

$$\frac{A_j^{n+1} - A_j^n}{\Delta t} = \frac{1}{2}\left[(\alpha + \beta|A_j^n|^2)(A_j^{n+1} + A_j^n) + \frac{\gamma}{(\Delta x)^2}\left((A_{j+1}^{n+1} - 2A_j^{n+1} + A_{j-1}^{n+1}) + (A_{j+1}^n - 2A_j^n + A_{j-1}^n)\right)\right],$$

where $A_j^n = A(x_j, t_n)$ and Δt, Δx are the time and space step respectively. This gives a tridiagonal implicit system that may be solved using standard band-diagonal techniques (Press *et al* [1992] §2.4). The integration code imposed zero boundary conditions at $x = 0, L = 20$ and started with an initial condition of small amplitude noise.

For the parameter values (6.4) together with $\mu + \mu_0 = 1$, this reproduces the qualitative behaviour observed by Bretherton & Spiegel [1983] in their Figure 3

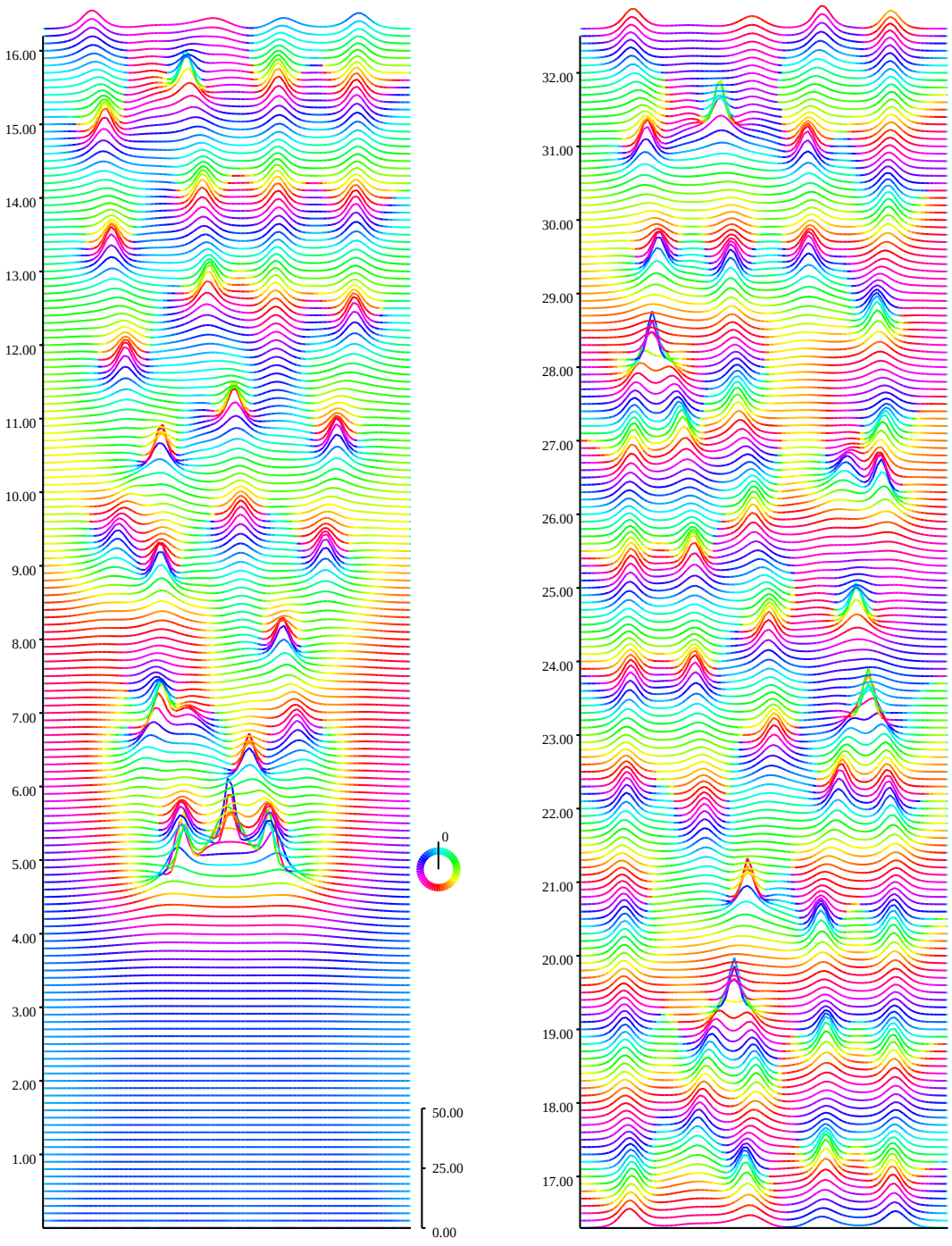

Figure 6.2 Numerical integration of the Ginzburg-Landau equation (6.5) with $\mu + \mu_0 = 1$ with zero boundary conditions at $x = 0, 20$, displaying aperiodic behaviour. Diagram was produced by a fixed timestep Crank-Nicholson method with $\Delta t = 0.005$. Time runs vertically up the page, with the height of the curve at each x given by $|A|^2$, and with the colour of the curve given by arg A.

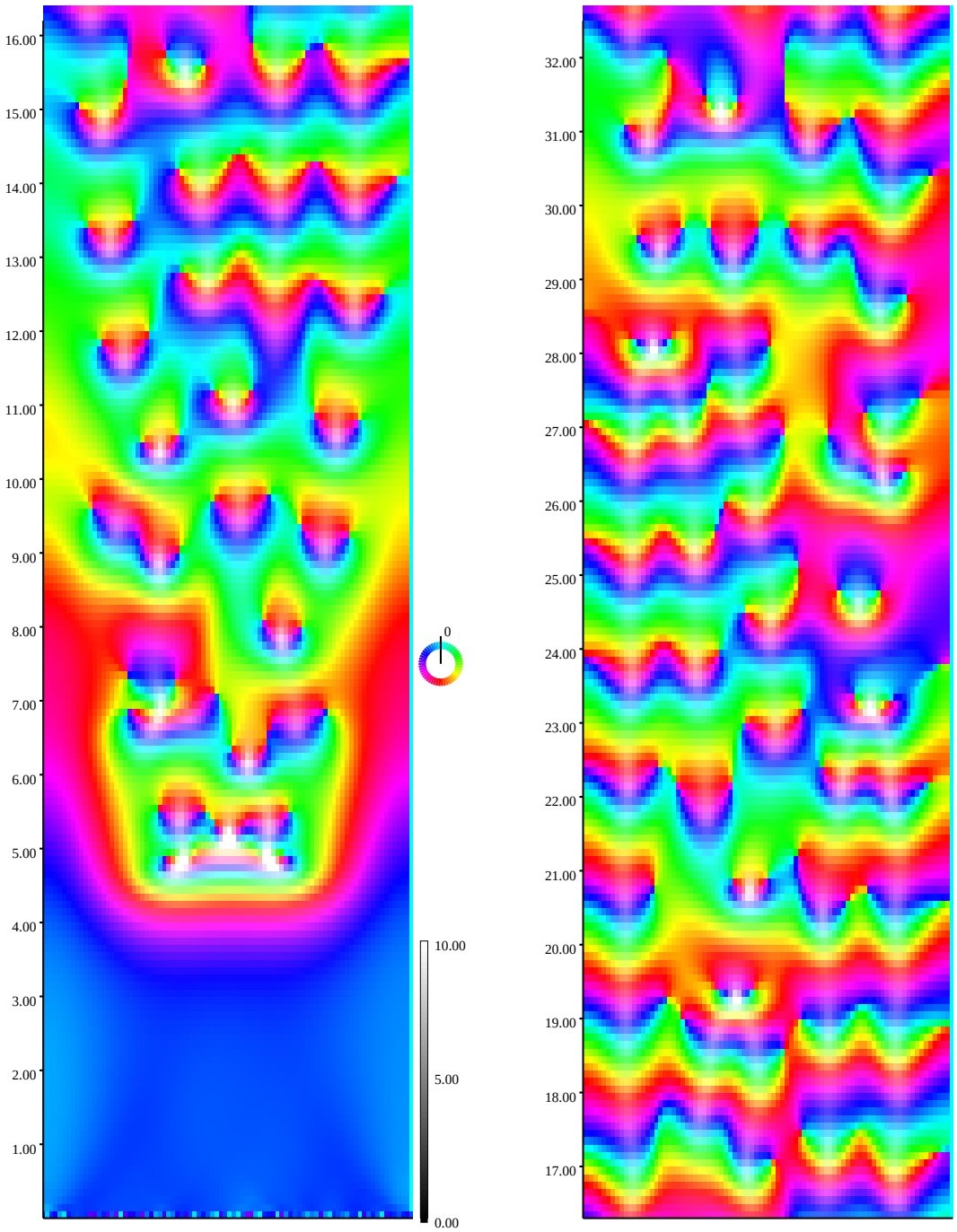

Figure 6.3 Alternative visualization of the previous diagram. Colour is used to represent the phase of the solution, with the intensity of the colour representing the norm.

(produced by a pseudo-spectral code). We would expect a homoclinic system to have aperiodic orbits that come close to the homoclinic orbit, and thus exhibit the sort of "pulse" behaviour shown in Figure 6.2 for $\mu + \mu_0 = 1$, $L = 20$.

We hope to simulate the behaviour of the equation on an infinite domain, and setting $L = 20$ is hardly infinite. However, when we examine (in Figure 6.4) the results of an integration with domain size $L = 200$, in a section $[100, 120]$, we see that the qualitative behaviour is the same, thus indicating that edge effects do not overly influence the results of the integration.

In addition to this Crank-Nicholson method, two other methods of integration were used, both taken from the NAG `FORTRAN` libraries. Both of these methods use the method of lines (Ames [1992] §1.9) to reduce the partial differential equation to a system of ordinary differential equations. The first method, NAG library routine `D03PGF`, then implements Gear's method to integrate these ordinary differential equations. The second method, NAG library routine `D03PCF`, implements a backwards differentiation formula method to integrate the ODEs. Both of these methods produced results at $\mu + \mu_0 = 1$ that were again qualitatively similar to those obtained with the Crank-Nicolson method and those depicted in Bretherton & Spiegel [1983].

Moreover, despite the complicated spatio-temporal structure observed in Figure 6.2, when these three methods were all started with the same initial condition (namely $A(x, 0) = (1 + i)e^{(x-10)^2}$), with the same gridsize ($N = 1025$) and the same timestep ($\Delta t = 0.001$), they remained in close correlation for a considerable period (relative to the timescale of "pulses"), as shown in Figure 6.5. Similarly, when intermediate values from one integration were used as starting points for

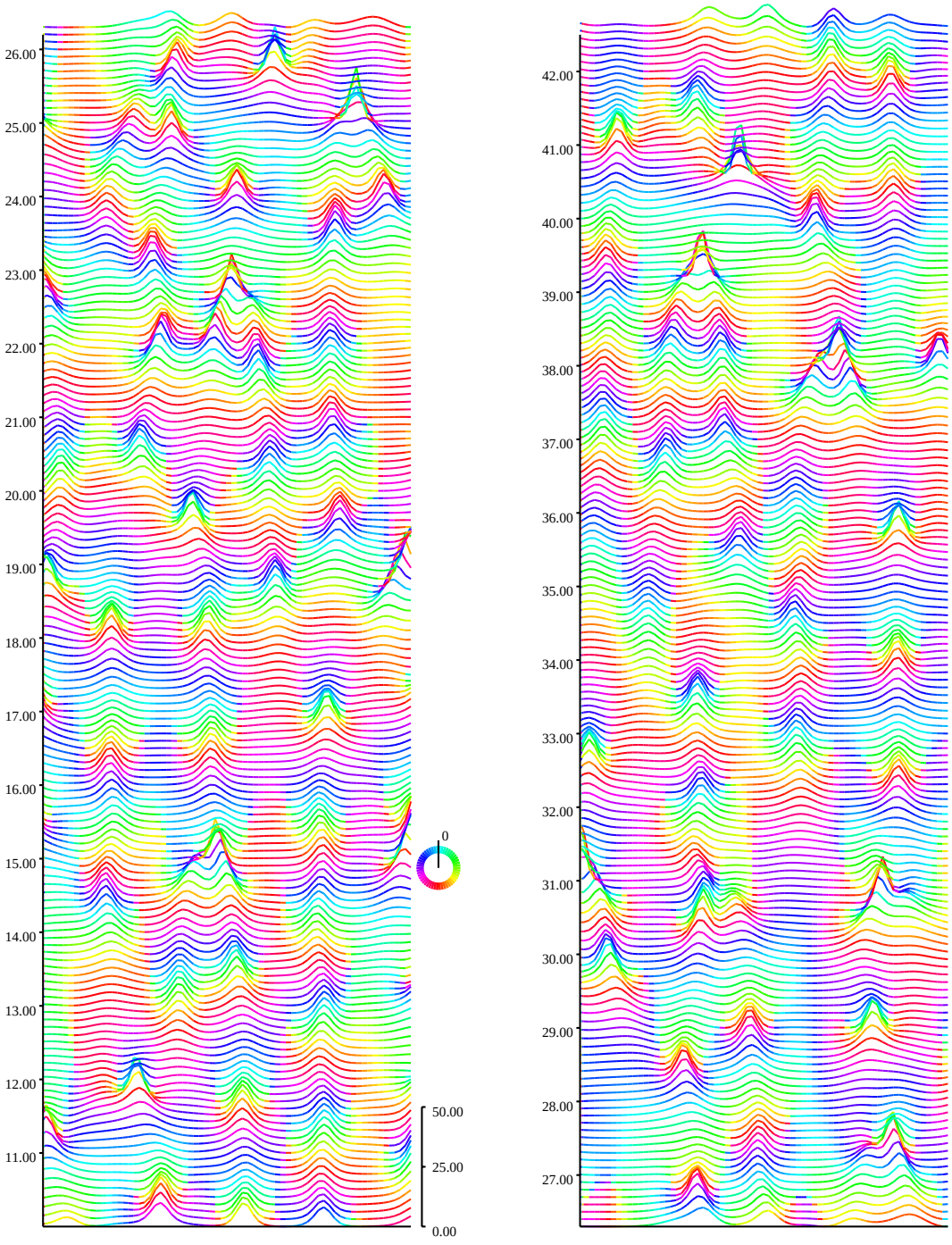

Figure 6.4 Numerical integration of the Ginzburg-Landau equation (6.5) with $\mu + \mu_0 = 1$, on the space domain $x \in [0, 200]$, depicting only the section $x \in [100, 120]$. Diagram was produced by a fixed timestep Crank-Nicholson method with $\Delta t = 0.005$.

the three integration methods, we again saw close correlation as shown in Figure 6.6.

We note, however, that these numerical results do not extend to larger parameter values. Integrations using the Crank-Nicholson method for $\mu + \mu_0 = 100$ did not match those in Bretherton & Spiegel [1983]; integrations of the system approached fixed point behaviour for large μ, and displayed periodic behaviour for values around $\mu + \mu_0 = 10$.

The alternative numerical simulation using `D03PGF` and Gear's method also produced different results from both the results given in Bretherton & Spiegel [1983] and from the results obtained with the Crank-Nicolson integrator, becoming numerically unstable so that at $\mu + \mu_0 = 100$ finite time blow-up was observed with this method. The third numerical method, using `D03PCF`, produced results at $\mu + \mu_0 = 100$ that were different again from any of the previously described simulations, giving spatio-temporally chaotic solutions.

However, since the methods all agree within the range of our investigations, we do not concern ourselves further with the inconsistencies observed at more extreme parameter values.

The integrations of the Ginzburg-Landau system (6.5) near $\mu + \mu_0 = 0$ produce aperiodic, "pulse"-like structures. Our hypothesis is that these pulses correspond to orbits of the system that are close to a homoclinic orbit, and which should therefore have space and time separations governed by the finite-dimensional map (6.8).

In order to attempt to compare the numerical results with the theoretical results, the following procedure was adopted. For a given value of $\mu + \mu_0$, the system

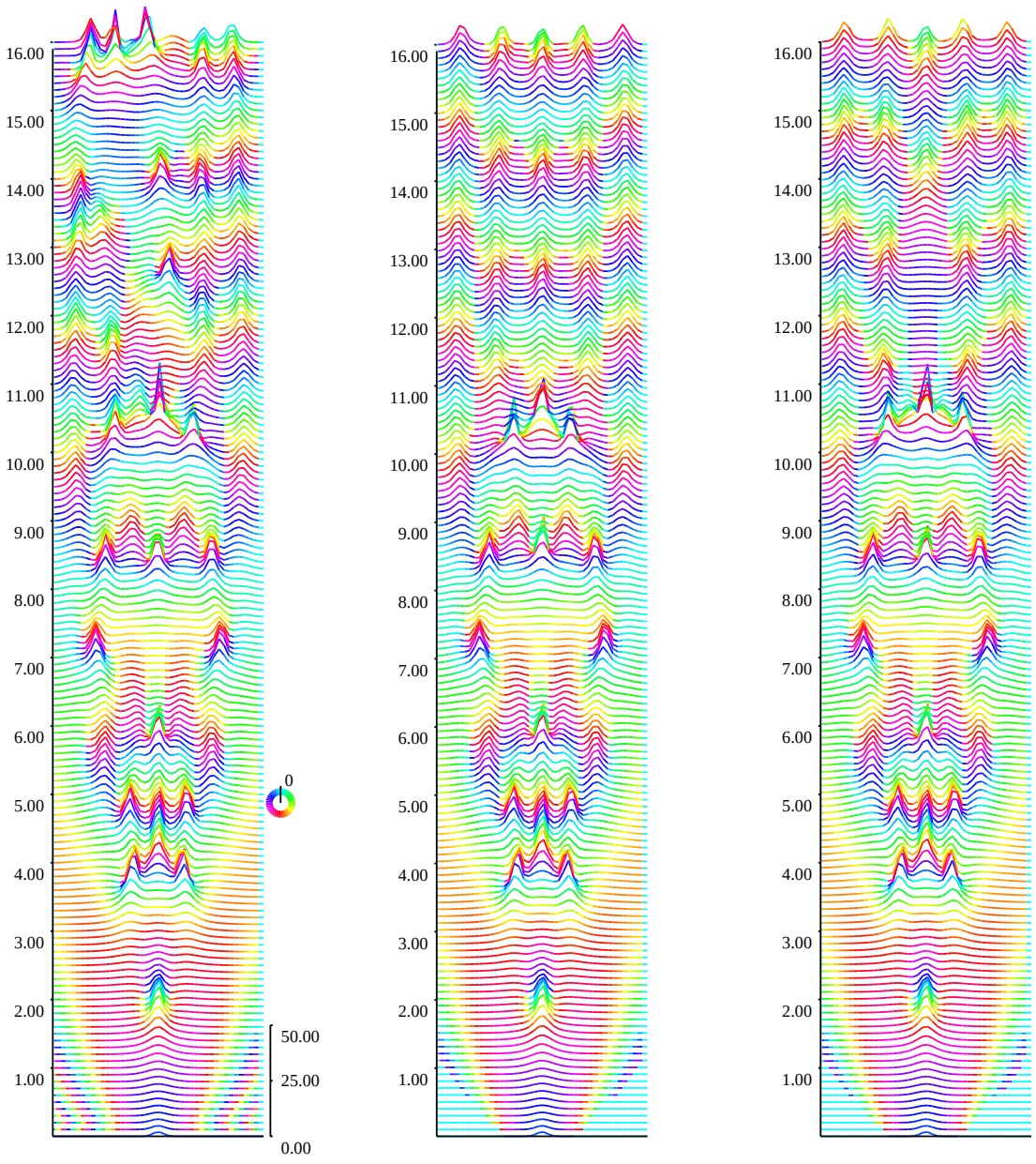

Figure 6.5 Numerical integrations of the Ginzburg-Landau equation (6.5) with $\mu + \mu_0 = 1$ and with zero boundary conditions, for three different integration methods. From left to right, these are: Crank-Nicholson method implemented in `C++`, NAG routine `D03PGF` using the method of lines and Gear's method, and NAG routine `D03PCF` using the method of lines and a backwards differentiation formula method, all with timestep 0.001 and 1025 gridpoints.

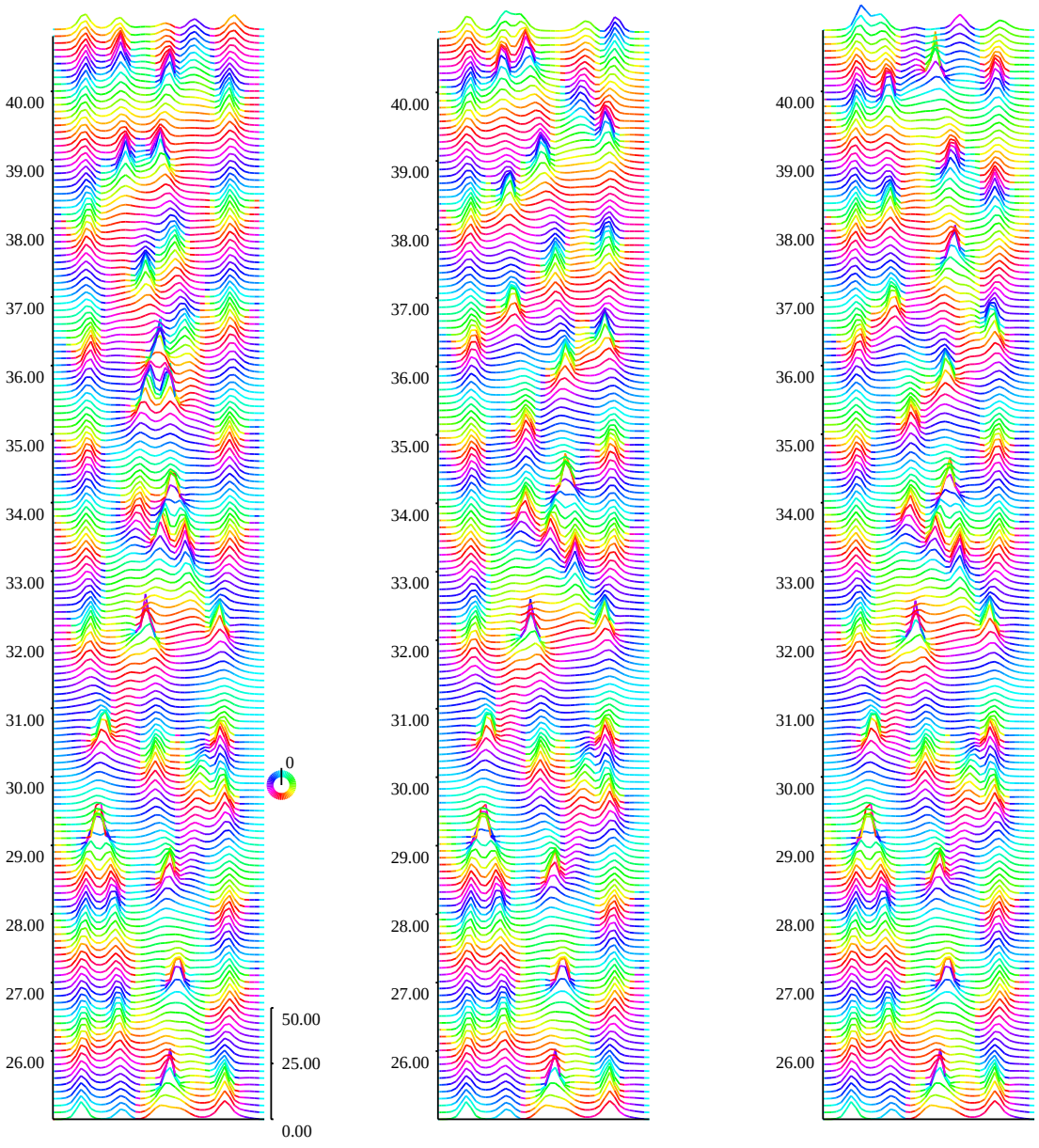

Figure 6.6 Numerical integrations of the Ginzburg-Landau equation (6.5) with $\mu + \mu_0 = 1$ and with zero boundary conditions, for three different integration methods, as in the previous diagram. In each case, the initial data was taken from a previous run of the Crank-Nicolson integrator.

was integrated forwards to $t = 70$ with the Crank-Nicolson integration system. The output from this integration was fed into a program that searched for local maxima, as depicted in Figure 6.7, where the dots indicate a local maximum in just the x direction (we shall call these "ridge points"), and the crosses indicate a local maximum in both the x and t directions.

We then attempt to determine recurrence times P between local maxima along a "ridge". We do this by attempting to follow the ridge between maxima, by looking for the nearest ridge point in the next timestep to the current ridge point. If the nearest ridge point is too far away from the current ridge point, we abandon the search for this local maximum. If the nearest ridge point is also a local maximum, we have found the connected local maximum, and we calculate the difference P in t values, and the difference L in x values.

These lists of P and L values for different μ values are then plotted. As the procedure described above is automatically implemented, the results are not as clear as they might be; owing to numerical fluctuations it is often the case that we have two local maxima apparently two time steps apart. Also, for long period recurrences we may well have a small local maximum between two large local maxima, leading to a smaller value of P than we would expect.

Regardless of these limitations, the data obtained is instructive. The orbit diagram of μ versus P is plotted in Figure 6.8 (whose grid-like structure is a symptom of the fixed timestep, and which has closer μ steps near to zero). This diagram clearly reveals decay in P with μ away from $\mu + \mu_0 = 0$.

Examination of the bifurcation structure of μ versus L reveals Figure 6.9, which has much less clear structure. We also note here that in terms of the criterion

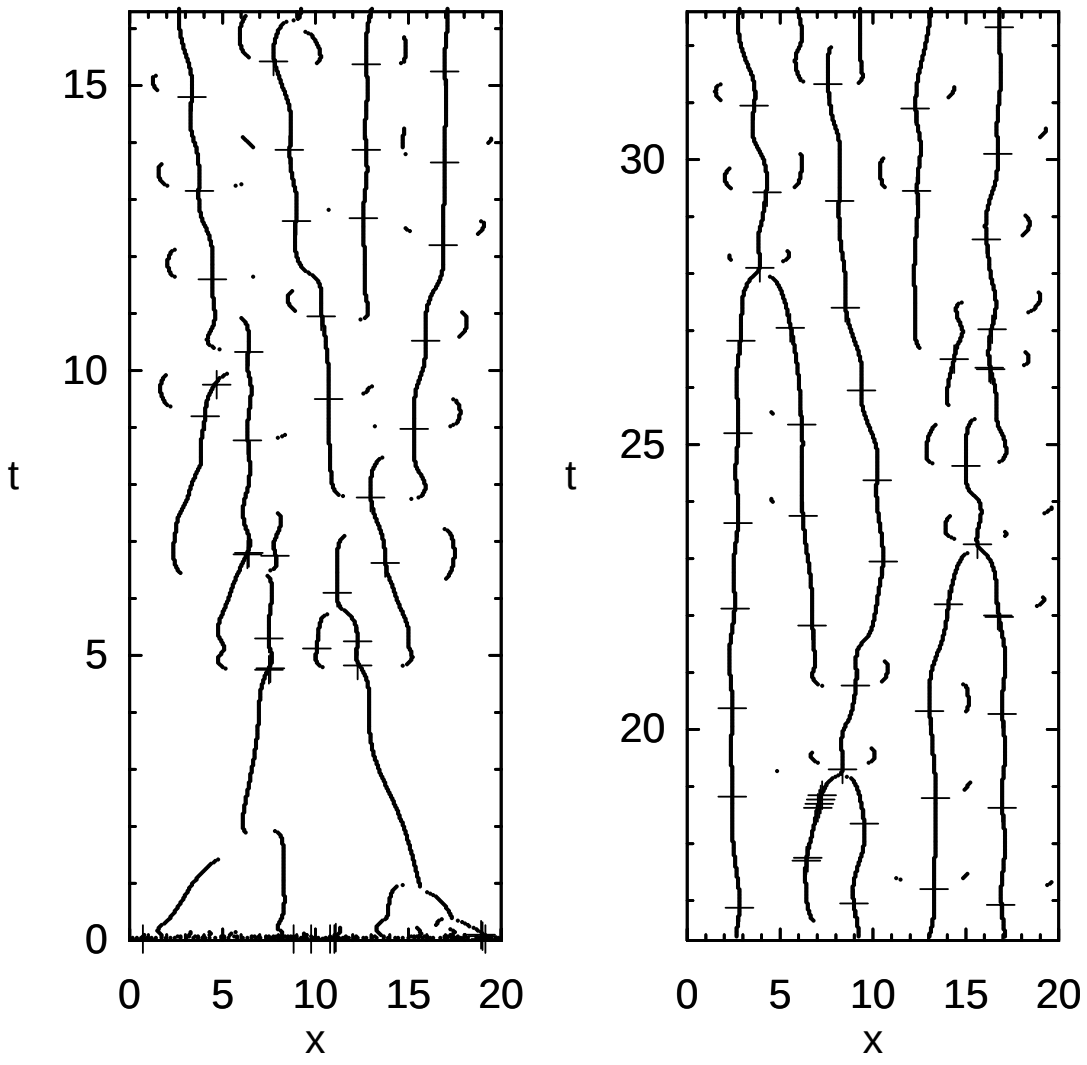

Figure 6.7 Local Maxima of Crank-Nicolson integration of the Ginzburg-Landau equation (6.1) with $\alpha = 1$, $\beta = i$, $\gamma = 1 + 10i$ and zero boundary conditions. Dots indicate local maxima in the x-direction, crosses indicate local maxima in both the x and t directions.

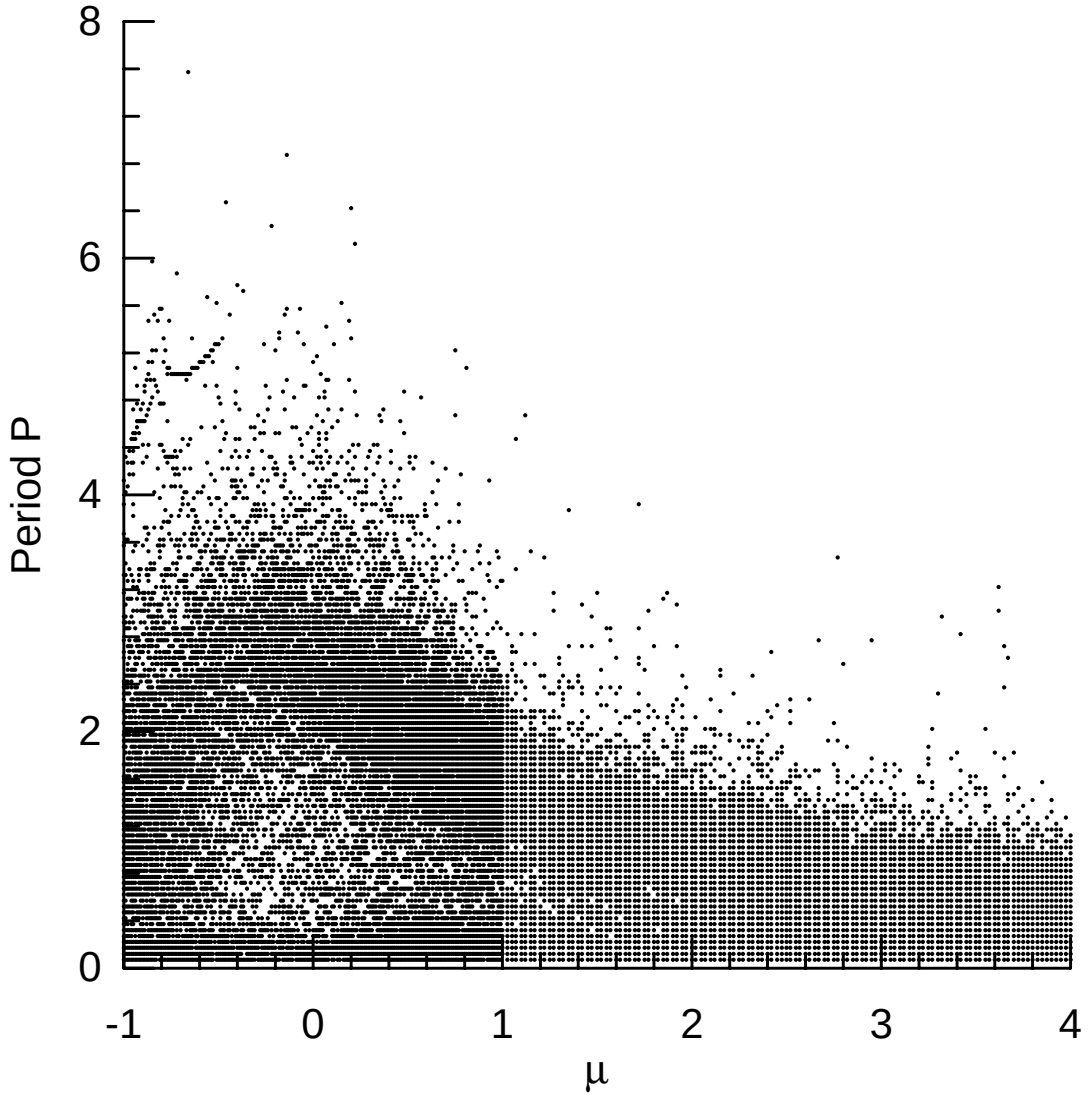

Figure 6.8 μ-P orbit diagram for Ginzburg-Landau system. A finer μ step was used near $\mu = 0$.

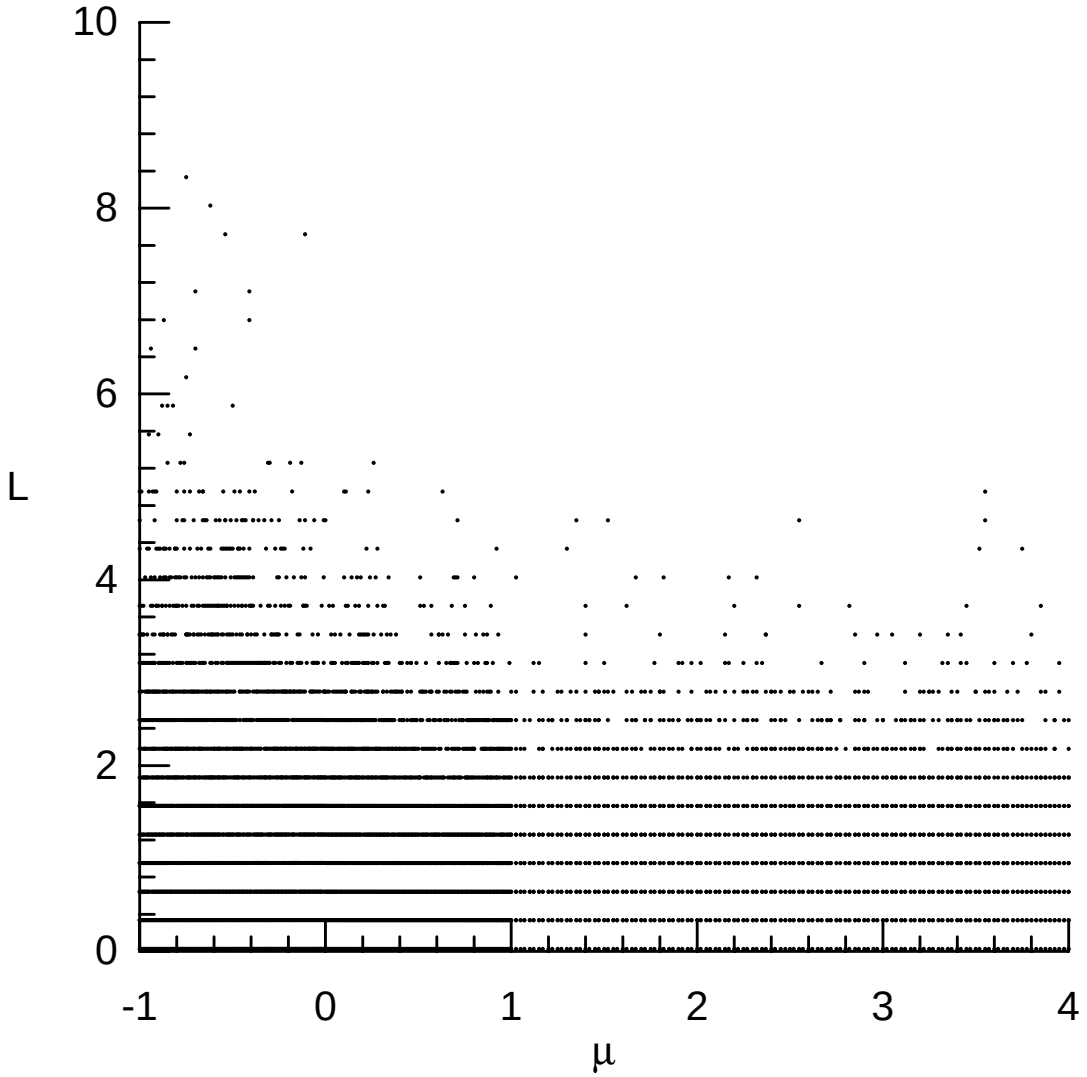

Figure 6.9 μ-L orbit diagram for Ginzburg-Landau system. A finer μ step was used near $\mu = 0$.

(5.35), we have a quadratic dispersion relation, giving $d = 2$, the spatial domain size is $L = 20$ and that the observed P and P' values are in the range $[0, 10]$. Hence we see that

$$P \ll L^d, \tag{6.9}$$

so that we should expect to see behaviour governed by the infinite domain case finite-dimensional map (6.8).

6.3 Parameter Fitting

We use the numerical results of the previous section to return to the problem previously deferred, that of finding values for the coefficients c_{j1}, c_{j2} and D_j for $j = 1, 2, 3$ and μ_0. We construct a list of observed results in the form $(\mu, P; P', L, \Delta)$, using the methods of the previous section, which we then use to fit the model (6.8).

The fitting method used is an adapted Levenberg-Marquardt method, based around that described in Press *et al* [1992] §15.5. Complications are introduced, however, because here we are trying to fit a function $\mathbf{f}{:}\mathbb{R}^2 \to \mathbb{R}^3$ from $(\mu, P) \mapsto (P', L, \Delta)$ that is defined implicitly by the finite-dimensional map equations (6.8) for $j = 1, 2, 3$, and which depends on the unknown coefficients as parameters.

We write $\mathbf{x} = (\mu, P)$ and $\mathbf{y} = (P', L, \Delta)$, so that our list of observed values is $(\mathbf{x}_i, \mathbf{y}_i)$ for $i = 1, \ldots, N$. We define a χ^2 merit function by

$$\chi^2(\mathbf{a}) = \sum_{i=1}^{N} \|\mathbf{y}_i - \mathbf{f}(\mathbf{x}_i; \mathbf{a})\|^2 \tag{6.10}$$

where

$$\mathbf{a} = (c_{11}, c_{21}, c_{31}, c_{12}, c_{22}, c_{32}, D_1, D_2, D_3, \mu_0) \in \mathbb{R}^M,$$

with $M = 19$, since we consider parameters in $\mathbb{C}$ as being in $\mathbb{R}^2$. Our aim is to minimize the function $\chi^2(\mathbf{a})$ over $\mathbf{a}$. If we are at parameter values $\mathbf{a}_{\rm cur}$ that are close to a minimum, we expect to be able to approximate $\chi^2(\mathbf{a})$ in a quadratic form:

$$\chi^2(\mathbf{a}_{\rm cur} + \mathbf{a}) \approx \gamma - \mathbf{d}.\mathbf{a} + \frac{1}{2}\mathbf{a}.\mathbf{D}.\mathbf{a}, \tag{6.11}$$

where $\gamma = \chi^2(\mathbf{a}_{\rm cur})$, $-\mathbf{d}$ is the M-dimensional gradient vector at $\mathbf{a}_{\rm cur}$, and $\mathbf{D}$ is the $M \times M$ Hessian matrix at $\mathbf{a}_{\rm cur}$. If this is an accurate approximation, we can jump straight to the minimizing value $\mathbf{a}_{\rm min}$ of $\mathbf{a}$ by using the inverse of the Hessian matrix:

$$\mathbf{a}_{\rm min} = \mathbf{a}_{\rm cur} + \mathbf{D}^{-1}.\left[-\nabla\chi^2(\mathbf{a}_{\rm cur})\right]. \tag{6.12}$$

On the other hand, if (6.11) is a poor approximation, we may take steepest descent steps of the form:

$$\mathbf{a}_{\rm next} = \mathbf{a}_{\rm cur} - \text{constant} \times \nabla\chi^2(\mathbf{a}_{\rm cur}). \tag{6.13}$$

In either case, we need first to calculate the gradient $\mathbf{d}$ and Hessian matrix $\mathbf{D}$ of $\chi^2(\mathbf{a})$. From (6.10), we see that the gradient vector is

$$\frac{\partial\chi^2}{\partial a_k} = -2\sum_{i=1}^{N}(\mathbf{y}_i - \mathbf{f}(\mathbf{x}_i;\mathbf{a})).\frac{\partial\mathbf{f}}{\partial a_k}(\mathbf{x}_i;\mathbf{a}) \tag{6.14}$$

and the Hessian matrix is

$$\frac{\partial^2\chi^2}{\partial a_k \partial a_l} = 2\sum_{i=1}^{N}\left[\frac{\partial\mathbf{f}}{\partial a_k}(\mathbf{x}_i;\mathbf{a}).\frac{\partial\mathbf{f}}{\partial a_l}(\mathbf{x}_i;\mathbf{a}) - (\mathbf{y}_i - \mathbf{f}(\mathbf{x}_i;\mathbf{a})).\frac{\partial^2\mathbf{f}}{\partial a_k \partial a_l}(\mathbf{x}_i;\mathbf{a})\right]. \tag{6.15}$$

Under the assumption that the model is accurate, the second of the terms in this sum, that involving the second derivative of $\mathbf{f}$, may be ignored, and we will use the approximation

$$\frac{\partial^2\chi^2}{\partial a_k \partial a_l} = 2\sum_{i=1}^{N}\left[\frac{\partial\mathbf{f}}{\partial a_k}(\mathbf{x}_i;\mathbf{a}).\frac{\partial\mathbf{f}}{\partial a_l}(\mathbf{x}_i;\mathbf{a})\right]. \tag{6.16}$$

Thus, in order to calculate the gradient and Hessian of the χ^2 function, we must first calculate $\partial\mathbf{f}/\partial a_k$ for $k = 1, \ldots, M$. Since f is only defined implicitly, by equations (6.8), this involves the solution of more implicit equations. Writing (6.8) as

$$\mathbf{g}(\mathbf{x}, \mathbf{y}; \mathbf{a}) = \mathbf{0}$$

and setting $\mathbf{y} = \mathbf{f}(\mathbf{x}; \mathbf{a})$ we see that the relevant equations are

$$\frac{\partial \mathbf{g}}{\partial a_k} + \left(\frac{D\mathbf{g}}{D\mathbf{y}}\right) . \frac{\partial \mathbf{f}}{\partial a_k} = 0,$$

and are linear in $\partial\mathbf{f}/\partial a_k$, so that we have

$$\frac{\partial \mathbf{f}}{\partial a_k} = -\left(\frac{D\mathbf{g}}{D\mathbf{y}}\right)^{-1} . \frac{\partial \mathbf{g}}{\partial a_k}.$$

The Levenberg-Marquardt method combines the inverse Hessian method (6.12) together with the steepest descent method (6.13). To do this, we write

$$\alpha_{jj} = \frac{1+\lambda}{2} \frac{\partial \chi^2}{\partial a_j^2}$$
$$\alpha_{jk} = \frac{1}{2} \frac{\partial \chi^2}{\partial a_k \partial a_j} \qquad (j \neq k)$$

and then solve the system

$$\sum_{l=1}^{M} \alpha_{kl} \Delta a_l = \frac{-1}{2} \frac{\partial \chi^2}{\partial a_k}$$

for $k = 1, \ldots, M$. When λ is large, the diagonal terms of the matrix $[\alpha]$ are dominant, and we are solving

$$\Delta a_l = \text{constant} \times \frac{\partial \chi^2}{\partial a_k},$$

which is just the steepest descent method (6.13). On the other hand, when λ is small, we are solving

$$\sum_{l=1}^{M} \frac{\partial^2 \chi^2}{\partial a_k \partial a_l} \Delta a_l = \frac{-\partial \chi^2}{\partial a_k},$$

which is the inverse Hessian method (6.12).

The choice of the parameter λ is then controlled as follows. At each iteration, we examine whether the proposed step $\Delta\mathbf{a}$ in parameters causes an increase or a decrease in the merit function χ^2. If it causes an increase, so that $\chi^2(\mathbf{a}+\Delta\mathbf{a}) \geqslant \chi^2(\mathbf{a})$, then we increase λ by some factor (say 10), in order to favour the steepest descent method more, and try again. If the step in parameter space causes an improvement in the merit function, that is $\chi^2(\mathbf{a}+\Delta\mathbf{a}) \leqslant \chi^2(\mathbf{a})$, then we reduce λ by the same factor, and moreover take the step in parameter space $\mathbf{a} \leftarrow \mathbf{a}+\Delta\mathbf{a}$. The iteration is terminated when a step is taken that only reduces χ^2 by a negligible amount.

These techniques for parameter fitting were applied to a set of N=16,560 points $(\mu, P; P', L, \Delta)$, obtained as described in the previous section. Because of the large dimension of the parameter space to be searched, several hundred different sets of random starting values were used in the parameter fitting. As the best fit obtained, this yielded the parameter values:

$$\begin{array}{lll} c_{11} = -2.53 - 7.56i & c_{12} = -8.61 - 7.59i & D_1 = -10.49 - 9.29i \\ c_{21} = -1.90 + 3.02i & c_{22} = -4.44 - 8.54i & D_2 = -7.26 - 8.86i \\ c_{31} = -4.31 - 10.66i & c_{32} = -1.58 - 8.08i & D_3 = -4.63 - 4.90i \end{array} \tag{6.17}$$

with $\mu_0 = 0.0771459$, which we use from now on.

The underlying assumption of this chapter is that the Ginzburg-Landau system (6.5) has a homoclinic orbit at $\mu = 0$. Now that we have determined a value for μ_0, we can attempt to obtain a rough approximation to such an orbit. In order to do this, we perform an integration starting from initial data of low amplitude noise. This initial data will then grow in magnitude in the directions appropriate to the unstable eigenspace, and map out an orbit close to the homoclinic orbit as

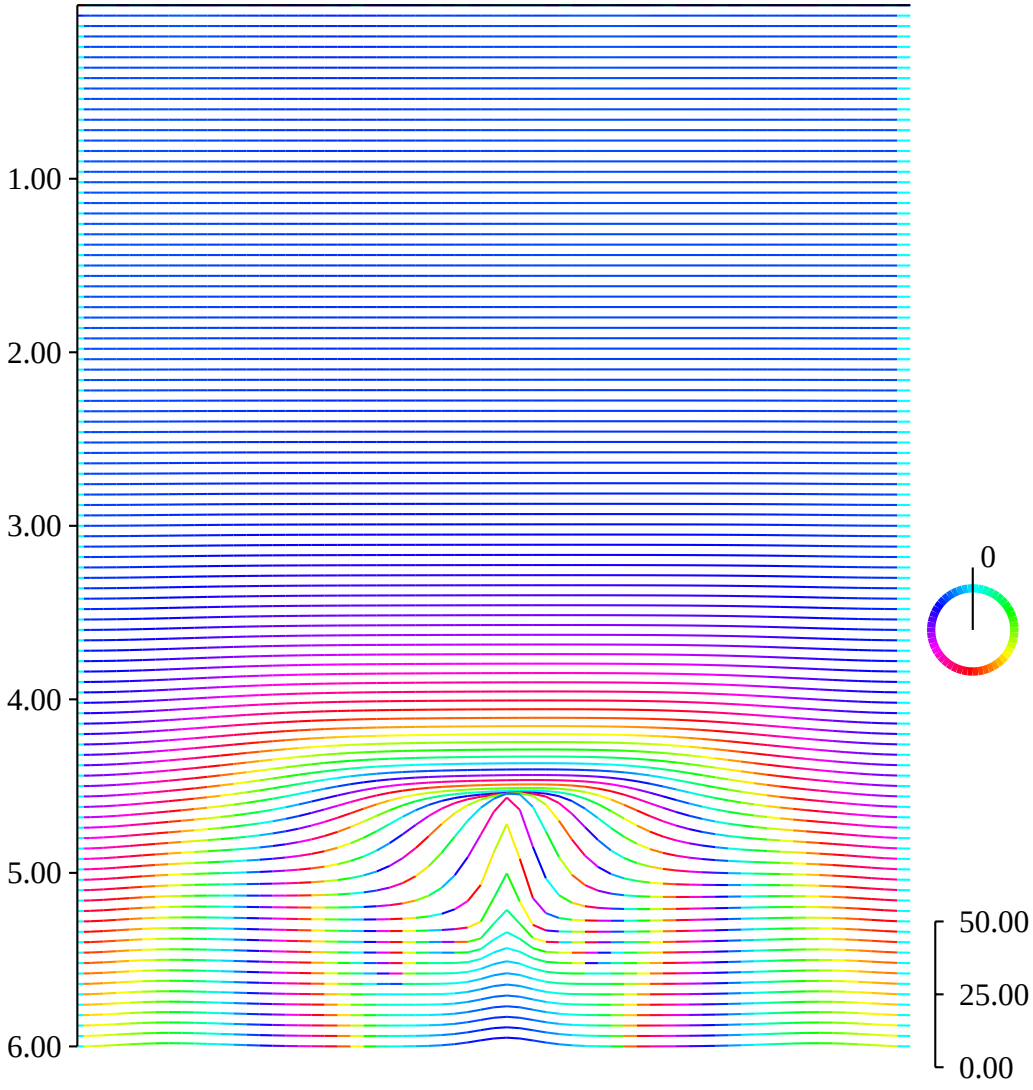

Figure 6.10 Numerical integration of the Ginzburg-Landau equation (6.5) with $\mu + \mu_0 = \mu_0$ from (6.17) and with zero boundary conditions, using a Crank-Nicolson integration method. This integration should be close to the underlying homoclinic orbit.

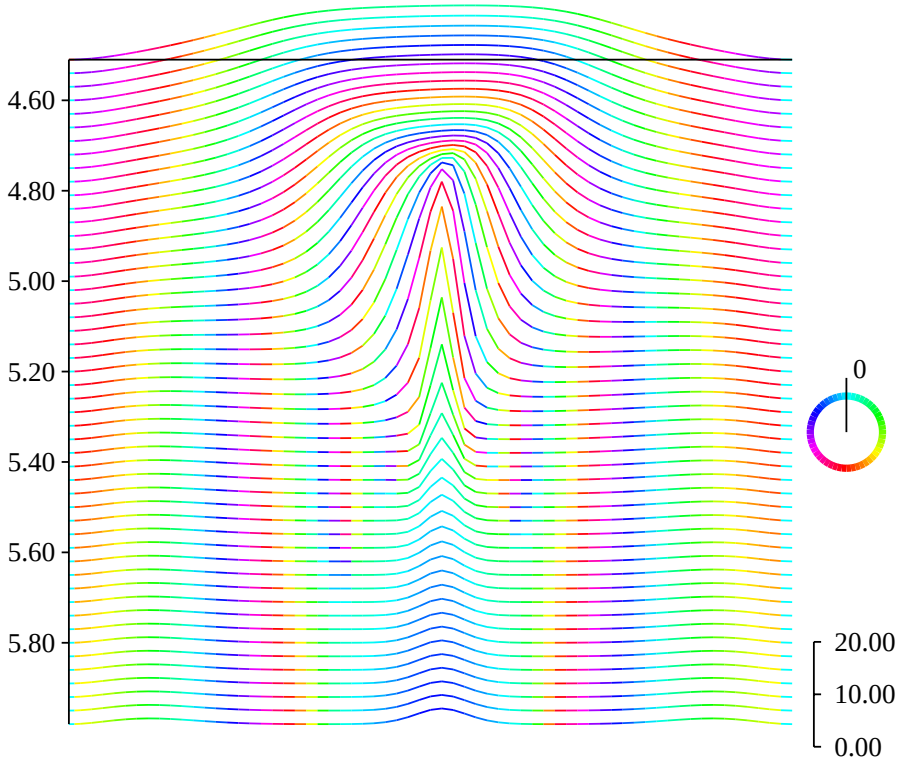

Figure 6.11 Closer examination of the previous diagram.

depicted in Figure 6.10 and Figure 6.11; the maximum value of $|A(x,t)|$ at each timestep is shown in Figure 6.12. This is clearly an *ad hoc* method, but may yield some indication of the possible shape of the homoclinic orbit.

6.4 Finite-Dimensional Map Results

Now that we have a set of feasible parameter values, we can now examine the theoretical bifurcation structure of the finite-dimensional map (6.8):

$$\frac{c_{j1}e^{i\mu_0 P'}e^{i(L-\Delta)}}{P'} + \frac{c_{j2}e^{i\mu_0 P'}e^{-i(L+\Delta)}}{P'} = \frac{D_j e^{-i\mu_0 P}}{P} + \mu.$$

This will not generally have fixed points with $P' = P$, $L = \Delta = 0$, but it may have fixed points with $P' = P$, $L \neq 0$, $\Delta \neq 0$ corresponding to modulated travelling

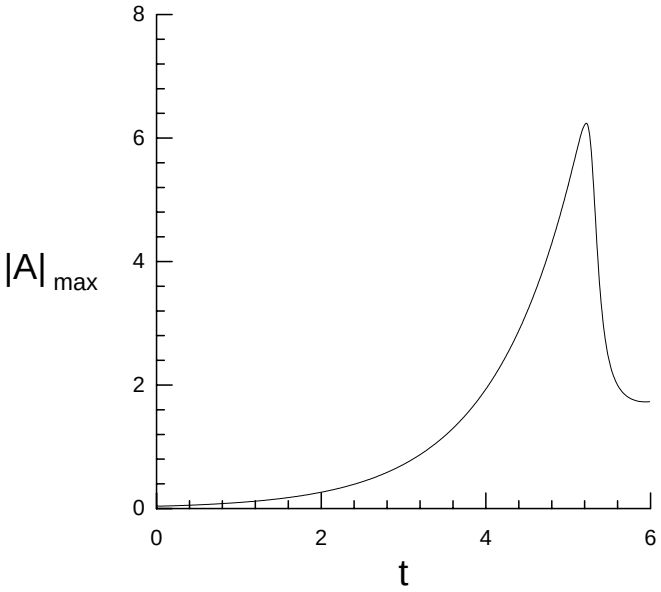

Figure 6.12 Plot of the maximum value of $|A(x,t)|$ for each timestep, from the preceding two diagrams.

waves, which will have $\mu \sim P^{-1}$ as $P \to \infty$. Thus we seek solutions $(\mu; P, L, \Delta)$ of

$$c_{j1}e^{i\mu_0 P}e^{i(L-\Delta)} + c_{j2}e^{i\mu_0 P}e^{-i(L+\Delta)} = D_j e^{-i\mu_0 P} + \mu P \tag{6.18}$$

for $j = 1, 2, 3$.

We have numerically investigated the existence of these fixed points, using the bifurcation-following techniques and software described in Doedel [1986], and in Chapter 4. In this case, we are no longer investigating the fixed points of a one-dimensional map $P \mapsto P'$, but instead searching for solutions with $P = P'$ of a map $P \mapsto (P', L, \Delta)$. This map is defined implicitly by the three equations (6.8); the continuation equations equivalent to equations (4.30) then give a four-dimensional root finding problem, which we again solve with a globally convergent Newton's method.

This investigation yields bifurcation diagrams as depicted in Figure 6.13 and

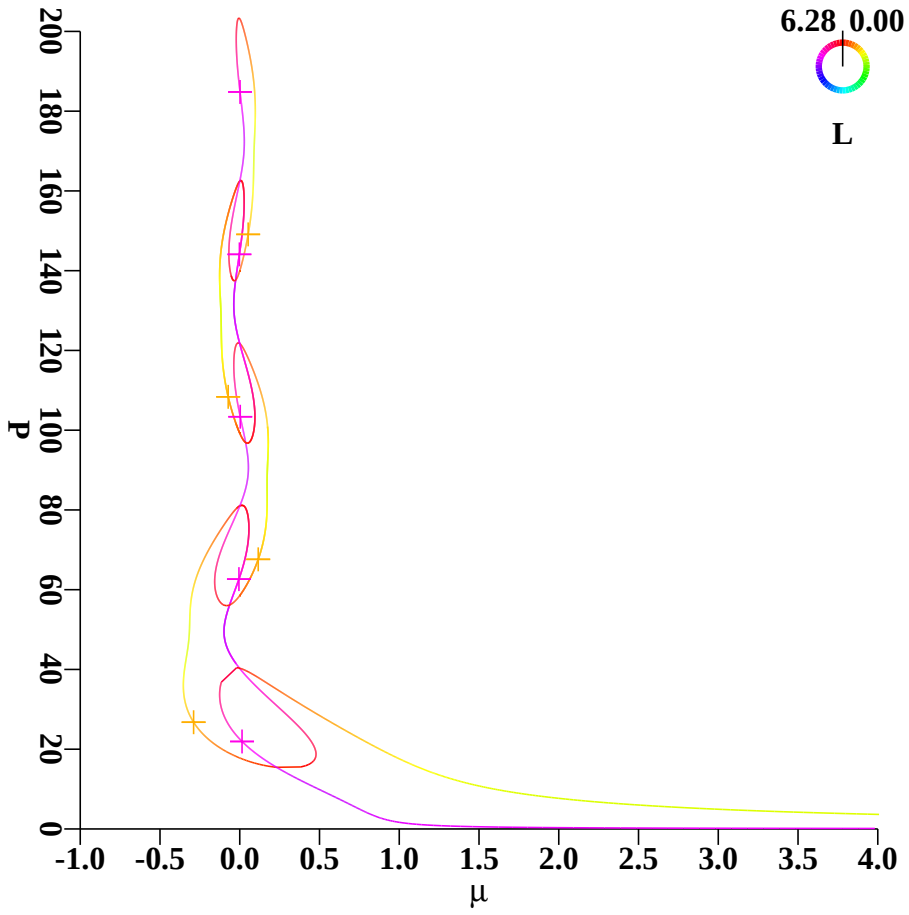

Figure 6.13 μ-P bifurcation diagram for Ginzburg-Landau system (6.18), where colour indicates the value of L, and where crosses indicate Hopf bifurcation points.

Figure 6.15. In Figure 6.13, we show the μ-P bifurcation diagram, with colour being used to indicate the value of L. We note from (6.18) that L is only defined modulo 2π, hence we use colour as an angular variable. This diagram has an interesting sequence of overlapping isolas extending up the $\mu = 0$ axis, together with the lowest branch which sweeps out to higher μ values. These structures are similar to a combination of two of the bifurcation structures shown in Chapter 4, those in Figure 4.8 and Figure 4.9. However, in practice only behaviour near

to the bifurcation branch with lowest P values will be observed, as evinced by comparison of this branch with the numerical integration data shown in Figure 6.8. This lowest branch is more closely examined in Figure 6.14.

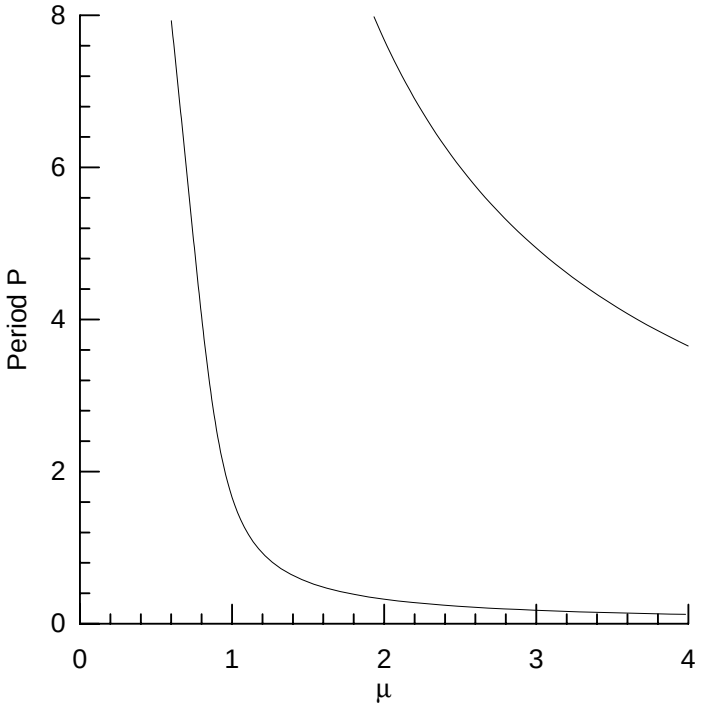

Figure 6.14 Closer examination of the lowest branch of the bifurcation diagram, for comparison with Figure 6.8.

When we plot the μ-P-L bifurcation diagram in Figure 6.15, we see that these isolas are interlocking and do not intersect, forming a chain up the $\mu = 0$ axis. Thus, in contrast to the cases studied in Chapter 4, the L component is not just a function of P but is of vital importance in understanding the shape of the bifurcation diagram. We also include on Figure 6.15 an indication of the value of Δ at each point on a branch, given by the colour. Again, by examining (6.18), we see that Δ is only defined modulo 2π, and we use colour as an angular variable.

On both Figure 6.13 and Figure 6.15, the crosses indicate Hopf bifurcation points,

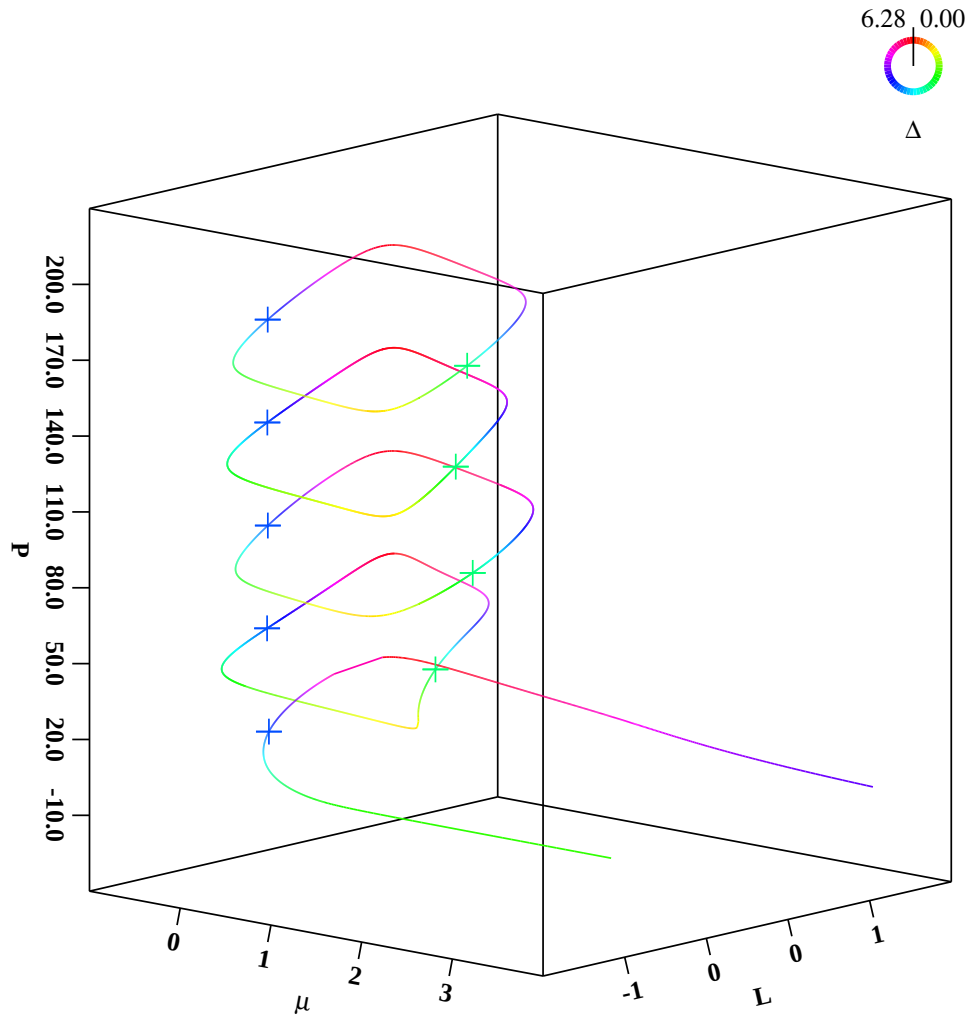

Figure 6.15 μ-P-L bifurcation diagram for Ginzburg-Landau system (6.18), where the colour indicates the phase of Δ. Crosses indicate Hopf bifurcation points.

where a complex conjugate pair of eigenvalues of the Jacobian of (6.18) cross the imaginary axis, yielding an invariant circle in (P, L, Δ) space (see Wiggins [1988] §3.2C, where such bifurcations are referred to as Naimark-Sacker bifurcations).

To see how the fixed points of the map arise, we may produce, for each fixed μ, a picture of the map $P \mapsto P'$ induced by (6.8). This is created numerically, and yields maps as shown in Figure 6.16 for a range of parameter values. The alternative values of P' on the map correspond to different L values.

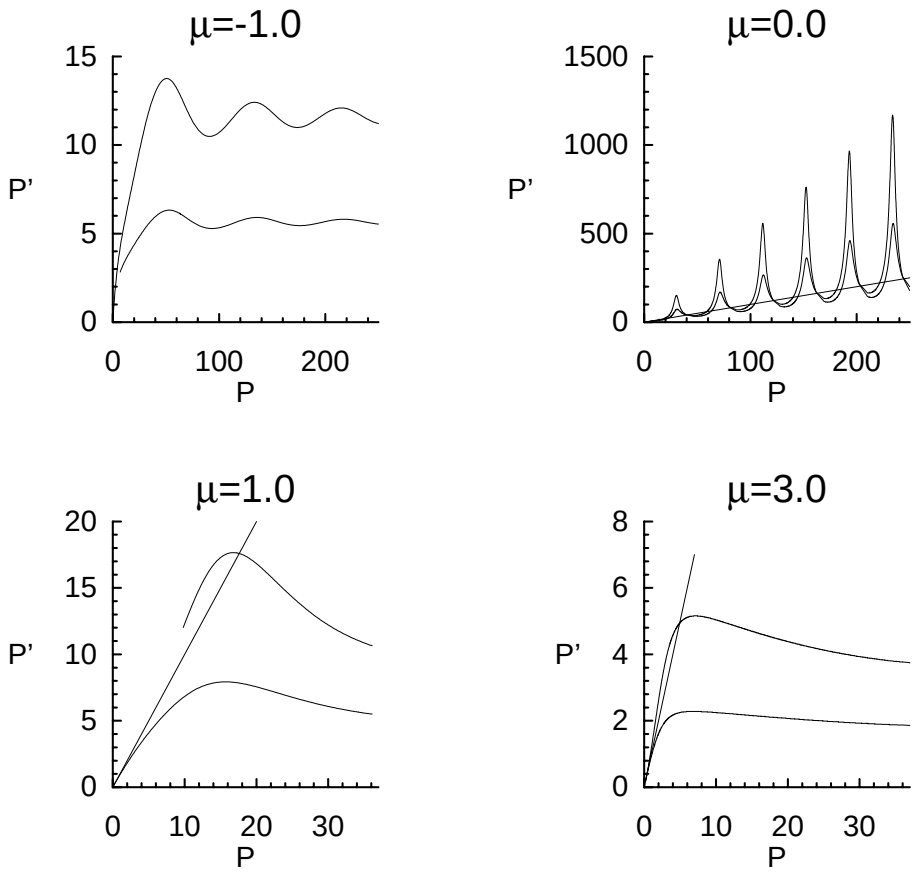

Figure 6.16 Numerically calculated map $P \mapsto P'$ induced by the finite-dimensional map (6.8) at various μ values. Where appropriate, the line $P' = P$ is also marked.

6.5 Summary

In this chapter we have tried to apply the theoretical results of Chapter 3 to a specific example, the complex Ginzburg-Landau equation. We have used a particular parameterization of the one-dimensional Ginzburg-Landau equation, taken from Bretherton & Spiegel [1983], that gives numerical results displaying spatio-temporal chaos in a manner consistent with the hypothesis of an underlying homoclinic orbit.

In the first section, we produced the finite-dimensional map for the system with the methods described in Chapter 4. However, this map (equation (6.8)) had a number of undetermined coefficients. In Chapter 4 we saw that the values of coefficients in such finite-dimensional maps can have a significant effect on the bifurcation diagrams produced, so we deferred further investigation of the map until some suitable values for these coefficients could be found.

In the second section, we presented some numerical results obtained from integrations of the system, together with a description of the method used to convert such integration data into recurrence coordinates $(\mu, P; P', L, \Delta)$ appropriate to the finite-dimensional map.

The third section described the method used to fit the unknown coefficients of the finite-dimensional map, using the numerical data obtained in the previous section. We used a standard nonlinear model fitting method, the Levenberg-Marquardt method. However, this did involve some numerical complications due to the form of the map (6.8) being fitted and the number of parameters being fitted.

Finally, the fourth section used the coefficient values obtained in the third section together with the finite-dimensional map (6.8) from the first section to obtain a bifurcation diagram. This diagram showed correspondence with the numerical recurrence data, and moreover displayed an interesting chain of interlocking isolas, extending up the P axis.

7 Conclusions

In the present work, we have studied homoclinic bifurcations, one of the most important global bifurcation phenomena occurring in parameterized dynamical systems. There are standard techniques for analysing homoclinic bifurcations in specific low-dimensional and general n-dimensional ordinary differential equations. The main thrust of this work has been the formal extension of these techniques to a class of partial differential equations, with special attention paid to symmetry considerations.

The standard method of attack for homoclinic systems in ordinary differential equations is the creation of a Poincaré return map. To create this map, we consider two Poincaré surfaces close to the homoclinic point. We create an inside map between the two surfaces, which is governed by the behaviour of the equations linearized at the homoclinic point. We also create an outside map, where we assume that we are close enough to the homoclinic orbit (in both phase space and parameter space) to linearize about the homoclinic orbit, giving an affine map. The composition of these two maps gives a Poincaré return map on one of the two Poincaré surfaces.

Having obtained this return map, we can examine its behaviour. In the specific low-dimensional cases previously studied this behaviour has been comprehensively analysed, to give a full bifurcation structure together with information about the existence of horseshoes, subsidiary homoclinic orbits, secondary bifurcations and so on. The essentials of this material were summarized in Chapter 1.

In the case of general n-dimensional ODEs, as studied in Chapter 2, such detail is beyond us. However, we deduced the primary bifurcation structure by reducing

the return map to a one-dimensional map, using approximations suggested by the geometry of the system. This one-dimensional map involved the return time between successive visits to the Poincaré surface, and from it we deduced the shape of the bifurcation curve of the principal periodic orbit.

These techniques were extended to a suitable class of partial differential equations in Chapter 3, by considering these PDEs as evolution equations in a suitable function space, and then extending the concepts of Poincaré maps to these spaces. This extension involved considerably more technicalities, including those concerning the effects of symmetries.

Upon considering this class of partial differential equations, we discovered that the symmetries of the equations play a much more important rôle than in ordinary differential equations. In ordinary differential equations, a continuous one-parameter group of symmetries will in general reduce the order of the equation by one. Thus, only specific cases of discrete symmetries can be considered (and in fact, few symmetries other than representations of $\mathbb{Z}_2$ have been studied). However, in our given class of partial differential equations, we have two one-parameter symmetry groups, namely time and space translation invariance, and we may well have more (notably phase shift invariance, in the case of complex valued equations such as the Ginzburg-Landau equation). Thus, any homoclinic orbit is non-unique in this case—a symmetry translation of the homoclinic orbit is still an orbit and is still homoclinic. This had important consequences for the construction of the Poincaré return map.

For the inside map, in the region where we assume the flow is governed by the equations linearized about the homoclinic point, these symmetries have no effect.

However, for the outside map, we produced an approximation under the assumption that points start, and remain, close to the homoclinic orbit. Since we have a family of symmetry-transform related homoclinic orbits, to be returned to the Poincaré surface, a point need only start near to any one of this family, not just the specific instance of the homoclinic orbit we have chosen.

In fact, we inverted this—instead of thinking of our starting point for the outside map as being close to a symmetry transform of the specific homoclinic orbit, we considered a symmetry transform of our starting point to be close to the homoclinic orbit. Thus, our full Poincaré map involved not only the return time between successive visits to the Poincaré surface, but also the symmetry transform parameters needed to move orbits to be close to our specific homoclinic orbit.

In Chapter 4, we then approximated this Poincaré map by a finite-dimensional map, in an analogous manner to the reduction to a one-dimensional map in the ordinary differential equation case. This finite-dimensional map involved the return time between visits to the Poincaré surface, together with the symmetry transform parameters. The time translation invariance of the system occupied a special place, essentially corresponding to the return time, so that overall we had a finite-dimensional map whose dimension corresponded to the number of one-parameter continuous symmetry groups that the equation is invariant under. Two of the simplest examples of this finite-dimensional map were also considered, yielding a remarkable range and complexity of results.

The most important feature of the map produced for partial differential equations is the algebraic decay in the period as the parameter moves away from its homoclinic value, as opposed to the exponential decay encountered for ordinary

differential equations. If we think of the behaviour in the ODE case as being governed by the least unstable eigenvalue of the linearization at the origin, we see an indication of why, in the continuous spectrum case, this behaviour is altered. An example providing clear confirmation of this result would provide strong support for the results of Chapter 3

In addition to the infinite domain partial differential equations studied in Chapter 3, we also considered the finite domain case in Chapter 5. Here, we assumed the existence of a countable, complete set of orthonormal eigenfunctions of the system linearized about the homoclinic point. As such the analysis of the system became similar to the analysis of general n-dimensional systems of ordinary differential equations in Chapter 2, but here dealing with countably infinite matrices. However, in this case, the effect of continuous symmetry groups could legitimately be considered, giving a finite-dimensional map with considerable structural similarity to that produced in the infinite domain case.

The boundary between the two cases, finite and infinite domain, was also briefly explored. We sought and found a practical criterion for distinguishing when each case would be applicable in an approximation of an infinite domain system. This criterion is invaluable for the consideration of any numerical simulation of an infinite domain system, which must necessarily be finite.

Chapter 6 then attempted to apply these results to the Ginzburg-Landau equation. This equation is a canonical example of a nonlinear partial differential equation displaying spatio-temporally chaotic behaviour. Although no homoclinic orbit could be found explicitly, numerical integrations of the system display behaviour that we would expect of such systems.

As demonstrated in Chapter 4, the specific values of coefficients in the finite-dimensional map may significantly alter the bifurcation structure. Hence the first procedure to be performed on data taken from numerical integrations of the Ginzburg-Landau equation was that of fitting these coefficients. This involved an algorithm for reducing the full integration data to recurrence coordinates, followed by an adapted Levenberg-Marquardt method to fit the coefficients. This numerical data was also plotted in Figure 6.8, for later comparison with the bifurcation diagram.

Having obtained the necessary coefficients for the finite-dimensional map, we then produced a bifurcation diagram for the map. The bifurcation diagram introduced an interesting chain of interlocking isolas, that required full use of μ-P-L bifurcation space to unravel the loops. This was in contrast to the examples in Chapter 4, where L was fully determined as a function of P.

In addition to this chain of isolas, the bifurcation diagram also had a branch sweeping out to higher μ values. This branch had lower P values, and corresponded to the previously obtained numerical data.

Homoclinic bifurcations are an organizing centre in chaotic ordinary differential equations. The present work involved the creation of analogous results for partial differential equations. This has involved considerably more technical problems than in the ODE case. The results thus obtained, although themselves difficult to apply, have shown a great variety of bifurcation behaviours in even simple cases. When applied to the Ginzburg-Landau equation, these methods have yielded results which correlate with numerics, and which give a possible indication of the underlying reasons for the complexity of spatio-temporal behaviour observed.

Bibliography

Ames W.F. [1992], "Numerical methods for partial differential equations", *Academic Press*

Arnéodo A., P.Coullet & C.Tresser [1981], "A possible new mechanism for the onset of turbulence", *Phys. Lett.* **81A**, *197–201*

Arnéodo A., P.Coullet, E.Spiegel & C.Tresser [1985], "Asymptotic chaos", *Physica* **14D**, *327–347*

Bedford T. & J.Swift [1988], "New directions in dynamical systems", *LMS lecture notes 127, C.U.P.*

Bender C.M. & S.A.Orszag [1978], "Advanced mathematical methods for scientists and engineers", *McGraw-Hill*

Blázquez C.M. [1986], "Bifurcation from a homoclinic orbit in parabolic differential equations", *Proc. Roy. Soc. Edinburgh* **103A**, *265–274*

Bretherton C.S. & E.A.Spiegel [1983], "Intermittency through modulational instability", *Phys. Lett.* **96A**, *152–156*

Carrier G.F., M.Krook & C.E.Pearson [1966], "Functions of a Complex Variable", *McGraw-Hill*

Chow S.N. & B.Deng [1989], "Bifurcation of a unique stable periodic orbit from a homoclinic orbit in infinite-dimensional systems", *Trans. Am. Math. Soc.* **312**, *539–587*

Coddington E.A. & N.Levinson [1955], "Theory of Ordinary Differential Equations", *McGraw-Hill*

Deng B. [1989], "The Shil'nikov Problem, Exponential Expansion, Strong λ-Lemma, C^1-Linearization, and Homoclinic Bifurcation", *J. Diff. Eqns.* **79**, *189–231*

Devaney R.L. [1989], "An Introduction to Chaotic Dynamical Systems, 2nd edition", *Addison-Wesley*

Doedel E. [1986], "`AUTO`: Software for Continuation and Bifurcation Problems in Ordinary Differential Equations", *Applied Mathematics, California Institute of Technology*

Doering C.R, J.D.Gibbon, D.D.Holm & B.Nicolaenko [1988], "Low-dimensional behaviour in the complex Ginzburg-Landau equation", *Nonlinearity* **1**, *279–309*

Feigenbaum M.J. [1978], "Quantitative universality for a class of nonlinear transformations", *J. Stat. Phys.* **19**, *25*

Feigenbaum M.J. [1979], "The universal metric properties of nonlinear transformations", *J. Stat. Phys.* **21**, *669*

Feigenbaum M.J. [1980], "Universal Behaviour in Nonlinear Systems", *Los Alamos Science* **1**, *4–27*

Fowler A.C. [1990a], "Homoclinic bifurcations in n dimensions", *Studies in Applied Math.* **83**, *193–209*

Fowler A.C. [1990b], "Homoclinic bifurcations for partial differential equations in unbounded domains", *Studies in Applied Math.* **83**, *329–353*

Fowler A.C. & C.Sparrow [1991], "Bifocal homoclinic orbits in four dimensions", *Nonlinearity* **4**, *1159–1182*

Gaspard P. & G.Nicolis [1983], "What can we learn from homoclinic orbits in chaotic dynamics?", *J. Stat. Phys.* **31**, *499–518*

Gaspard P. [1984a], "Generation of a countable set of homoclinic flows through bifurcation", *Phys. Lett.* **97A**, *1–4*

Gaspard P. [1984b], "Generation of a countable set of homoclinic flows through bifurcation in multidimensional systems", *Bull. Class. Sci. Acad. Roy. Belg. Serie 5* **LXX**, *61–83*

Gaspard P., R.Kapral & G.Nicolis [1984], "Bifurcation phenomena near homoclinic systems : a two-parameter analysis", *J. Stat. Phys.* **35**, *697–727*

Glendinning P. [1984], "Bifurcations near homoclinic orbits with symmetry", *Phys. Lett.* **103A**, *163–166*

Glendinning P. [1988], "Global bifurcations in flows", *in Bedford & Swift [1988], 120–149*

Glendinning P. [1989], "Subsidiary bifurcations near bifocal homoclinic orbits", *Math. Proc. Camb. Phil. Soc.* **105**, *597–605*

Glendinning P. & C. Sparrow [1984], "Local and global behaviour near homoclinic orbits", *J. Stat. Phys.* **35**, *645–696*

Gottlieb D. & S.P.Orszag [1977], "Numerical analysis of spectral methods : theory and applications", *SIAM*

Guckenheimer J. & P.J.Holmes [1983], "Nonlinear oscillations, dynamical systems and bifurcations of vector fields", *Springer-Verlag*

Hartman P. [1982], "Ordinary differential equations, 2nd edition", *Birkhäuser, Basle*

Head A.K. [1991], "`MULIE`", *IBM PC software*

Holmes P.J. [1980], "A strange family of three-dimensional vector fields near a degenerate singularity", *J. Diff. Eqns.* **37**, *382–404*

Hutson V. & J.S.Pym [1980], "Applications of Functional Analysis and Operator Theory", *Academic Press*

Keefe L.R. [1985], "Dynamics of Perturbed Wavetrain Solutions to the Ginzburg-Landau Equation", *Studies in Applied Math.* **73**, *91–153*

Kreyszig E. [1978], "Introductory Functional Analysis with Applications", *John Wiley & Sons*

Kuramoto Y. & T.Tsuzuki [1975], "On the formation of dissipative structures in reaction-diffusion systems", *Progr. Theoret. Phys. Suppl.* **54**, *687–699*

Lanford O.E. [1982], "A computer-assisted proof of the Feigenbaum conjectures", *Bull. Am. Math. Soc.* **6**, *427*

Lin X.B. [1986], "Exponential Dichotomies and Homoclinic Orbits in Functional Differential Equations", *J. Diff. Eqns.* **63**, *227–254*

Lorenz E.N. [1963], "Deterministic nonperiodic flow", *J. Atmos. Sci.* **20**, *130–141*

Numerical Algorithms Group [1992], "NAG `FORTRAN` library, version 16", *256 Banbury Road, Oxford*

Olver P.J. [1986], "Applications of Lie Groups to Differential Equations", *Springer-Verlag*

Parker T.S. & L.O.Chua [1989], "Practical Numerical Algorithms for Chaotic Systems", *Springer-Verlag*

Press W.H., B.P.Flannery, S.A.Teukolsky & W.T.Vetterling [1992], "Numerical recipes in C, 2nd edition", *C.U.P.*

Sarkovskii A.N. [1964], "Coexistence of cycles of a continuous map of a line onto itself", *Ukranian Math. J.* **16**. *61*

Sherratt J.A. [1994], "On the Evolution of Periodic Plane Waves in Reaction-Diffusion Systems of λ-ω Type", *SIAM J. Appl. Math.* **54**, *1374–1385*

Shil'nikov L.P. [1965], "A case of the existence of a countable number of periodic motions", *Soviet Math. Dokl.* **6**, *163–166*

Shil'nikov L.P. [1967a], "Existence of a countable set of periodic motions in a four-dimensional space in an extended neighbourhood of a saddle-focus", *Soviet Math. Dokl.* **8**, *54–58*

Shil'nikov L.P. [1967b], "On a Poincaré-Birkhoff problem", *Math. USSR Sb.* **3**, *353–371*

Shil'nikov L.P. [1968], "On the generation of a periodic motion from trajectories doubly asymptotic to an equilibrium state of saddle type", *Math. USSR Sb.* **6**, *427–438*

Shil'nikov L.P. [1969], "On a new type of bifurcation of multidimensional dynamical systems", *Soviet Math. Dokl.* **10**, *1368–1371*

Shil'nikov L.P. [1970], "A contribution to the problem of the structure of an extended neighbourhood of a rough equilibrium state of saddle-focus type", *Math. USSR Sb.* **10**, *91–102*

Sparrow C. [1982], "The Lorenz Equations", *Springer-Verlag*

Takáč P. [1991], "Invariant 2-Tori in the Time-Dependent Ginzburg-Landau Equation", *Preprint* `MCS-P244-0691`, *Argonne National Laboratory, Chicago*

Temam R. [1988], "Infinite-Dimensional Dynamical Systems in Mechanics and Physics", *Springer-Verlag*

Tinkham M. [1975], "Introduction to Superconductivity", *McGraw-Hill*

Tresser C. [1984], "Homoclinic orbits for flows in $\mathbb{R}^3$", *J. Physique* **45**, *837–841*

Wiggins S. [1988], "Global Bifurcations and Chaos", *Springer-Verlag*

Wiggins S. [1990], "Introduction to Applied Nonlinear Dynamical Systems and Chaos", *Springer-Verlag*

Wolfram S. [1991], "Mathematica: a system for doing mathematics by computer, 2nd edition", *Addison-Wesley*